AN ABSTRACT OF THE THESIS OF

Richard H. Fifarek for the degree of Doctor of Philosophy in Geology presented on May 8, 1985.

Title: Alteration Geochemistry, Fluid Inclusion, and Stable Isotope Study of the Red Ledge Volcanogenic Massive Sulfide Deposit, Idaho

Abstract approved:

Cyrus W. Field

The Red Ledge Zn-Cu-Ag deposit is hosted by island arc volcanic and sedimentary rocks correlative with the Lower Permian Hunsaker Creek Formation of the Seven Devils Group. Mineralization is genetically related to a dacite-rhyodacite domal complex, and consists of a stockwork feeder system and an overlying strata-bound cap of stacked stringer and massive sulfide lenses (3-4 couplets). Footwall alteration assemblages grade outward from silicified vein selvages through zones of sericite and sericite-chlorite to a propylitic halo. Altered host rocks have been variably enriched in SiO_2, Fe_2O_3, MgO, K_2O, and ^{18}O, and consistently depleted in FeO, CaO, and Na_2O. Average $\delta^{18}O$ values of felsic rocks in the propylitic, phyllic and silicified alteration zones are 9.6, 10.6, and 12.2 permil, respectively. Homogenization temperatures of primary-appearing vapor-liquid inclusions in vein minerals average 274 °C. Calculated $\delta^{18}O$ values of the feeder vein fluids vary from ~0 $^{o}/oo$ during early

amethyst deposition, to 4-5.5 $^{o}/_{oo}$ during intermediate quartz-sulfide deposition, and finally to 0-1 $^{o}/_{oo}$ during late barite-carbonate deposition. This paragenetic trend is consistent with isotopic exchange between convecting seawater and volcanic rocks at reasonable temperatures and integrated water to rock ratios with respect to the water (w/r_w): early fluids at ~250 °C and moderate w/r_w, intermediate fluids at 400-450 °C and low w/r_w (deep in the volcanic pile), and late fluids at 250-290 °C and moderate w/r_w. Average $\delta^{34}S$ values of sulfides and barite decrease upward from vein (-2.8 & 15.2 $^{o}/_{oo}$, resp.), through stringer (-5.1 & 14.5 $^{o}/_{oo}$, resp.), to massive (-5.1 & 12.7 $^{o}/_{oo}$) mineralization. These isotopic shifts are consistent with the progressive addition of Permian seawater (~0 °C, $\delta^{34}S$ = 10.5 $^{o}/_{oo}$) to the rising intermediate fluids (~275 °C, $\delta^{34}S$ = 12-23 $^{o}/_{oo}$). Small additions (10% seawater) resulted in equilibrium cooling to 240 °C and a sympathetic decrease in sulfide and barite $\delta^{34}S$ values. Additional mixing resulted in nonequilibrium cooling and a further decrease in barite values. The isotopic variablilty of vein carbonates ($\delta^{13}C$ = -10.8 to -0.8 $^{o}/_{oo}$ & $\delta^{18}O$ = 9.1 to 20.1 $^{o}/_{oo}$) and vein sulfates ($\delta^{34}S$ = 13.6-19.0 $^{o}/_{oo}$ & $\delta^{18}O$ = 7.8-10.5 $^{o}/_{oo}$) suggest that seawater also mixed with late fluids up to +1000 feet below the seafloor. Hydrothermal carbon was leached from the country rocks, whereas hydrothermal sulfur, both in the Red Ledge and analagous deposits of the western Cordillera, was largely derived from seawater via an intermediate step involving the inorganic reduction of seawater sulfate.

Alteration Geochemistry, Fluid Inclusion, and Stable Isotope Study of the Red Ledge Volcanogenic Massive Sulfide Deposit, Idaho

by

Richard H. Fifarek

A THESIS

submitted to

Oregon State University

in partial fulfillment of
the requirements for the
degree of

Doctor of Philosophy

Completed May 8, 1985

Commencement June 1985

APPROVED:

Redacted for privacy

Professor of Geology in charge of Major

Redacted for privacy

Head of Department of Geology

Redacted for privacy

Dean of Graduate School

Date thesis is presented May 8, 1985

Typed by researcher for Richard H. Fifarek

ACKNOWLEDGEMENTS

Financial support for this investigation was provided by grants from the ASARCO Foundation and Texasgulf, Inc. and through temporary employment with the Branch of Central Mineral Resources, U. S. Geological Survey. Major and minor element analyses were furnished by the Branch of Marine Geology, U. S. Geological Survey. For arranging this monetary support, I would like to thank Cyrus W. Field of Oregon State University, Richard B. Taylor, Charles H. Thorman, and Tracy L. Vallier of the U. S. G. S., and Allan P. Juhas formerly of Texasgulf, Inc.

Michael L. Cummings of Portland State Univerity kindly allowed the use of a petrographic microscope.

Sample material and unpublished geologic data on the Red Ledge deposit were provided by Texasgulf, Inc. and Roney C. Long. Most of the samples and data on other volcanogenic massive sulfide deposits in the western Cordillera were released to the author by Conoco, Inc. Two samples from the Lynx Mine were supplied by Arthur E. Soregaroli of Westmin Resources Ltd., and one sample from the Keating District and unpublished geologic data on the Blue Jacket were contributed by Ronald Willden of J. L. Carroll Mineral Exploration. The generous assistance of these companies and individuals is gratefully acknowledged.

I would like to sincerely thank Robert O. Rye for the opportunity to utilize the isotopic and fluid inclusion facilities at the Branch of Isotope Geology, U. S. G. S. (Denver, Co.) and for his guidance during the initial phase of this study. Moreover, I would

like to express my gratitude to Joseph F. Whelan, Mark A. Huebner, and Michael Wasserman for their patience and amiability during many training sessions in various laboratory techniques. Generous and warm hospitality were extended to the author and his family while in Denver by Robert O. Rye, Joseph F. Whelan, Gary P. Landis, and Roberta H. Dixon and their respective families.

The concepts expressed in this investigation greatly benefited from discussions with Cyrus W. Field, Robert O. Rye and Ronald G. Senechal (Oregon State University). Editorial comments from Cyrus W. Field and Ronald G. Senechal were most welcome.

Finally, I am deeply grateful for the encouragement and support provided by my wife, Katheryn, and by my family throughout graduate school.

Table of Contents

List of Tables

List of Figures

ALTERATION GEOCHEMISTRY, FLUID INCLUSION, AND STABLE ISOTOPE STUDY OF THE RED LEDGE VOLCANOGENIC MASSIVE SULFIDE DEPOSIT, IDAHO

Introduction

Volcanogenic massive sulfide deposits have been the subject of intensive research during the last 25 years. It is now widely accepted that: 1) these deposits formed on or near the seafloor and typically around the discharge vents of hydrothermal convection cells, 2) the hydrothermal fluids consisted principally of seawater that had evolved chemically via reactions with rocks during convection, 3) the precipitation of sulfide and gangue minerals resulted from the physiochemical changes caused by mixing ambient seawater with the hydrothermal fluids, and 4) convection was driven by the heat released from crystallizing bodies of mafic magma at mid-ocean ridges or of felsic magma in volcanic arc settings. However, many critical factors concerning the origin of these deposits have yet to be established and are a matter of current debate. For example, the mixing of seawater and hydrothermal fluids in the area above the discharge vent is supported by several lines of evidence (e.g. Sato, 1972; Solomon and Walshe, 1979; Francheteau et al., 1979), but the mixing of these two solutions in permeable rocks below the seafloor, which is suggested by theoretical considerations (e.g. Cathles, 1983), has not been convincingly demonstrated. Moreover, certain features of these deposits, such as the mineral zonation and upward decrease in sulfide $\delta^{34}S$ values, have been explained by both equili-

brium (e.g. Kajiwara, 1971; Rye and Ohmoto, 1974; Bryndzia et al., 1983) and nonequilibrium (e.g. Ohmoto et al., 1983) mechanisms of chemical and isotopic exchange. Finally, the principal source(s) of metals, carbon and other major components (except sulfur) of the hydrothermal phases is still unresolved.

The major purpose of this investigation was to address these and other problems involving the genesis of volcanogenic massive sulfide mineralization through a study of the alteration geochemistry, fluid inclusion record, and stable isotope systematics of the Red Ledge deposit. The specific objectives of this investigation were to establish: 1) the spatial and temporal variations in the isotopic composition of ores, gangue, and altered wallrocks, 2) the thermal history of mineral deposition, and 3) the origin of the fluids and the source of the components of the mineral phases deposited therefrom. Previous investigations (Long, 1975; Juhas and Gallagher, 1981; unpublished report by Texasgulf, Inc.) have established that the Red Ledge prospect is a large "Kuroko type" massive sulfide deposit of Early Permian age which consists of massive, strata-bound stringer, and stockwork feeder mineralization. The coincidence of these features, and the presence of barite and carbonate in the stockwork zone, permitted the characterization of the hydrothermal fluids prior to venting and the effects attendant with the mixing of seawater and hydrothermal fluids upon venting.

The more important results of this investigation that pertain to a general model for volcanogenic mineralization include: 1) the isotopic composition of the fluids in submarine hydrothermal systems may result from the interaction of convecting and stagnant seawater

with volcanic rocks at specific temperatures and integrated water/rock ratios, 2) temporal variations in the isotopic composition of the fluids may reflect differences in the conditions under which the predominant fluids were generated, 3) the commonly noted upward decrease in the $\delta^{34}S$ ratios of sulfides may be produced by equilibrium isotopic exchange between SO_4 and H_2S that accompanies the admixing of a minor amount of seawater into the hydrothermal solutions at shallow depths below the seafloor, 4) pristine seawater may infiltrate the stockwork systems to considerable depths below the seafloor and mix with rising hydrothermal fluids during the waning stages of hydrothermal activity, and 5) carbon in the hydrothermal solutions may be derived from country rocks, seawater, or both.

Regional Geologic Setting

The Red Ledge prospect is located in the Seven Devils mining district, Adams County, Idaho, about 120 miles northwest of Boise and two miles southeast of the Oregon-Idaho border at Hells Canyon dam on the Snake River, as shown in Figure 1. The deposit is largely in the SE1/4 sec. 23, T. 22 N., R. 3 W. (Cuprum 15' quadrangle) and is exposed between 2800 and 5200 feet of altitude in the valley of Deep Creek, a tributary to the Snake River. Peaks of the Seven Devils Mountains and Hells Canyon, the deepest canyon in North America, dominate the rugged physiographic setting of the deposit.

The Hells Canyon area, as depicted in Figure 2, is one of numerous erosional inliers of Paleozoic and Mesozoic eugeosynclinal rocks which occur throughout the Blue Mountains geomorphic province of northeastern Oregon and westernmost Idaho. The inliers are exposed through an extensive cover of Cenozoic continental volcanic and sedimentary rocks along a northeast-trending belt of uplifts and incised rivers. Notable among these younger strata are the Miocene flood basalts of the Columbia River Basalt Group. Rocks of the Cretaceous Idaho batholith and Precambrian Belt Supergroup adjoin the eugeosynclinal sequence to the east near the 0.706 $^{87}Sr/^{86}Sr$ line and western margin of the North American craton (Armstrong et al., 1977).

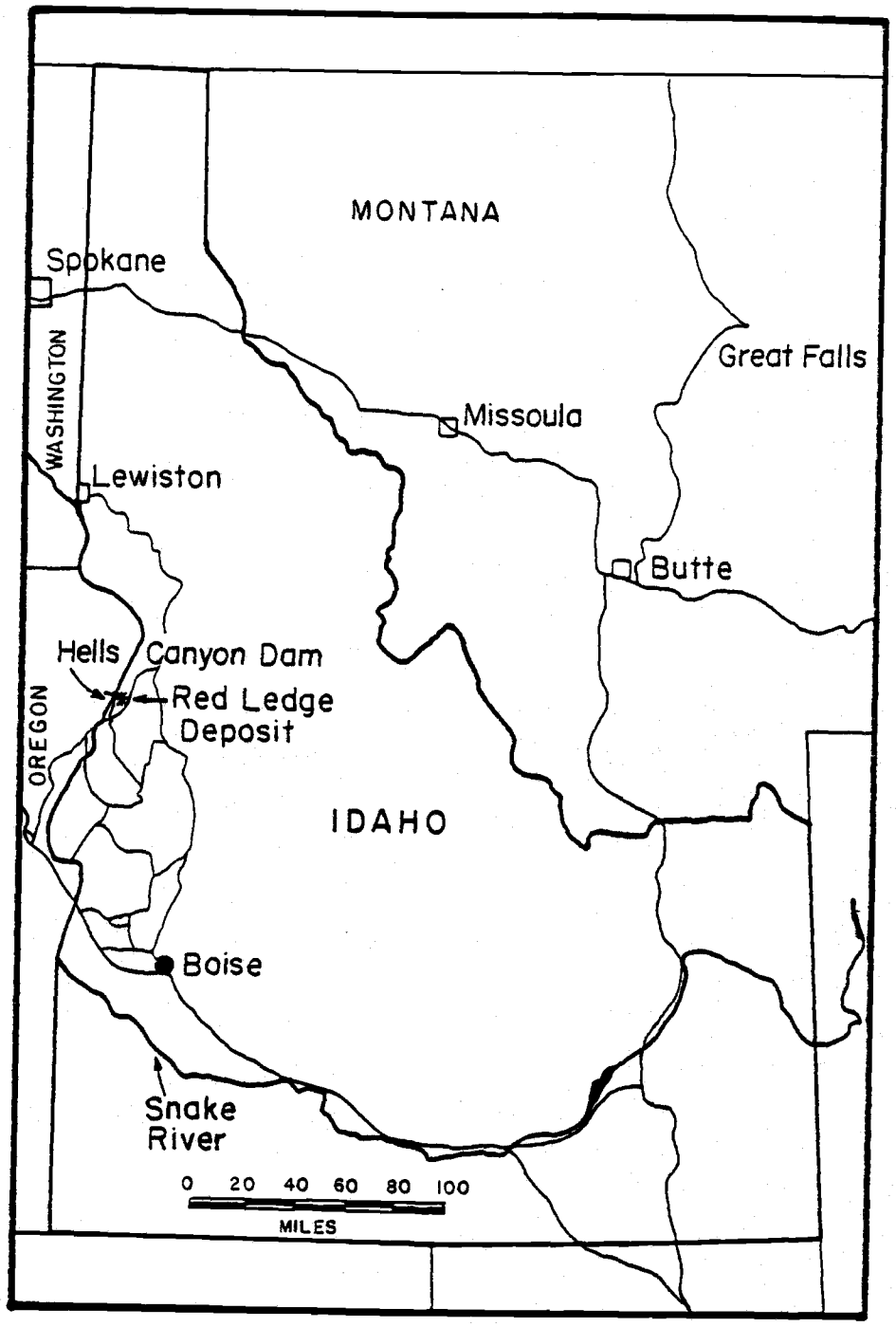

Figure 1. Location of the Red Ledge deposit. Also shown are the Snake River, major regional highways, and secondary roads in the vicinity of the Red Ledge.

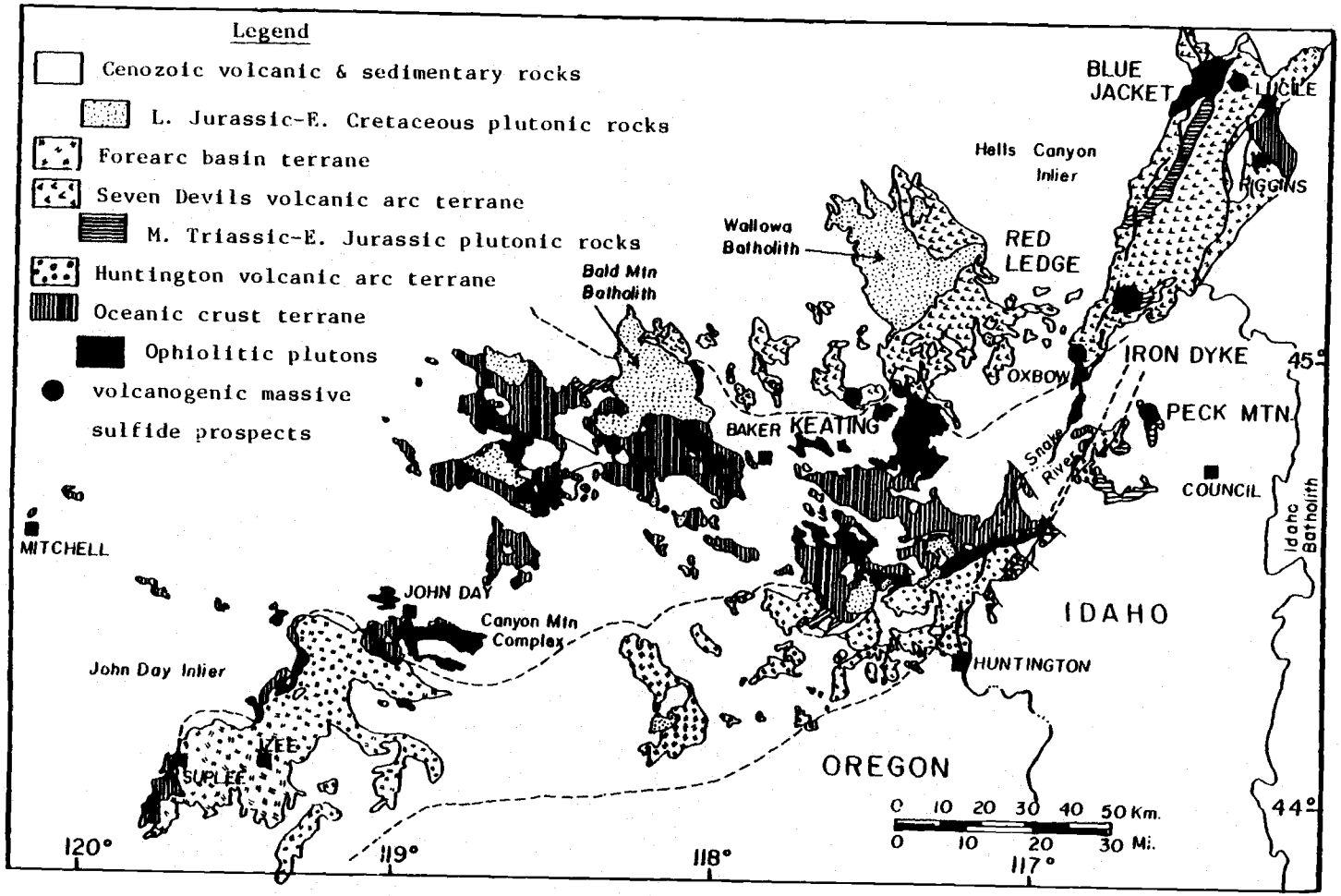

Figure 2. Geology of the Blue Mountains province (modified after Vallier et al., 1977, Fig. 2; Brooks and Vallier, 1978, Fig. 4; and Brooks, 1979, Fig. 4) and location of principal volcanogenic massive sulfide prospects.

Blue Mountains Province

Pre-Cenozoic rocks of the Blue Mountains province are divisible into four northeast-trending petrotectonic terranes: 1) oceanic crust terrane, 2) forearc basin terrane, 3) Seven Devils volcanic arc terrane, and 4) Huntington volcanic arc terrane as portrayed in Figure 2 (Brooks et al., 1976; Vallier et al., 1977; Brooks and Vallier, 1978; Dickinson and Thayer, 1978; Brooks, 1979; Dickinson, 1979). Each terrane is metamorphosed, bounded by major faults or unconformities, and intruded by Jurassic-Cretaceous plutonic rocks of intermediate composition. Intraterrane units, fold axes, and faults generally parallel terrane boundaries.

The oceanic crust terrane is comprised of tectonic blocks of dismembered ophiolite in a supracrustal assemblage of chert, argillite and locally abundant tuff and lava flows. Exotic limestone pods, containing fossil faunas of both Tethyan and American affinity, range from Devonian to mid-Triassic in age. A rare occurrence of blueshcist near Mitchell, Oregon has yielded a K-Ar date of 225 m.y. (Swanson, 1969; Hotz et al., 1977). Ophiolitic rocks, representative of the crustal basement, are well exposed in the Canyon Mountain Complex (Fig. 2) where gabbroic and ultramafic cumulates and a sheeted dike complex once formed the substructure to Permian and Triassic volcanoes (Thayer, 1963, 1977; Thayer and Brown, 1964; Ave Lallemant, 1976).

The forearc basin terrane consists of a thick, extensive flysch of Late Triassic to Late Jurassic age. Lithologies are predominantly

volcanic sandstone, siltstone, shale and tuff with lesser amounts of lava flows, conglomerate, limestone and gypsum. This succession is typically in fault contact with the oceanic crust and Huntington volcanic arc terranes and conceals their mutual boundary. In a few significant localities, however, sedimentary rocks of the flysch sequence rest unconformably on rock types of the oceanic and volcanic arc units and contain their detritus.

The volcanic assemblages of the Huntington and Seven Devils volcanic arc terranes closely resemble those of modern volcanic arcs and host the principal massive sulfide prospects in the region (Fig. 2). They largely consist of volcaniclastic breccia, agglomerate, tuff, conglomerate, sandstone and siltstone, and minor flows, dikes, hypabyssal intrusions, and limestone lenses. Igneous compositions are basalt, basaltic andesite, andesite, dacite and rhyolite. Fossil suites indicate a Late Triassic (late Karnian to middle Norian) age for the Huntington volcanic arc terrane and a Early Permian and Mid to Late Triassic (Ladinian to Karnian) age for the Seven Devils volcanic arc terrane. The latter terrane includes a basement of ophiolitic and associated metamorphic rocks, and a sequence of Late Triassic to Late Jurassic platform carbonate and fine-grained marine epiclastic rocks unconformably overlying the volcanic section. Neither of these assemblages, however, has been found in the Huntington volcanic arc terrane.

Granitic plutons intruded the Blue Mountains province during three principal intervals: Middle Triassic-Early Jurassic, Late Jurassic-Early Cretaceous, and Late Cretaceous (Armstrong et al.,

1977). The oldest group (200-220 m.y.) is represented by small metamorphosed plutons in the Huntington arc terrane and the intermediate (95-160 m.y.) and youngest (64-95 m.y.) episodes include the Wallowa and Bald Mountain batholiths, and Idaho batholith, respectively.

It is evident that the pre-Cenozoic rocks of the Blue Mountains province record a complex history of plate convergence and accretion. Dickinson (1979) proposed a coherent hypothesis that interrelates three of the four terranes. He suggested the oceanic terrane constitutes an accretionary melange which formed in an arc-trench gap between a southeast plunging subduction zone to the northwest and the Huntington volcanic arc to the southeast. Structural adjustments within the arc-trench gap produced the forearc basin which subsequently filled with detritus mostly from the Huntington arc during Late Triassic-Late Jurassic time.

The tectonic evolution of the Seven Devils arc, however, is less certain and the subject of recent debate. At question is: 1) whether the Seven Devils and Huntington terranes are fragments of the same arc, and 2) whether the Seven Devils arc is part of Wrangellia, an exotic terrane discontinuously exposed along the British Columbia coastline and in southern Alaska. The connection to Wrangellia is based on time-stratigraphic similarities (Jones et al., 1977, 1978; Silberling, 1983), although Sarewitz (1983) has suggested the stratigraphic, lithologic and geochemical dissimilarities between the terranes preclude their consanguinity. Using stratigraphic and paleontologic data, Silberling (1983) concluded the Seven Devils and

Huntington terranes were not fragments of the same arc. However, Walker (1983) has interpreted U/Pb ages of zircons from these terranes as evidence favoring a close association in part of a single convergent system. Finally, paleomagnetic pole determinations on volcanic rocks from all three terranes (Wrangellia, Seven Devils and Huntington) permit a common subequatorial origin during Late Triassic time (Hillhouse, 1977; Schwarz et al., 1980; Yole and Irving, 1980; Hillhouse and Gromme, 1981; Hillhouse et al., 1982). In any case, the Blue Mountains fragment collided with North America by the Late Jurassic Epoch (Wilson and Cox, 1980; Ave Lallemant, 1983), and from Late Jurassic to Eocene time the region underwent approximately 60 degrees of clockwise rotation (Wilson and Cox, 1980).

Hells Canyon Inlier

The Red Ledge volcanogenic massive sulfide deposit is hosted by volcanic rocks of the Seven Devils arc terrane (Fig. 2). This assemblage is particularly well exposed in Hells Canyon where a volcanic section, 6000 meters thick, has been formally termed the Seven Devils Group and divided into four formations by Vallier (1977), as summarized in Figure 3. The Windy Ridge Formation, of Early Permian or older age, is comprised of quartz keratophyre flows and tuff. The restricted distribution and lack of epiclastic rocks for this unit imply that it represents a local accumulation of silicic volcanic rocks and is a lithofacies of the overlying Lower Permian Hunsaker Creek Formation. This latter unit and the

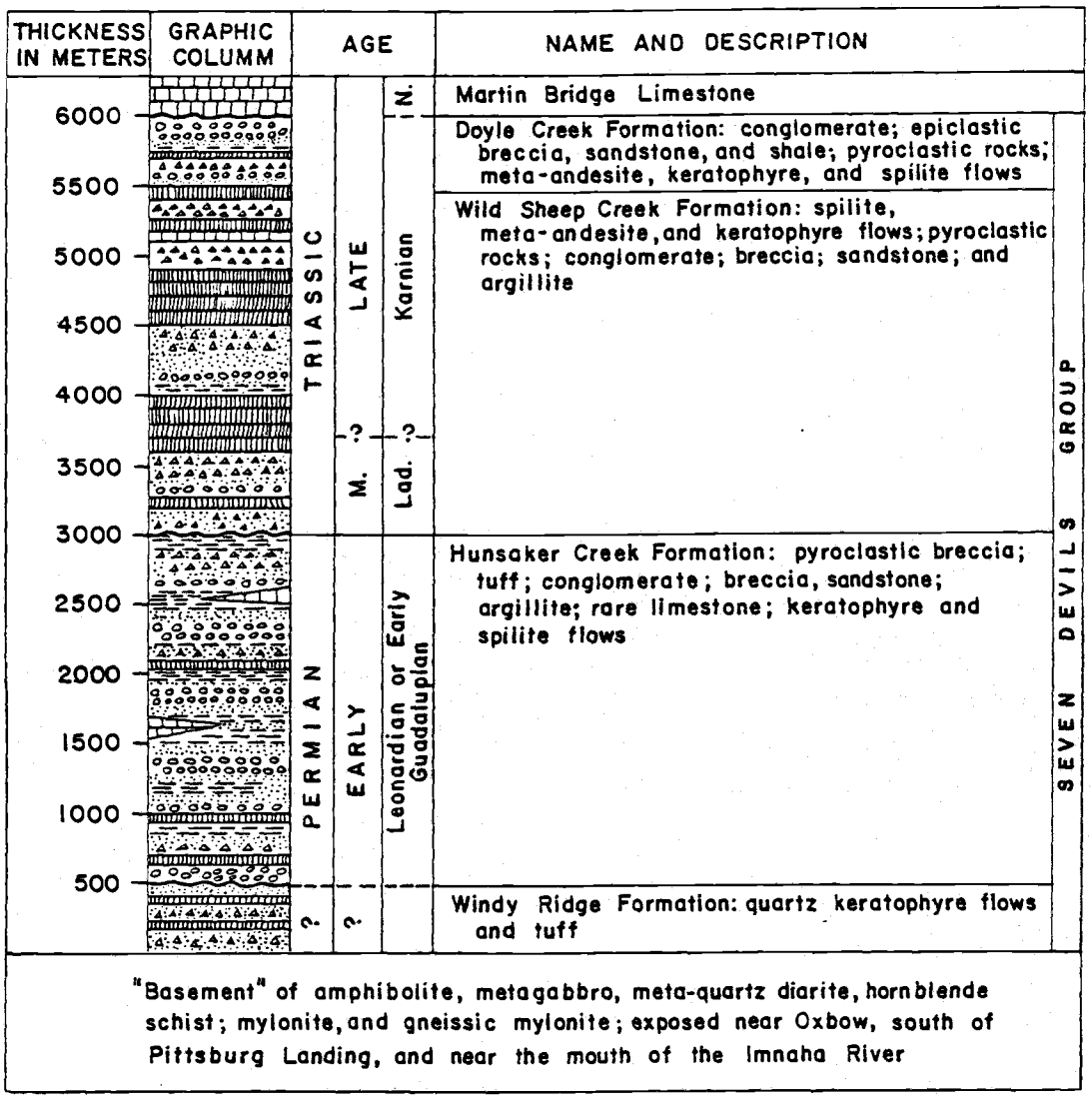

Figure 3. Composite stratigraphic column of the Seven Devils Group, Snake River Canyon, Oregon and Idaho (after Vallier et al., 1977).

succeeding Middle and Upper Triassic Wild Sheep Creek and Upper Triassic Doyle Creek Formations are principally composed of pyroclastic and epiclastic rocks interspersed with flows, hypabyssal intrusions, dikes and minor limestone. Clastic rock types range from volcanic tuff and agglomerate or breccia, to epiclastic shale and conglomerate. Common features of the units include rapid lithofacies changes, a small but ubiquitous component of plutonic debris, and graded beds and pillow structures. Igneous compositions change from an apparently bimodal assemblage of spilite and quartz keratophyre in the Lower Permian Hunsaker Creek Formation to predominantly spilite and keratophyre in the Middle and Late Triassic formations. This change in magma composition coincides with a regional unconformity of low angular discordance that represents a 30-40 m.y. hiatus in the stratigraphic record. Thus, the Seven Devils Group records at least two petrologically distinct and overlapping episodes of arc volcanism.

Mineralogies in the rocks of the Seven Devils Group are diagnostic of the greenschist facies of regional metamorphism and include secondary albite, chlorite, epidote, quartz, sphene, calcite and prehnite (Vallier and Batiza, 1978). Spilites of Permian age have mineral assemblages more nearly representative of equilibrium than those of Triassic age, probably indicating deeper burial. Albite is characteristic of Permian rocks, whereas more calcic plagioclase, occasionally rimmed by albite, and zeolite and relict clinopyroxene distinquish the Triassic assemblage. Foliation is also more common in the Permian rocks, although penetrative deformation is

generally absent. Despite extensive ion mobility most elements have apparently been conserved and clinopyroxene compositions, ratios of relatively immobile elements, and major oxide abundances indicate the spilite, keratophyre and quartz keratophyre rocks represent a low-K differentiation series of tholeiite-andesite-dacite-rhyolite (Vallier and Batiza, 1978).

The Seven Devils Group is unconformably overlain by shallow-water reef limestone and minor limestone breccia and dolomite of the Upper Triassic Martin Bridge Limestone (Fig. 3) which are successively superseded by argillaceous limestone, argillite and volcaniclastics of the Upper Triassic and Lower Jurassic Hurwall Formation and mudstone, minor siltstone, sandstone and conglomerate of the Middle and Upper Jurassic Coon Hollow Formation.

Pre-Cenozoic rocks of this region are moderately deformed. Bedding and fold axes typically strike northeast and northwest (Vallier, 1974). Significant displacement has occurred on reverse faults and along three major shear zones characterized by extensive cataclasis, metamorphism and plutonism. The present topography has been greatly influenced by block faulting and broad regional warping of Late Miocene to Recent age.

Geology of the Red Ledge Deposit

The Red Ledge prospect is a large, zinc-copper-silver deposit of Permian age and island-arc volcanogenic massive sulfide affiliation. Geologic features of this deposit grossly resemble those of many others found throughout the geologic column and in a variety of locations around the world such as the Kuroko deposits, Japan; Buchans, Newfoundland; Roseberry, Tasmania; and Noranda, Quebec. Mineralization is comprised of a well-developed stockwork feeder system and an overlying cap of stratiform and strata-bound sulfides. These are spatially and genetically related to a domal complex of dacitic and rhyolitic composition.

Detailed investigations of the Red Ledge deposit include those by Livingston and Laney (1920), Long (1975) and Juhas and Gallagher (1981). These, and unpublished reports, maps, sections and drill logs furnished by Texasgulf, Inc., provided the overall geological basis for this investigation. Subsurface geologic interpretations were based on approximately 50,000 feet of exploratory drilling and over 2000 feet of accessible mine workings. Most of the 220 samples utilized in this study were selected from 38,000 feet of diamond drill core distributed among 26 drill holes that have intercepted this deposit.

Stratigraphic Units

Interfingered volcanic, volcaniclastic and sedimentary rocks constitute the country rocks to the Red Ledge domal complex and host rocks to the majority of the mineralization (Fig. 4). Folding has rotated the section approximately 90 degrees such that the stratigraphic units and strata-bound mineralization generally strike northeast and dip steeply, and the originally near-vertical zone of stockwork mineralization is now essentially horizontal (Fig. 5). Rocks in the Red Ledge area have been previously regarded as Permian, Triassic, or undifferentiated Permo-Triassic in age. However, based on the recent find of a Permian brachiopod near the horizon of strata-bound mineralization (T. Vallier, pers. comm.) they are herein considered to be Permian in age and informally correlated with the Lower Permian Hunsaker Creek Formation. This age determination is in agreement with that interpreted for the mineralization based on the sulfur isotopic composition of syngenetic barite (Fifarek et al., 1983; see this investigation). Thick sections of alternating volcanic and sedimentary rocks of Mid to Late Triassic age are well exposed 0.5 miles northwest of the Red Ledge deposit.

Stratigraphic rock types adjacent to the Red Ledge intrusion are primarily volcanic breccia, lapilli tuff, tuff, flows, and volcanic conglomerate, wacke and siltstone. Examples of some stratigraphic lithologies are shown in Figure 6A. Field distinctions between epiclastic volcanic rocks and volcaniclastics are commonly ambiguous because the sedimentary units are immature, massive to faintly

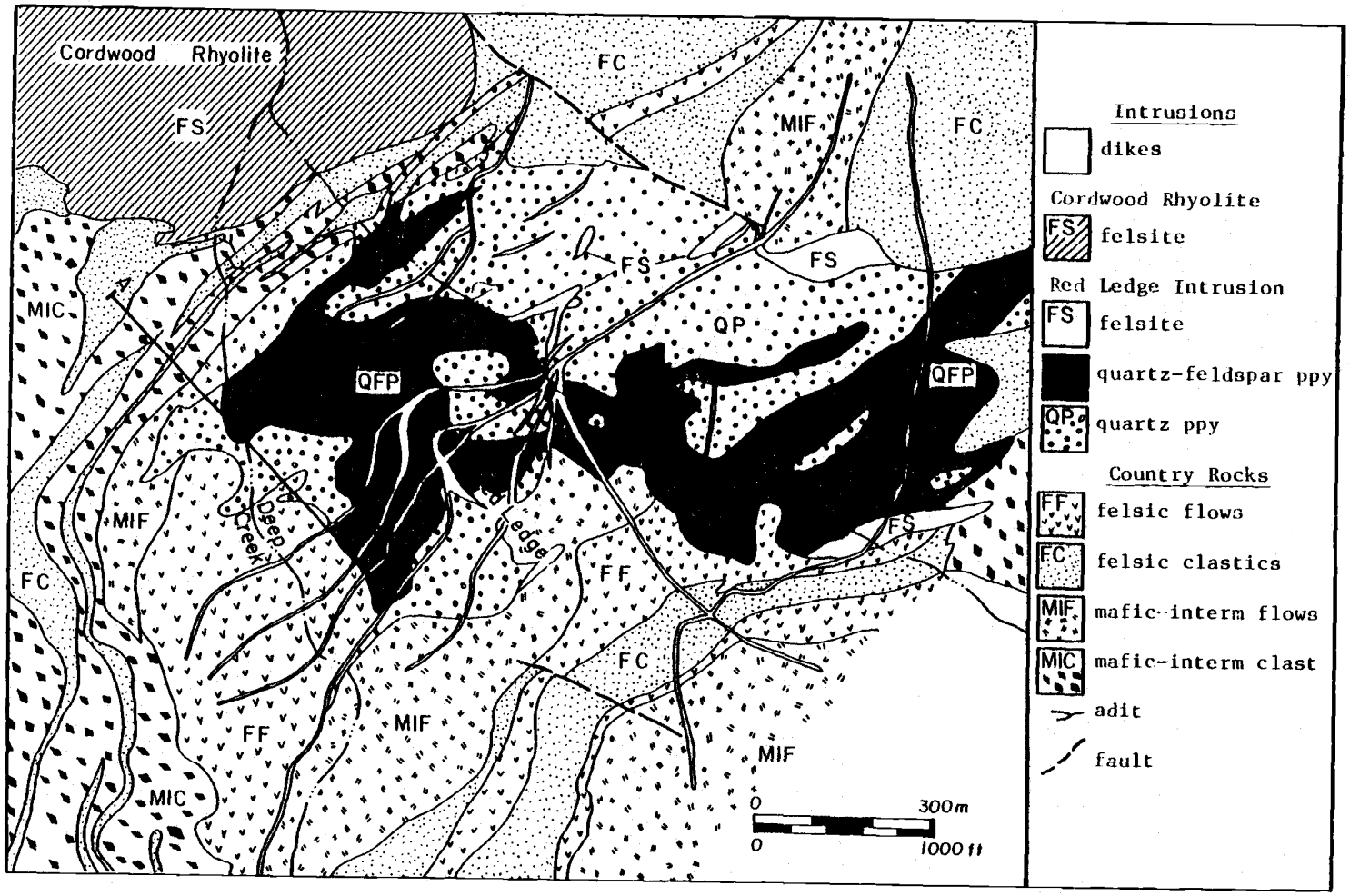

Figure 4. Geology of the Red Ledge area (modified from Long, 1975; Texasgulf, Inc., unpublished map).

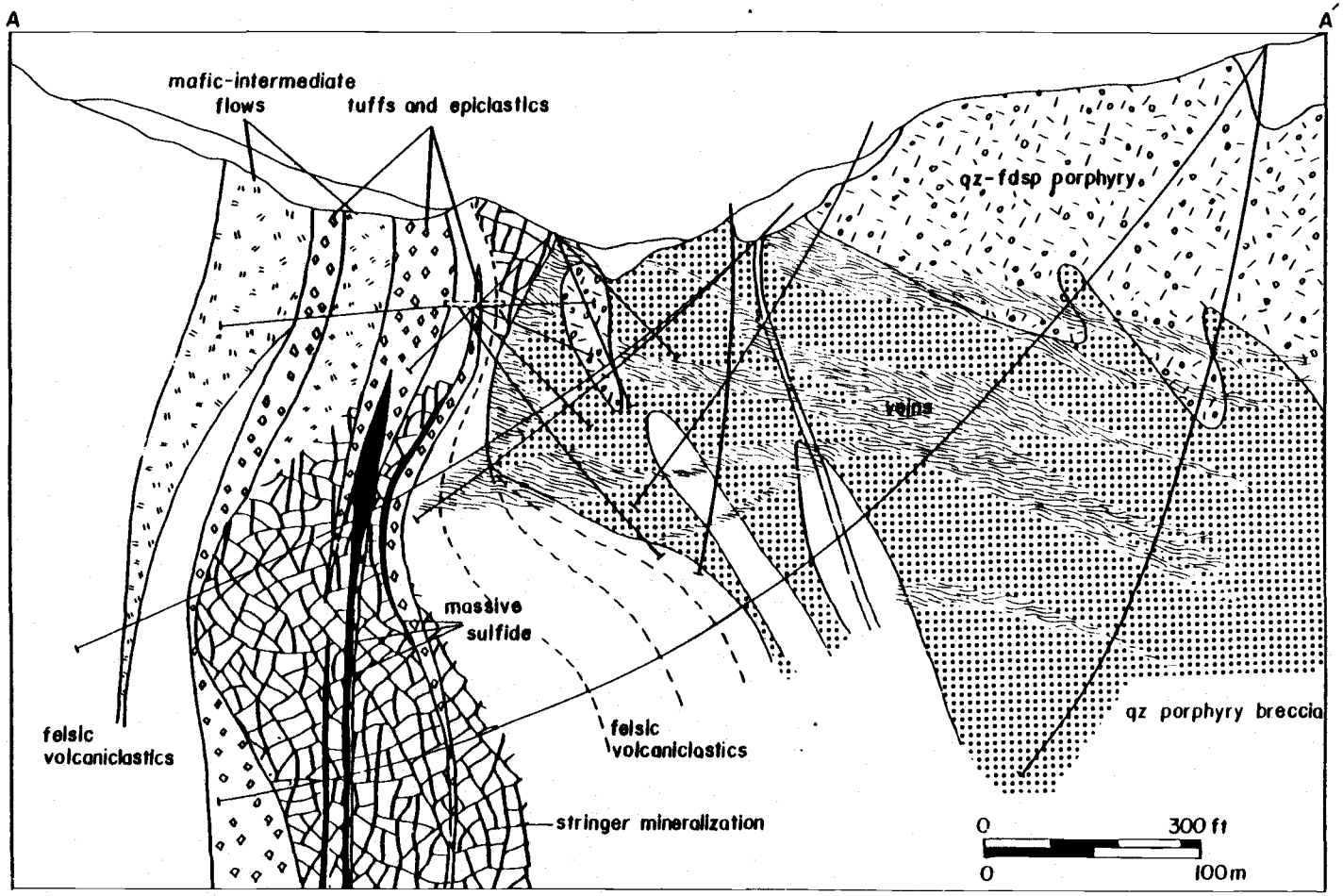

Figure 5. Geology and mineralization along cross section A-A' of Figure 4 (modified from Juhas and Gallagher, 1981).

A.

B.

Figure 6. A. Stratigraphic host rocks: quartz-eye tuff (left); volcanic epiclastics (center and right); B. Intrusive host rocks: hematitic QFP of Red Ledge domal complex (top left); felsite of Cordwood Rhyolite (top right); QFP dike (lower left);

bedded, and monolithologic. Many of these represent slighty reworked volcanic precursors. Similarly, mafic and intermediate rocks are difficult to distinquish by field criteria although they contrast markedly with felsic rocks characterized by phenocrysts and xenocrysts of quartz or having a leucocratic siliceous appearance. Because of the aforementioned problems, and in order to clarify genetic relationships, the stratigraphic units depicted in Figure 4 are grouped into clastics or flows of either mafic-intermediate or felsic composition. Major and trace element data indicate that most of the felsic rocks are dacites, the principal exception being a rhyodacite or rhyolite post-mineralization intrusion (Cordwood Rhyolite), and that rocks of the mafic-intermediate clan are basalts (see Protolith Compositions).

Geologists of Texasgulf, Inc. have noted the following megascopic features of the various stratigraphic lithologies. Tuffaceous rocks are typified by chloritic or sericitic aphyric fragments which may exhibit a eutaxitic-like structure aligned in the direction of a weak foliation. Equidimensional, subangular fragments of volcanic breccias range up to 10 cm in width and include quartz and quartz-feldspar porphyries of the Red Ledge intrusion as well as aphyric phases. Tuffaceous epiclastic rocks are commonly thin, massive to finely laminated, and of uniform fine-grain size. An unusual interbedded unit of volcanic wacke and siltstone, near the top of the interval containing strata-bound mineralization, displays graded bedding, scour and fill, load cast and flame structure features that are typical of turbidites. Lava flows variably

manifest massive structures, flow brecciated tops, aphyric textures, vesicles, amygdules of calcite, chlorite and quartz, rounded and embayed quartz phenocrysts, and plagioclase phenocrysts and microlites that are partially or completely replaced by secondary minerals.

Although most of the stratified rocks are greenish-gray to buff in color, a few exhibit dark reddish gray or dusky red colors produced by pervasively disseminated hematite. This hematite occurs as veinlets, diffuse zones that crosscut the stratigraphic units, and a cement in sandstone units of Triassic age. Such features imply that this hematite was produced during diagenesis (e.g. prior to sandstone induration) by oxidizing solutions that were largely confined to zones of high permeability. Marked differences in distribution and associated minerals imply that the regional hematite is genetically unrelated to a hydrothermal hematite that is spatially associated with mineralization.

Intrusions

The Red Ledge intrusion is a large composite hypabyssal intrusion of felsic composition. As exposed, the main part of the intrusion is approximately 1100 meters long, 600-800 meters wide and tapers to the east into a major feeder dike at least 1300 meters long (Fig. 4). Overall, the intrusion is discordant to the stratified country rocks, but locally it is concordant or sill-like along the northwest, southwest and southeast margins (Long, 1975). Mappable

phases include quartz-feldspar porphyry (QFP), quartz porphyry (QP), and minor felsite (FS) (Fig. 4). The quartz-feldspar porphyry, as illustrated in Figure 6B, is distinguished by phenocrysts of subangular to rounded quartz, 1-4 mm in diameter, and relict plagioclase feldspar that displays albite and (or) Carlsbad twins. Petrographic and chemical analyses of the least altered QFP samples respectively indicate that the plagioclase is Andesine (An_{33-38}) and the rock composition is dacite. Feldspars from intensely altered samples have been pseudomorphically replaced by aggregates of finely crystalline sericite and minor kaolinite. Quartz porphyry is mineralogically similar to QFP except for an absence of plagioclase feldspar and the presence of minor disseminated barite. Although QP is coextensive with QFP, it is characteristically brecciated, veined, and intensely altered. Consequently, these features suggest that the QP unit is primarily a volcaniclastic derivative of QFP, rather than a distinct intrusive phase. Felsite is typically massive and siliceous, and contains minor replacement clots of chlorite. Crosscutting relationships indicate that it is temporally later than QFP and QP.

A large body of felsite, informally termed the Cordwood Rhyolite, intruded the stratigraphic section overlying the Red Ledge intrusion (Fig. 4). Columnar jointing, an almost white color on fresh surfaces, and a homogenous aphyric to weakly porphyritic texture are its diagnostic features (Fig. 6B). Relict microphenocrysts and groundmass crystals of plagioclase feldspar are evident in thin section, whereas quartz-eye phenocrysts are notably absent. Although

post-mineralization, the Cordwood Rhyolite is pervasively altered to a quartz-sericite-calcite assemblage and is sparsely veined by calcite, quartz-calcite, and hematite. Nevertheless, its major element chemistry closely resembles that of unaltered rhyolite (e.g. 74.3% SiO_2, 2.23% K_2O; see Table 2). Collectively, these characteristics imply that the Cordwood Rhyolite is contemporaneous with the felsite bodies in the Red Ledge intrusion and presumably is consanquineous with QFP.

Several dikes of mafic or intermediate composition crosscut all other rock types in the vicinity of the Red Ledge deposit (Fig. 4). Phenocryst assemblages include calcic plagioclase feldspar and augite, hornblende, and quartz and andesine which are consistent with basalt, andesite and dacite compositions, respectively (Long, 1975).

Geologic Environment

The lithologic character and distribution of the felsic rocks comprising the Red Ledge intrusion are suggestive of a volcanic domal complex. Accordingly, QFP is interpreted as an intrusive phase that was emplaced as sills, dikes and irregularly-shaped plugs. The QP breccia that mantles the intrusion accumulated as an apron of talus around the base of the dome. Beds of felsic tuff and QP breccia in the stratigraphic section near the top of the dome were produced by phreatic and phreatomagmatic explosions. These latter units thin or pinch-out over the inferred apex of the dome, but drape over the flanks and thicken towards adjacent depressions: patterns consistent

with a topographically positive source area. Thus, the domal complex and its extrusive equivalents were produced through repeated intrusions and extrusions of magma and the deposition of volcanic debris resulting from the disintegration of the dome by explosions and gravity slides. In the section overlying the dome the felsic units are intercalated with mafic flows, and tuffaceous wackes and siltstones. They record the waning stages of dome development and the progressive influx of sediment and extraneous volcanic material from nearby vents.

The geology of the Red Ledge area and the bimodal character of the Hunsaker Creek Formation imply, by comparison with modern analogs, that the Red Ledge deposit formed in a back-arc tectonic setting. Such an environment was probably characterized by extensional faulting, caldera development, and high heat flow.

Hydrothermal Alteration

All rocks types in the vicinity of the Red Ledge deposit were hydrothermally altered shortly after their deposition or emplacement. This event was essentially contemporaneous with mineralization and resulted in alteration assemblages spatially zoned about the mineral deposit as illustrated in Figure 7. An outward succession through silicified, phyllic and propylitic alteration facies was established by geologic mapping and logging of drill core (Long, 1975; Texasgulf, Inc.). The phyllic assemblage is mineralogically similar to that of the sericite-chlorite alteration zone associated with Kuroko deposits (e.g. Iijima, 1974; Izawa et al., 1978). However, because chlorite is a minor sporadically distributed constituent in the outer portion of the phyllic zone, and is generally absent from the inner portion, this facies is herein divided into sericite-chlorite and sericite subfacies. Thus, the sericite-chlorite assemblage associated with the Red Ledge deposit represents a transition between the sericite and propylitic zones with respect to its mineralogy and inferred chemical environment. Petrographic evidence suggests that the propylitic assemblage represents a metamorphosed equivalent of the montmorillonite zone of Kuroko deposits (see Date et al., 1983; Green et al., 1983), whereas evidence for the former existence of a zeolite facies has not been recognized. The petrography of both major and minor alteration types, based on the study of 55 thin sections, and the geochemistry of their major and minor elements are discussed subsequently.

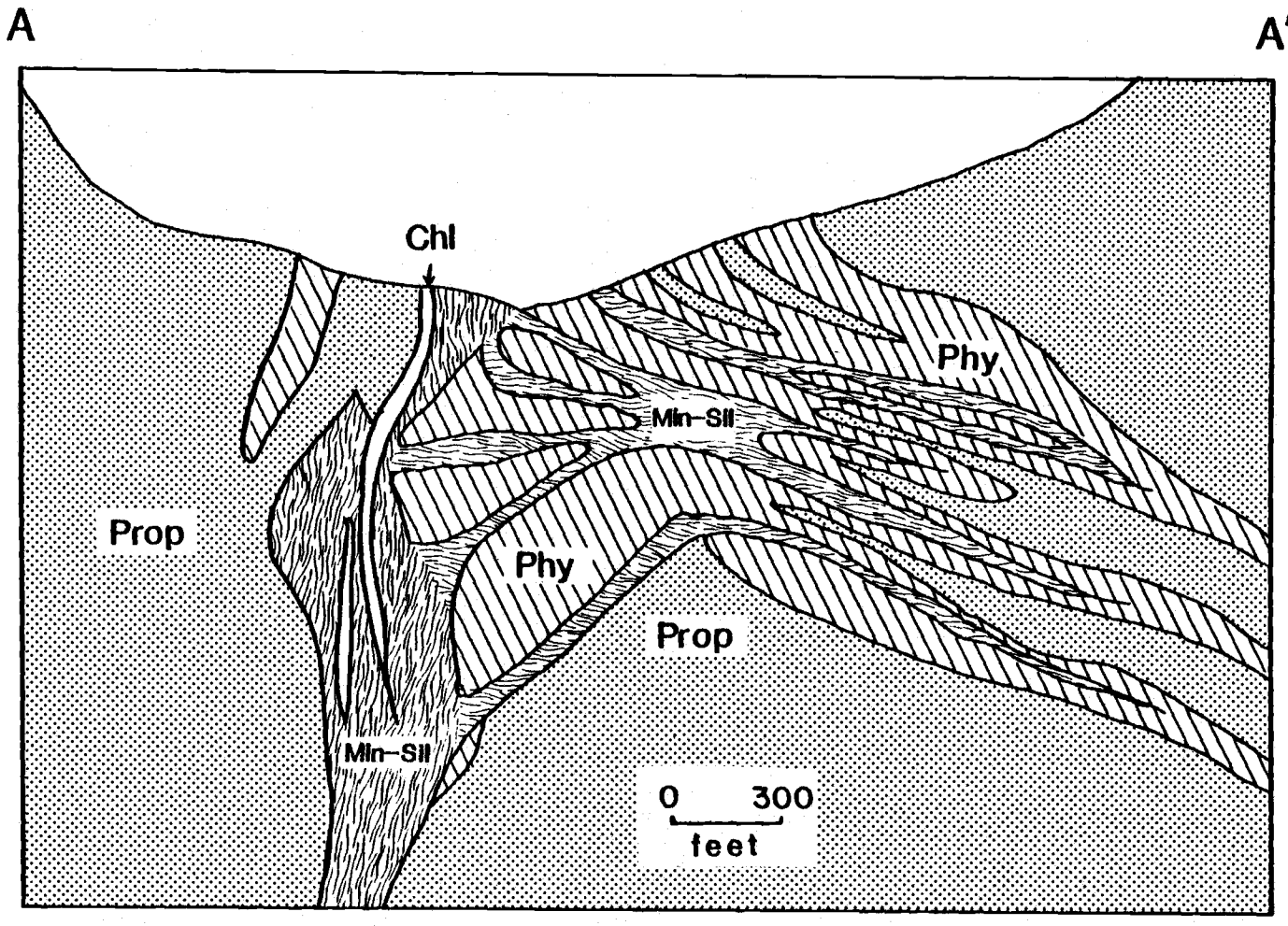

Figure 7. Zonation of hydrothermal alteration assemblages along cross section A-A', Fig. 4 (modified from Juhas and Gallagher, 1981). Min-Sil: mineralization-silicification; Phy: phyllic; Prop: propylitic; Chl: chloritic;

Petrography

Silicification is a prominent type of alteration within the major zones of stockwork veins in the feeder system and in the volcaniclastic host rocks to stringer mineralization. It is distinguished by abundant veinlets of quartz, replacement by microcrystalline quartz in the groundmass, and significant recrystallization along the margins of embayed and fractured ellipsoidal phenocrysts of quartz. Sericite and pyrite are prevalent in silicified rock. The sericite occurs as wispy aggregates that pervasively replace the host, and the pyrite occurs as veinlets, streaks, and finely disseminated euhedra. Barite, as ragged disseminated crystals or polycrystalline aggregates, is typically found in silicified rocks associated with the stringer mineralization, but less commonly in those associated with the stockwork system.

The zone of sericite alteration encases the silicified rocks and is particularly well-developed within and immediately below (or footwall to) the strata-bound mineralization. This alteration in felsic rocks, as shown in Figure 8A, is distinguished by 15% or more sericite, 3-10% pyrite, 0-5% clay, 0-4% barite and the absence of chlorite, calcite and relict plagioclase feldspars. Sericite is pervasively disseminated throughout the groundmass, and in places, accentuates the presence of narrow shear planes, veinlets, or a weak foliation. In addition, sericite may be abundantly concentrated with

A.

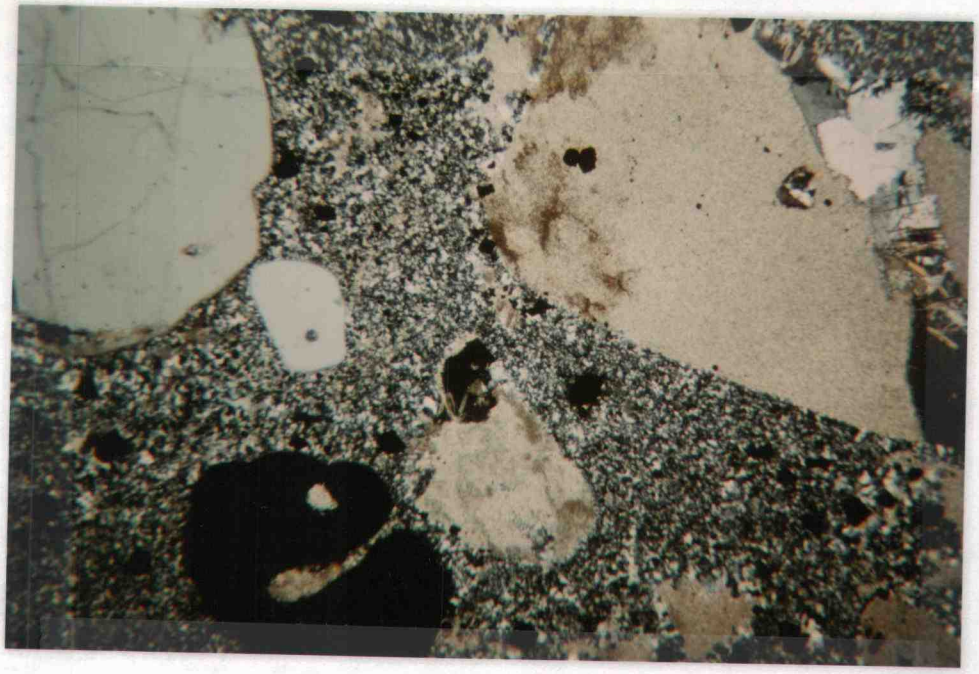

B.

Figure 8. Photomicrographs of QFP altered to: A) phyllic assemblage (sericite subfacies) with aggregates of sericite-pyrite pseudomorphic after phenocrysts of feldspar, and resorbed phenocrysts of quartz; B) propylitic assemblage with phenocrysts of andesine partially replaced by albite and calcite; (field of view is 7.8 mm long);

quartz in aggregates pseudomorphically replacing phenocrysts of plagioclase feldspar (Fig. 8A), in pressure shadows adjacent to quartz phenocrysts and pyrite cubes and in alteration-recrystallization rinds around quartz phenocrysts. The hydrothermal quartz of this rind typically contains abundant small liquid-vapor inclusions. Textures defined by the pyrite disseminations and quartz phenocrysts are similar to those in the silicified rocks, and clay is commonly present as fine intergrowths associated with sericite. Long (1975) identified kaolinite in sericitized quartz-feldspar porphyry and suggested that some of this clay may have been produced by late supergene processes.

Subequal amounts of sericite, chlorite, and clay may represent the sericitic rank of alteration in rocks of mafic to intermediate composition.

The sericite-chlorite alteration assemblage is transitional between the propylitic and sericitic zones. Minerals and textures of this assemblage largely resemble those of the sericitic subfacies, except for the absence of barite and the sporadic presence of either wispy chlorite or calcite (both characteristic of the propylitic zone). The chlorite is a Mg-rich variety according to the optical criteria of Albee (1962).

Propylitic alteration has been recognized at least up to 500 feet away from the intrusion (Long, 1975) and in the country rocks stratigraphically above the deposit. In mafic to intermediate rocks it is expressed by 10-35% chlorite, 3-20% sericite, 5-15% calcite, 3-5% clay and 0-3% pyrite whereas in felsic rocks, as shown in Figure

8B, it is represented by 5-10% sericite, 5-15% calcite, 0-3% pyrite and only minor amounts of chlorite. A Mg-rich chlorite predominates in both rock clans, although minor amounts of Mg-Fe and Fe-Mg chlorite are also present. Phenocrysts of ellipsoidal quartz show less embayment and recrystallization than do their counterparts in zones of more intense alteration. The sporadic association of small bipyramidal quartz phenocrysts with the larger ellipsoidal variety suggests that two generations of quartz crystallized from the magma, possibly because of fluctuations in P_{H2O}, and that some of the "rounding" resulted from magmatic resorption. Relict phenocrysts of andesine are diagnostic of propylitic alteration, although most crystals of this phase have been variably altered to albite, sericite, chlorite and calcite (Fig. 8B). Partially altered plagioclase is also characteristic of the montmorillonite alteration zone associated with Kuroko deposits, where it contrasts with unaltered and completely altered plagioclase of the zeolite and sericite-chlorite zones, respectively (Green et al., 1983, and references cited therein). At the Red Ledge deposit, the outer margin of propylitic alteration grades transitionally into the mineralogically nearly identical greenschist facies of regional metamorphism. Distinctions are based on abundances of sericite and (or) pyrite greater than 2-3%, and a paucity or absence of epidote in the propylitic zone (see Vallier and Batiza, 1978, Table 1, for regional "background" abundances).

The alteration zones are concentrically distributed about the Red Ledge mineral deposit. They are widest at the top of the feeder

system and around stringer mineralization and become progressively restricted with depth (Fig. 7). Although the chronology of their development is not well-established, sparse paragenetic relationships between sericite and chlorite or calcite suggest that the sericitic zone formed at the expense of the sericite-chlorite and propylitic zones. These mineral relationships imply an outward growth of the alteration assemblages with time in a manner similar to that documented for vein selvages by Meyer and Hemley, (1967).

Hematitic alteration of sporadic distribution has also been recognized in the Red Ledge deposit. It is characterized by diffuse veins of hematite and pervasively disseminated, amorphous clusters of moderate red hematite with minor calcite and barite. This latter assemblage commonly replaces wallrocks and fragment margins adjacent to vein fillings of maroon hematite, barite and chlorite. The hematitic alteration is in isolated patches throughout the deposit, but is especially prevalent at the top of the stockwork system and in the overlying southwest limb of stringer mineralization where it partially replaces the sulfides.

Some tuffaceous beds in the interval of strata-bound mineralization have been significantly replaced by Fe-Mg chlorite (Fig. 7). However, they are distinguishable from a chloritic exhalite by the presence of quartz-sericite replacement textures, calcite and plagioclase feldspar, and small amounts of hematite.

Major Element Chemistry

Fourteen samples were analyzed for their major element abundances to document, in preliminary fashion, the chemical variations associated with hydrothermal alteration and to infer protolith compositions. Chemical changes imposed on the rocks by hydrothermal alteration were investigated by comparing the chemistry of the Red Ledge samples with that of unaltered or weakly altered rocks. Volcanic rocks from the Hunsaker Creek formation and Fiji were selected as approximations to Red Ledge protoliths because the former represent weakly modified products of the same volcanic episode and the latter are unmetamorphosed low-K dacites from a shallow marine island arc setting with concentrations of relatively immobile major oxides (e.g. TiO_2, P_2O_5, MnO) similar to those of the QFP. The mineralogy and textures of the samples analyzed, arranged by lithologic and alteration type, are summarized in Table 1. Data for their chemistry and specific gravity are presented in Table 2, and the comparative analyses are reproduced in Table 3.

For relatively simple assemblages, the variations of certain major element oxides are primarily a function of the abundance of one or two mineral phases. In terms of the Red Ledge alteration assemblages, the oxides MgO, FeO and H_2O+ are major components of chlorite, K_2O and H_2O+ of sericite, Na_2O and CaO of plagioclase feldspar, and CaO and CO_2 of calcite. A ternary plot of the principal oxides components in chlorite, sericite, and

Table 1. Mineralogy, Alteration Assemblages and Textures of Analyzed Host Rocks, Red Ledge Deposit, Idaho

Smpl No	Field No	Phen[1]		Secondary Minerals[1]								Alt[2]	Textures[3]
		Qz	Pl	Qz+Ab	Ch	Cc	Sr	Ep	Ba	Py	Cl		
Quartz-Feldspar Porphyry													
1	RL4-79	15	20	20	10	2	18	6	--	6	3	PR	P,F,M
2	TG20-570	25	25	23	2	5	10	--	--	--	3	PR	P,V,FM
3	TG13-597	20	25	30	6	15	5	--	--	1	1	PR	P,F,V,MF
4	TG14-472	12	5	55	Tr	13	10	--	--	3	2	PR	P,F,V
5	TG3-239	22	--	45	5	--	15	--	2	2	1	SC	P,V,S,PS,M
6	TG10-259	15	--	45	Tr	Tr	30	Tr	Tr	4	1	SC	P,F,V
7	TG17-182	20	--	50	5	--	15	2	--	7	--	SC	P,S,PS,M
8	RL72-141[4]	20	--	45	--	--	30	--	1	3	--	S	P,V
Felsic Tuff													
9	TG2-1519	--	--	55	--	--	25	--	2	7	--	SR	F,V,S
Intermediate Tuff													
10	TG1-1494	--	--	50	8	7	25	1	--	2	1	PR	M
Mafic Flows													
11	RL2-81	--	12	15	20	35	10	--	--	--	4	PR	V,A,PS,M
12	TG10-1761	--	--	55	10	25	3	--	--	--	5	PR	A,V,FM
Chloritized Tuff													
13	TG9-1332	--	--	5	25	--	50	--	Tr	--	10		FM
Exhalative													
14	RL5-79	--	--	15	60	--	--	--	10	--	--		FM
Cordwood Rhyolite													
15	TG19-622	--	5	65	--	20	7	--	--	--	1	PR	P,F,V

Notes: 1. Modal estimates in volume percent exclusive of veins; Phen-phenocrysts (partially altered quartz and andesine); Secondary minerals from left to right: quartz+albite, chlorite, calcite, sericite, epidote group, barite, pyrite, clay; minor accessories include: rutile, zircon, hematite; 2. Alt-alteration facies: PR-propylitic, SC-sericite-chlorite, SR-sericitic; S-silicified; 3. P-porphyritic; F-weakly foliated; A-amygdules of calcite, chlorite, quartz; V-veins of quartz+/-carbonate+/-gypsum, calcite, chlorite, sericite; S-minor shearing; PS-pressure shadows of sericite or quartz around quartz phenocrysts and pyrite cubes; M:Mg chlorite, MF:Mg-Fe chlorite, FM:Fe-Mg chlorite; 4. sample collected by R. C. Long;

Table 2. Major, Minor and Trace Element Composition of Host Rocks, Red Ledge Deposit, Idaho

	Quartz-Feldspar Porphyry							
Smpl No:	1	2	3	4	5	6	7	8[2]
SiO2 %	67.2	68.7	71.4	66.7	70.9	68.8	73.2	80.82
TiO2	0.50	0.39	0.39	0.37	0.49	0.50	0.39	0.34
Al2O3	15.3	13.4	12.4	11.7	15.3	16.5	12.2	9.85
Fe2O3	1.93	1.20	0.36	2.01	1.77	1.77	4.55	2.41
FeO[1]	2.25	1.64	2.00	1.14	0.92	0.36	0.20	0.34
MnO	<0.02	0.19	0.08	0.12	0.02	<0.02	<0.02	tr
MgO	3.22	0.84	1.22	1.29	2.66	3.35	1.24	0.07
CaO	3.51	3.32	3.05	4.87	0.20	0.34	0.23	0.10
Na2O	1.90	3.95	3.94	1.65	0.34	0.58	0.28	0.41
K2O	1.32	1.63	0.90	2.27	3.34	2.70	2.45	1.74
P2O5	0.1	0.09	0.08	0.09	0.12	0.09	0.09	0.07
H2O+	2.40	1.25	1.42	1.30	2.74	3.25	2.01	2.94
H2O-	0.17	0.10	0.09	0.13	0.27	0.46	0.20	0.45
CO2	0.26	2.88	2.21	5.42	0.03	<0.01	<0.01	----
Total	100.07	99.58	99.54	99.06	99.10	98.72	97.06	99.54
Li (ppm)	27	32	13	<4	<4	8	<4	
Ba	617	446	190	460	454	607	5000	
Rb	17	25	13	31	50	38	32	
Sr	237	138	101	88	21	61	61	
Sc	9	8	8	7	9	9	7	
Y	22	24	21	23	26	29	18	
Zr	201	169	177	175	213	246	173	
V	53	46	32	41	47	44	36	
Nb	6	6	7	6	7	6	6	
Mo	<4	<4	<4	6	<4	5	<4	
Cr	14	9	4	4	4	4	3	
Co	7	5	5	9	6	7	5	
Ni	<4	5	4	<4	<4	<4	<4	
Cu	23	27	48	23	290	36	170	
Zn	70	50	50	<40	120	150	50	
Pb	20	10	<8	8	<8	15	<8	
Ga	17	12	16	16	19	15	14	
As	<20	<20	<20	<20	<20	<20	<20	
La	15	12	12	9	14	8	<4	
Ce	26	18	23	14	29	15	<8	
Nd	16	12	18	14	19	10	9	
Dy	<8	<8	<8	<8	<8	<8	<8	
Yb	<2	<2	<2	<2	<2	<2	<2	
SG	2.73	2.69	2.68	2.72	2.74	2.70	2.75	2.62

Table 2. (continued)

	Felsic Tuff	Interm Tuff	Mafic flows		Chtd Tuff	Exhal	Cordwood Rhyol
Smpl No:	9	10	11	12	13	14	15
SiO2 %	72.6	60.4	45.4	49.9	35.9	26.9	74.3
TiO2	0.89	1.00	1.17	1.91	2.52	0.65	0.21
Al2O3	14.5	17.9	18.1	14.7	30.0	15.7	13.1
Fe2O3	3.43	2.68	1.12	1.1	1.5	16.8	0.65
FeO[1]	0.02	2.58	7.28	10.9	11.8	23.3	0.61
MnO	<0.02	0.13	0.17	0.21	0.07	0.09	0.07
MgO	0.12	3.48	8.55	4.16	4.09	3.64	0.86
CaO	0.24	0.96	4.61	4.99	0.81	0.17	1.49
Na2O	0.63	0.27	2.62	0.42	1.97	0.16	3.45
K2O	3.15	3.93	0.87	1.24	2.32	0.03	2.23
P2O5	0.18	0.23	0.23	0.22	0.43	0.21	0.08
H2O+	1.86	3.68	5.76	5.01	7.08	7.30	0.95
H2O-	0.19	0.13	0.19	0.18	0.42	0.07	0.07
CO2	<0.01	1.02	3.16	4.98	0.09	0.01	1.91
Total	97.83	98.39	99.23	99.92	99.00	95.03	99.98
Li (ppm)	<4	<4	53	57	59	58	<4
Ba	1280	1700	1310	1570	3990	>23500	216
Rb	35	60	16	19	41	34	25
Sr	149	41	134	48	256	762	100
Sc	8	23	36	45	60	7	<4
Y	18	40	21	31	33	9	30
Zr	166	124	90	104	158	119	140
V	69	210	280	450	540	92	5
Nb	7	10	9	8	12	5	9
Mo	6	6	<4	<4	<4	12	<4
Cr	<2	28	470	11	480	11	<2
Co	18	25	37	38	31	130	<2
Ni	<4	7	150	15	92	28	<4
Cu	66	54	52	17	7	29	<2
Zn	<40	60	60	100	<40	<40	<40
Pb	15	9	18	29	57	10	<8
Ga	15	20	23	19	32	<8	15
As	<20	30	<20	<20	20	<20	<20
La	<4	<4	8	6	7	4	18
Ce	<8	<8	16	<8	12	10	35
Nd	<8	13	10	<8	12	13	28
Dy	<8	<8	<8	<8	<8	10	<8
Yb	<2	<2	<2	2	3	<2	<2
SG	2.73	2.81	2.69	2.78	2.92	3.24	2.69

Table 2. (continued)

Notes: See Table 1 for field numbers and petrography. SG=specific gravity; 1. FeO determined by wet chemical methods, all other major elements and Ba, Rb, Sr, Y, Zr and Nb by X-ray fluorescence spectroscopy. All other trace elements were by Induction Coupled Plasma (ICP). The following trace elements were below ICP detection limits: Ag(4), Au(20), Be(2), Bi(20), Cd(4), Sn(8), Ta(80), Th(8), U(200), Pr(20), Eu(4), Tb(40), Ho(8), and Er(8). Analyses performed at Branch of Analytical Chemistry, U.S. Geological Survey, Lakewood, CO and Reston, VA. 2. From Long (1975).

Table 3. Average Chemical Composition of Selected Volcanic Rocks

	TB	SP	QK	LKD	BA	GD	GR
SiO2 (%)	50.83	54.27	72.6	75.8			
TiO2	2.03	1.56	0.56	0.36			
Al2O3	14.07	15.0	13.4	13.0			
Fe2O3	2.88	3.76	1.69	0.13			
FeO	9.06	5.66	1.75	1.86			
MnO	0.18	0.19	0.04	0.04			
MgO	6.3	4.54	0.33	0.34			
CaO	10.42	3.71	0.84	2.4			
Na2O	2.23	5.03	5.94	4.5			
K2O	0.82	0.15	0.48	0.86			
P2O5	0.23	0.30	0.13	0.11			
H2O+	--	2.95	0.77	--			
CO2	--	0.54	0.52	--			
Others	0.91	--	--	--			
Li (ppm)		--	--	--	10	25	30
Ba		75	30	117	250	500	600
Sr		250	20	100	465	450	285
Sc		50	5	8	38	10	5
Y		23	20	43	25	30	40
V		125	7	4	250	100	20
Nb		--	--	--	20	20	20
Mo		--	--	--	1	1	2
Cr		152	2	3	200	20	4
Co		25	--	<5	50	10	1
Ni		150	--	<5	150	20	0.5
Cu		40	1	6	100	30	10
Zn		--	--	--	100	60	40
Pb		--	--	2.5	5	15	20
Ga		--	--	--	12	18	18
As		--	--	--	2	2	1.5
La		--	--	--	11	36	5
Ce		--	--	--	35	40	46
Nd		--	--	--	26	18	26
Dy		--	--	--	3	3	0.5
Yb		--	--	--	1	4	0.01

****

TB-tholeiitic basalt (Nockolds et al., 1978, Table 12.1, p.128, av. of 137). Sp-Permian spilite, Hells Canyon, Oregon and Idaho (Vallier and Batiza, 1978, Table 4, av. of 7 for major and 2 for minor elements). QK-Permian quartz-keratophyre, Hells Canyon, Oregon and Idaho (ibid, Table 2, av. of 2 for majors; 1 analysis for minors). LKD-low-K dacite, Mathuandrove Supergroup, Fiji (Gill and Stork, 1979, Table 1, >68% SiO2, av. of 7). BA-basalt, GD-granodiorite, GR-granite (Levinson, 1974, Table 2-1). 1. Calculated by method of Irvine and Baragar (1971) from total iron.

feldspar+calcite (the latter two are generally coextensive), as portrayed by Figure 9, readily distinguishes the different alteration assemblages and rock types. A progression through the propylitic, sericite-chlorite, sericitic, and silicified alteration zones in felsic rocks of the footwall corresponds to a relatively marked decrease in Na_2O, CaO and CO_2. This trend is accompanied first by a possible enrichment in MgO and FeO at constant K_2O, then K_2O enrichment at constant MgO+FeO, and finally K_2O enrichment and depletion of MgO and FeO. The intensely chloritic rocks (samples 13 & 14) within the interval of strata-bound mineralization are notable for their extreme mafic composition. Figure 9 also implies that the propylitized mafic flow rocks are chemically similar to tholeiitic basalt and Hells Canyon spilite, and that the propylitized QFP resembles Hells Canyon quartz-keratophyre and low-K dacite from Fiji.

A consideration of absolute oxide concentrations provides a convenient means of evaluating the transfer of elements between alteration zones and a more accurate analysis of chemical trends and contrasts than relative plots. This technique is generally based on the assumption of the maintenance of constant volume or concentration of one or more relatively immobile elements, usually Al_2O_3 or TiO_2. In this investigation, oxide gains and losses were assessed for the quartz-feldspar porphyry (with the single exception of a felsic tuff). The preservation of pseudomorphic textures in some intensely altered specimens shows that volume appreciably after hydrothermal alteration. The average oxide concentrations of the

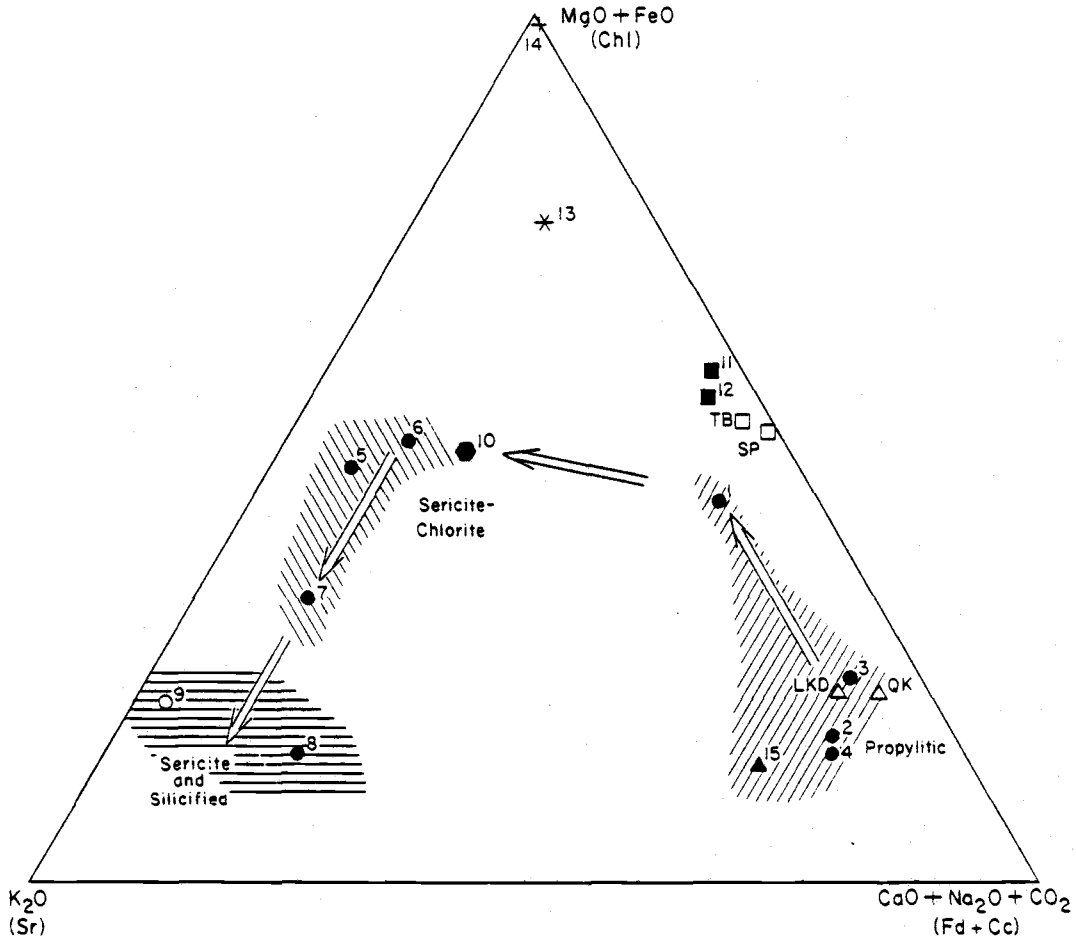

Figure 9. MgO+FeO - CaO+Na_2O+CO_2 - K_2O plot of hydrothermally altered rocks from the Red Ledge deposit and selected volcanic rocks (refer to Tables 2 and 3 for sample numbers and abbreviations). Arrows depict relative chemical variations with increasing alteration grade. normalized (H_2O^- free) data in weight percent;

alteration facies and changes between successively higher alteration grades are depicted in Figure 10. Some of the important chemical variations include:

1. SiO_2 progressively increases from propylitically altered QFP through silicified QFP (+274 g/1000 cm^3).

2. Al_2O_3 is enriched (+49 g/1000 cm^3) in felsic rocks of the sericite-chlorite and sericite zones, but is apparently depleted (-99 g/1000 cm^3) in silicified rocks, relative to its concentration in propylitized QFP.

3. Total Fe maintains a relatively uniform concentration in all hydrothermally altered rocks where it is apparently more abundant than in the unaltered equivalents (+32 g/1000 cm^3). However, there is a concomitant gain of Fe_2O_3 and loss of FeO up through the highest rank of alteration.

4. MgO is progressively added to the rocks up through the sericite-chlorite zone (+58.1 g/1000 cm^3) but is depleted in rocks of the sericite and silicified zones (-6.2 g/1000 cm^3) relative to its approximate concentration in the QFP protolith.

5. CaO and CO_2 vary sympathetically, showing a strong enrichment (+37 g/1000 cm^3 for CaO) in the propylitic zone and a strong depletion in the zones of more intense alteration.

6. K_2O is progressively enriched with alteration up through the rank corresponding to the sericite assemblage (+56.2 g/1000 cm^3) but is depleted with silicification. In contrast, Na_2O has been markedly depleted from all hydrothermally altered rocks.

The source of the elements added to the altered rocks and the

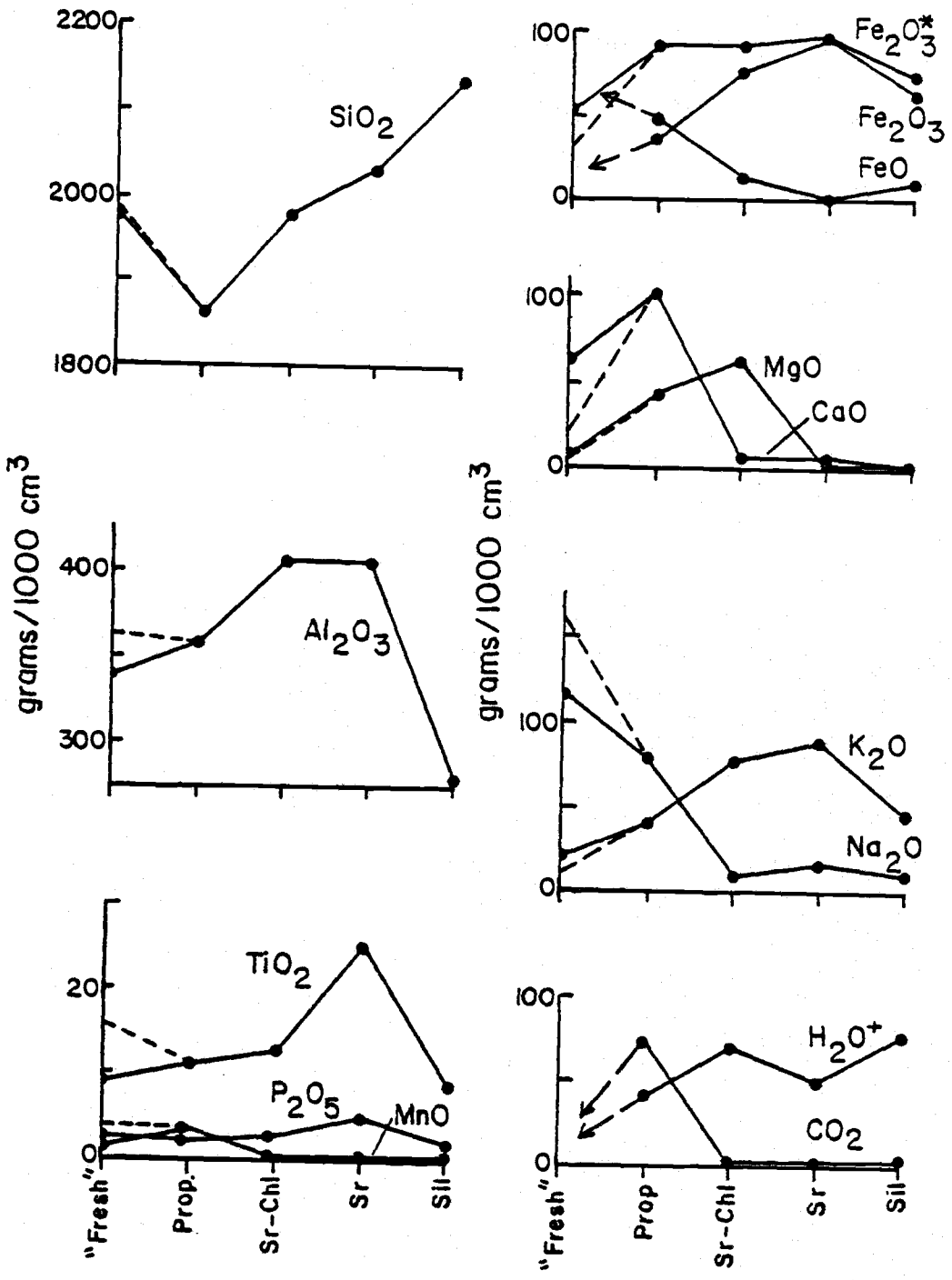

Figure 10. Absolute variations of the major oxides (in grams per 1000 cm^3) with increasing alteration grade (left to right). Fresh: assumed protoliths (low-k dacite-dashed line; quartz keratophyre-solid line); Prop: propylitic; Sr-Chl: sericite-chlorite; Sr: sericite; Sil: silicified;

fate of the depleted elements cannot, with the possible exception of CaO, be discerned from the distribution of analyzed samples. The sympathetic variation of CaO and CO_2 (Fig. 10) and the petrographic features of the altered rocks imply a loss of Ca from intensely altered rocks as a consequence of feldspar destruction and its transfer to the propylitic zone where it is fixed in calcite by aqueous carbonate of possible seawater derivation. This mechanism could explain the presence of calcite as disseminations and void-fillings, whereas the in situ fixation of Ca by aqueous carbonate during alteration within the propylitic zone can account for the calcite that replaces plagioclase feldspar.

Sources and sinks of the other major elements must be located outside of the sampled fossil hydrothermal system; either within the volcanic pile or seawater. Studies concerning experimental, natural and theoretical seawater-rock interactions indicate that Mg from seawater is added to, and SiO_2, Ca, K, Fe, Mn, Ba, Cu, Zn and Ag are generally leached from, reacted rock at temperatures ranging from less than 100 ^{o}C up to 500 ^{o}C and pressures of a few hundred bars (Mottl, 1983 and references cited therein; Reed, 1983). Sodium from seawater is added to the reacted rock at water/rock ratios of less than 5 and is leached at ratios greater than 10 (Mottl, 1983). These results suggest that greenschist, and possibly zeolite, metamorphic reactions in the predominantly mafic volcanic and volcaniclastic rocks surrounding the Red Ledge deposit provided a ready source of those elements now enriched in the hydrothermally altered host rocks and ores; except for Mg which was supplied by seawater. Sodium

leached from rocks in the vicinity of hydrothermal systems analagous to that represented by the Red Ledge deposit might be available to participate in spilitic reactions (characterized by Na metasomatism) within the volcanic pile wherever low water/rock ratios prevail.

The aforementioned variations of elements and oxides with respect to increasing alteration intensity and proximity to mineralization are similar to those reported for other volcanogenic massive sulfide deposits related to felsic igneous rocks: e.g. Kuroko deposits, Japan (Date and Tanimura, 1974; Iijima, 1974; Izawa et al., 1978; Date et al., 1983), Millenbach, Quebec (Riverin and Hodgson, 1980), Mattagami Lake, Quebec (Roberts and Reardon, 1978), Mattabi Lake, Superior (Franklin et al., 1975), Buchans, Newfoundland (Thurlow et al., 1975), Brunswick No. 12, New Brunswick (Goodfellow, 1975) and Woodlawn, New South Wales (Petersen and Lambert, 1979). The enrichment of MgO and total Fe, and the depletion of CaO and Na_2O, are the most consistent trends reported whereas other oxides exhibit more uncertain or variable behavior.

Minor and Trace Element Chemistry

Concentrations of selected minor and trace elements in rocks of the Red Ledge area are presented in Table 2. Similar analyses for samples from the Hunsaker Creek formation and Fiji, and for average igneous rocks are reproduced in Table 3 for comparative purposes. Concentrations of most elements in the least altered QFP (samples 1 & 2) are consistent with average values in comparable igneous rocks,

although the abundances of Nb, La and Ce are somewhat low. Concentrations of certain elements in QFP vary with intensity of alteration: Li, Sr and Cr markedly decrease, Pb, Ni, La, Ce and Nd slightly decrease, and Ba, Rb, Cu, Zn and possibly Mo erratically increase inward through the propylitic, sericite-chlorite and sericite zones. However, Sc, Y, Zr, V, Nb, Co and Ga abundances remain constant through the same interval and presumably were unaffected by hydrothermal alteration. The sample of Cordwood Rhyolite is depleted in most of the minor and trace elements relative to comparably altered QFP (and unaltered equivalents), except for a slight enrichment in the LREEs La, Ce, and Nd. The enrichment of the these elements may represent a primary effect that is related to more advanced magmatic differentiation. The chemistry of the Cordwood Rhyolite resembles that of the analyzed quartz-keratophyre from the Hunsaker Creek Formation (Table 3) with respect to most minor element concentrations.

The samples of mafic flow rocks show appreciable differences in the concentrations of Sr, V, Cr and Ni. The mafic rocks are depleted in Sr, highly enriched in Ba, and contain approximately equivalent concentrations of Sc, Y, Zr, Nb, Co, Ga and La relative to basalt. Those samples that have been intensely chloritized are anomalously enriched in Ba as a consequence of hydrothermally introduced barite.

Protolith Compositions

Because most of the major oxides in the host rocks to the Red Ledge deposit were mobilized during hydrothermal alteration, chemical analyses of these altered rocks are unsuited for determinations of protolith composition or magma series. Even the least altered samples yield inconsistent results according to the classification scheme of Irvine and Baragar (1971) for weakly modified and unaltered rocks. For example, the samples of propylitized QFP were variously classified as tholeiitic or calc-alkalic, and andesite or dacite according to their scheme.

Nevertheless, it was previously noted that SiO_2, TiO_2, Zr, Nb and Y, and a few other elements and oxides, were either immobile or slightly mobile during alteration. The SiO_2 content of QFP exhibits a minor variance (+/- 6%) between successive alteration zones that presumably is related to its overwhelming abundance. Thus, as a first approximation, it may be utilized for estimating protolith compositions of propylitized rocks. Accordingly, the mafic flows (av. 47.7% SiO_2) represent altered basalts, the QFP (av. 68.5% SiO_2) altered dacite and the Cordwood Rhyolite (av. 74.3% SiO_2) altered rhyolite. A plot of Zr/TiO_2 and Nb/Y ratios of all the volcanic rocks on the discrimination diagram of Winchester and Floyd (1977), given by Figure 11, supports these conclusions, except for the Cordwood Rhyolite, which falls in the dacite-rhyodacite field at a slightly higher differentiation index (Zr/TiO_2) than QFP. These ratios

Figure 11. A) Zr/TiO_2-Nb/Y discrimination diagram for volcanic rocks (after Winchester and Floyd, 1977) depicting protolith composition of QFP and mafic flows. B) Ti-Zr and Ti/100-Zr-Yx3 plots (after Pearce and Cann, 1973) depicting inferred tectonic setting of mafic flows. Ti-Zr diagram: A is island arc, low-k tholeiite (LKT); B is LKT, ocean floor basalt (OFB) and island arc calc-alkali basalt (CAB); C is CAB; D is ocean island or continental basalt;

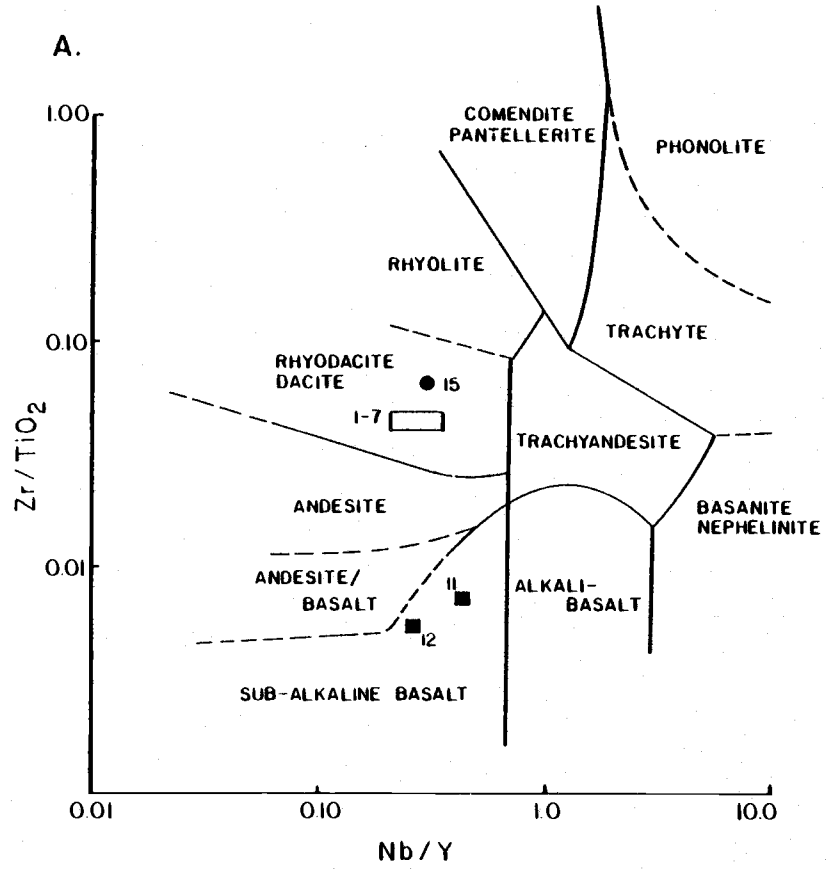
A.
1.00
0.10
0.01
Zr / TiO2
COMENDITE
PANTELLERITE
PHONOLITE
RHYOLITE
TRACHYTE
RHYODACITE
DACITE
15
1-7
TRACHYANDESITE
ANDESITE
BASANITE
NEPHELINITE
ANDESITE/
BASALT
11
ALKALI-
BASALT
12
SUB-ALKALINE BASALT
0.01
0.10
1.0
10.0
Nb / Y

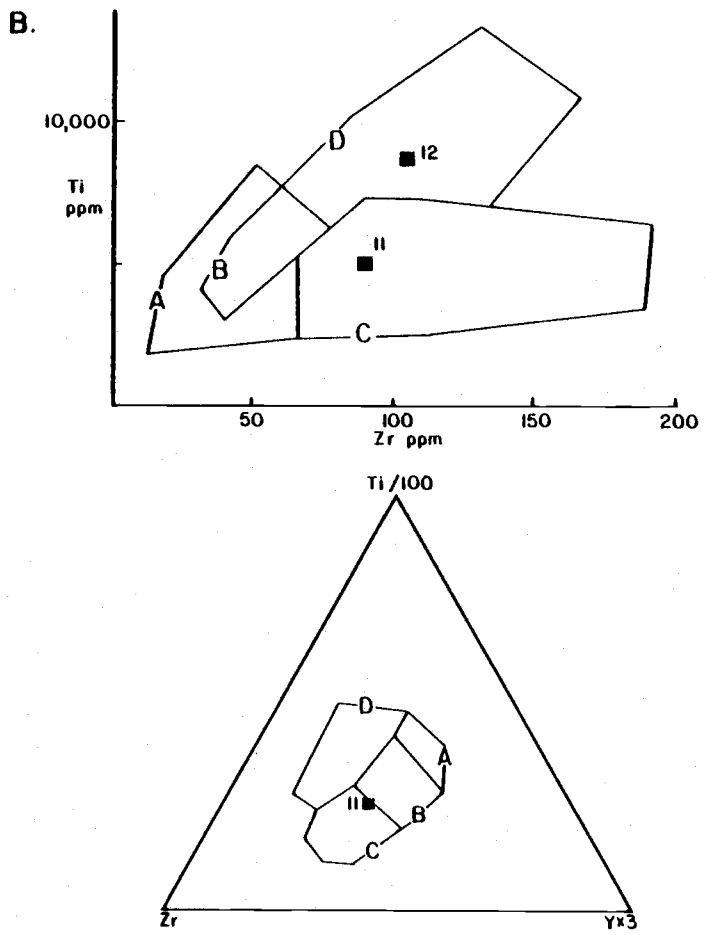
B.
10,000
Ti
ppm
D
12
11
B
A
C
50
100
150
200
Zr ppm
Ti /100
D
A
11
B
C
Zr
Yx3

Figure 11.

also indicate that the Red Ledge suite is subalkaline, but they do not distinguish between members of the tholeiitic and calc-alkalic series (Winchester and Floyd, 1977). However, the concentrations of some immobile trace elements in QFP (i.e. La, Ce, V and Cr) more closely resemble those of calc-alkalic dacites than island arc tholeiitic dacites (see Jakes and White, 1972, Table 2B). Additionally, one sample of the mafic flows (number 11) is classified as a calc-alkalic basalt on the Ti-Zr-Y discrimination diagram of Pearce and Cann (1973), whereas the other sample (number 12) apparently exhibits an ocean floor basalt affinity (Fig. 11). The preliminary petrogenetic work of Vallier and Batiza (1978) and Sarewitz (1983) indicate the presence of both calc-alkalic and tholeiitic (low-K) volcanic rocks in the Seven Devils Group, which according to the criteria of Jakes and White (1971), implies a relatively high stratigraphic level in a mature island arc.

Mineralization

Geology and Mineralogy

The Red Ledge deposit consists geometrically of a large mushroom-shaped zone of mineralization that formed through the cyclic deposition of epigenetic and syngenetic sulfides. Mineralization is almost exclusively hosted by, and genetically related to, the felsic rocks. The strata-bound "cap" of the deposit is comprised of stringer and massive sulfide lenses, whereas the "stalk" is composed of a zone of stockwork feeder mineralization (Fig. 5). Folding has rotated the deposit approximately 90 degrees such that the strata-bound cap dips steeply and the stockwork zone is essentially horizontal. Overall, the mineralization types, mineralogy, zonations, and metal abundances and ratios closely resemble those of the unmetamorphosed Kuroko deposits in Japan.

The wedge-shaped stockwork system is exceptionally large for this class of deposit. Drill hole data indicate that it crosscuts 370 meters (1200 feet) of stratigraphic section, is about 370 meters long, and averages 150 meters (500 feet) in width (Texasgulf, Inc., unpub. data). The subsurface data have not delineated its ultimate dimensions. This style of mineralization is localized along the margin of the Red Ledge intrusion in QP breccia, felsic tuff and, to a lesser extent, the QFP phase of the intrusion. It consists of discrete zones of anastomosing veins and veinlets that are separated by relatively barren wedges of rock. Three to four prominent

en-echelon, northwest-striking zones, up to 45 meters (150 feet) thick, form the base of the stockwork system but tend to branch and expand upward resulting in a greater density of narrower vein structures at higher levels.

Vein mineralization primarily consists of pyrite and chalcopyrite in a gangue of quartz, as illustrated in Figure 12. Other vein minerals include dolomite, barite, sphalerite, sericite, chlorite, gypsum, anhydrite, and calcite. These phases show a distinct stratigraphic and lateral zonation within the feeder system (Juhas and Gallagher, 1981). Pyrite is the dominant sulfide at depths greater than approximately 240 meters (790 feet) below the contemporaneous seafloor (measured from the stratigraphically lowest massive sulfide or sedimentary unit), whereas chalcopyrite generally predominates for several hundred feet above this level. Sphalerite is sporadically distributed to depths of about 300 meters (985 feet) but is most abundant in the upper portion of the stockwork zone and in veins cutting strata-bound mineralization. It is commonly associated wtih pyrite and chalcopyrite, and locally with minor galena and tetrahedrite. Barite is generally coextensive with sphalerite in veins and is locally abundant in the upper peripheral areas of the stockwork zone as a replacement of felsic rocks. Gypsum-bearing veins, with or without associated sulfides, range vertically from immediately below the sulfide cap to the hangingwall section. However, traces of anhydrite are restricted to veins crosscutting stringer mineralization. Barren quartz, quartz-dolomite, and quartz-dolomite-calcite veins are common in the

Figure 12. Pyrite-chalcopyrite mineralization of the stockwork feeder system.

hangingwall sequence, and within and peripheral to the stockwork zone in the footwall section.

The zone of strata-bound mineralization is generally lenticular, measuring approximately 120 meters thick at the center, 460 meters wide, and greater than 610 meters long (Texasgulf, Inc., unpub. data). It is centered over and aligned with the stockwork zone. The strata-bound zone is composed of three to four stacked blankets of stringer mineralization and intervening massive sulfide layers, tuffs, flows and fine-grained sedimentary rocks. These silicate rocks are weakly to moderately pyritized and variably altered. The base of the stratigraphically lowest or earliest mineralization blanket is gradational into and indistinguishable from the top portion of the stockwork zone.

Stringer mineralization, as used in this investigation and shown in Figure 13A, refers to stringers, blebs and disseminations of fine- to medium-grained sulfides that infill and partially replace the coarse-grained felsic volcaniclastic units. Hence, it is strata-bound but epigenetic. Such mineralization is comprised of moderate amounts of microcrystalline quartz, 10-20% barite, 10-35% pyrite, trace-10% sphalerite, trace-5% chalcopyrite, 0-1% galena, and less than 1% tetrahedrite (Texasgulf, Inc., unpub. data). Mineralization and intense quartz-sericite-barite-pyrite alteration have obscured many primary features of the host rocks. Nonetheless, the discernible clasts are commonly subangular to subrounded, 0.5 to 3 cm in diameter, and consist of QFP, QP and FS rock types. Veinlets confined to individual clasts indicate multiple episodes of

A.

B.

Figure 13. A. Pyrite-(chalcopyrite)-quartz-barite stringer mineralization hosted by felsic volcaniclastic rocks; B. Massive mineralization: granular pyrite-quartz (left); interlayered pyrite-barite and hematite-barite-chlorite (center); laminated sphalerite-pyrite-galena-barite with exotic clasts of chert (jasper) and pyritic mineralization;

fracturing and mineralization. A relatively late period of brecciation is conspicuous because the voids were filled by a maroon hematite-barite-chlorite assemblage, and the wallrocks are variably altered to an admixture of bright red hematite-barite-calcite. The inclusion of hematitically altered clasts in the lenses of massive sulfides records even later fracturing events.

Lenses and pods of massive sulfide generally overlie and flank major intervals of stringer mineralization. In plan view they are circular, lobate, and horseshoe-shaped, and up to 550 meters in diameter and 25 meters in thickness. However, their average dimensions are appreciably smaller (Texasgulf, Inc., unpub. data). Four principal units of massive sulfide, stacked in the center of the strata-bound cap, are recognized in addition to several smaller occurrences. The principal types of massive sulfide mineralization are illustrated in Figure 13B. Their mineralogy includes variable proportions of pyrite, sphalerite, chalcopyrite, barite, and quartz in association with subordinate amounts of galena, tetrahedrite and chlorite. Ratios of barite/quartz and sphalerite/chalcopyrite tend to be higher in peripheral massive sulfide beds than in those located over the center of the stockwork zone. Moreover, galena and chlorite are more abundant in peripheral lenses. Proximal units typically exhibit coarse-grained granular aggregates of pyrite (Fig. 13), indicative of recrystallization in a higher temperature environment (Rye et al., 1984), whereas distal beds are finely laminated and contain sparse angular clasts of massive pyrite or jasperoidal chert (Fig. 13B). The deflection of laminations around these clasts

suggest that previously formed and consolidated hydrothermal deposits were susceptible to repeated deformation. Indeed, these fragments of chert and a few intercepts of chert in drill core represent the only evidence for the development of siliceous iron formation (or tetsusekei horizon in the Kuroko ores) in the Red Ledge deposit.

Minor, restricted occurrences of exhalites other than deposits of massive sulfide include lenses of massive barite with minor finely disseminated pyrite, and thin, massive, finely laminated layers of hematite-barite-chlorite interbedded with massive pyrite-barite (Fig. 13B). The laminations, sharp interdigitated contacts, and absence of quartz boxworks indicate that the hematitic assemblage is of exhalative origin rather than the result of seafloor oxidation or recent weathering. It is the syngenetic counterpart to the void-filling hematitic assemblage previously mentioned. Although generally sparse, galena is commonly concentrated near these hematite-sulfide boundaries. Furthermore, rocks characterized by approximately 60% Fe-Mg chlorite and 10-15% each of hematite, barite and quartz possibly represent a distal silicate facies of the iron oxide layers. Spatial and paragenetic relationships indicate that the hematite event was an integral part of the hydrothermal cycle and that the mineralogical differences between the hematitic and sulfide assemblages imply episodic changes in the fugacity of sulfur (as implied by fig. 6 in Barton et al., 1977).

The massive sulfide bodies are overlain, underlain, or laterally contiguous with tuffs and flows of intermediate composition and fine-grained volcanic wackes. The rocks, although unmineralized, are

variably altered to propylitic, sericite-chlorite-clay, and intensely chloritized assemblages. They represent periods of quiescent felsic volcanism, when massive sulfide deposition was likely to occur, and they are part of three to four repetitive cycles of volcanism-mineralization-sedimentation within the interval of strata-bound mineralization (Juhas and Gallagher, 1981). A generalized cycle of mineralization begins with the deposition of felsic volcaniclastic rocks, followed by stringer and massive sulfide mineralization, and is culminated with the deposition of volcanic and epiclastic rocks. However, massive sulfide sedimentation was sporadic and was occassionally preceded by or penecontemporaneous with the deposition of clastic rocks. Moreover, each cycle of strata-bound mineralization may coincide with a distinct episode of fracturing as expressed by the three or four en echelon vein zones in the stockwork system (Juhas and Gallagher, 1981).

Mineral Paragenesis

The paragenetic order of mineral deposition in veins of the stockwork system is relatively constant throughout the Red Ledge deposit. It is based on crosscutting relationships and sequences of crustification deduced from the minerals contained in veins and vugs, as illustrated in Figure 14, and determined from both megascopic and microscopic scales of observation. Because the individual samples portray but a few periods of mineral deposition, the paragenetic scheme presented in Figure 15 was, of necessity, constructed by

A.

B.

Figure 14. Paragenetic relationships of vein minerals observed in drill core samples. A. Sulfide veinlets crosscutting amethyst and white quartz. B. White quartz vein with medial cavity filled successively by clear quartz druse and orange dolomite.

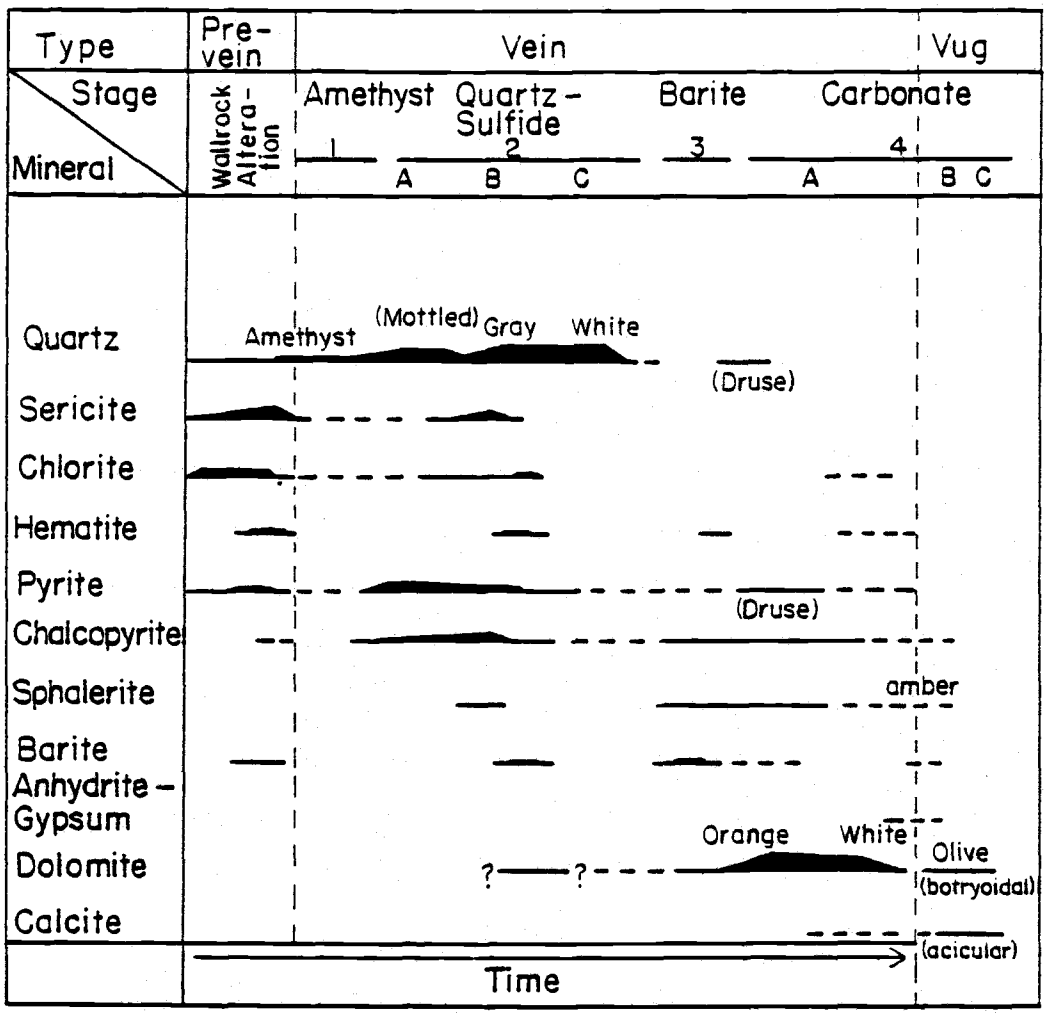

Figure 15. Paragenesis of vein (stages 1-4) and alteration minerals in the stockwork system.

correlating like minerals and assemblages of consistent temporal position throughout the stockwork zone. The assumptions implicit in this method treat contemporaneous but dissimilar mineral assemblages (i.e. spatial variations) as having been precipitated during different intervals. However, the consistency of depositional sequences from widely separate locations suggest that this effect is minimal.

The limited abundance and (or) distribution of vein sericite, chlorite, anhydrite and gypsum made it difficult to establish their precise paragenetic position and range. By contrast, determining the specific timing for much of the ubiquitous orange dolomite was difficult because of its apparent wide range, a general lack of associated coeval phases, and the paucity of barite which typically precedes dolomite formation.

Zones of pervasive alteration and pyritization are arranged about areas of abundant veins, yet individual veins rarely display alteration selvages. Furthermore, most early veins are typified by irregular, diffuse contacts with silicified or sericitized wallrocks, whereas intermediate and late veins exhibit straight, sharp vein walls. These features suggest that early quartz-sulfide veins formed concomitantly with wallrock alteration-replacement, but by the time of later vein deposition, the rocks had essentially acheived thermal and chemical equilibrium with the hydrothermal fluids.

In general, the paragenesis of the Red Ledge stockwork mineralization (Fig. 15) indicates that most of the pyrite and chalcopyrite were deposited early, followed successively by abundant

quartz, minor barite-sphalerite, and late carbonate-sphalerite. Quartz, volumetrically the most abundant vein mineral, varies from amethyst of stage 1, to finely crystalline mottled white and gray of stage 2A, to translucent gray of stage 2B, to moderately crystalline white and opaque of stage 2C, and finally to a sporadically distributed druse. In detail, the paragenesis is divided into three types, pre-vein, vein, and vug fillings, and into four stages (Fig. 15) of which the specific features are described as follows:

Stage 1. Amethyst: Amethyst forms the cores to relatively large (0.5 tO 2.0 cm) quartz clots embedded in altered rocks or later mineralization. These cores progressively grade outward to alternating zones of white opaque quartz and amethyst followed solely by white quartz. In thin section, the white quartz is distinguished from the amethyst by a greater abundance of fluid inclusions, which are commonly less than 2-3 microns in size, and unidentified solid inclusions.

Stage 2. Quartz-Sulfide: Pyrite and chalcopyrite, in amounts ranging from 10 to 80% of the vein constituents, are present as granular aggregates in mottled white and gray quartz (2A) and as crosscutting stringers associated with sericite, gray quartz and sporadic chlorite (2B). Invariably, the chalcopyrite is texturally later than pyrite, infilling and replacing pyrite aggregates and crosscutting crystals as veinlets with matching walls. White opaque quartz of stage 2C is more coarsely crystalline and vuggy than its earlier counterparts but it is associated with less than 5% sulfides and, rarely, dolomite.

Stage 3. Barite: Barite occurs as veinlets and as a crustification formed by prismatic crystals up to 6 mm long in white quartz of stages 2B and 2C. It is occassionally associated with minor amounts of sphalerite, pyrite, chalcopyrite, and dolomite.

Stage 4. Carbonate: Pink to orange dolomite (4A) infills the medial part of veins that are lined with quartz and barite crystals, and is also present as euhedral crystals in vugs. Coeval sulfides comprise less than 5% of the vein material, and pyrite is typically euhedral. This early event (4A) is followed by the deposition of botryoidal masses and euhedral aggregates of olive brown dolomite (4B) in vugs. Radiating clusters of acicular calcite (4C) crystals cap all other vug minerals and coat narrow fractures.

The mineral paragenesis of strata-bound mineralization is similar to that of vein mineralization. Invariably, pyrite is the earliest sulfide, and quartz the first-formed gangue mineral. Quartz, where present, is commonly associated with pyrite but it temporally overlaps and supersedes pyrite deposition. Other sulfides and barite crosscut, marginally replace, and fill the interstices between subrounded, embayed aggregates and networks of pyrite. The deposition of chalcopyrite appears to precede and partially overlap that of sphalerite, which in turn, exhibits the same relationship to barite. Galena and tetrahedrite, and sericite and chlorite, are minor coeval associates of sphalerite and barite, respectively. Carbonate, a major vein phase, is absent in strata-bound mineralization.

Metal Grades and Variations

Concentrations and variations of copper are primarily a function of the distribution of chalcopyrite. Overall, it shows a marked decrease upward and outward from the center of the stockwork system. Zones of abundant veins near the center of the system (150 to 250 meters below the paleo-seafloor) average about 1% Cu, although intercepts of 2-4% Cu are not uncommon, whereas those near the top and margins of the system average about 0.6-0.7% Cu. Strata-bound mineralization (stringer and massive) averages appproximately 0.6% Cu and locally reaches 6-7% Cu over appreciable thicknesses of the massive sulfide lenses. Copper is most concentrated in the central portion of the strata-bound mineralization, and near the present topographic surface (Juhas and Gallagher, 1981). The latter concentration is partly caused by the sporadic development of supergene oxide and sulfide-enriched zones at depths up to 60 meters below the surface (Livingston and Laney, 1920; Long, 1975). These are characterized by azurite, malachite, chrysacolla and chalcanthite, and chalcocite, covellite and bornite, respectively.

The distribution of zinc is directily related to that of sphalerite and increases upward through the deposit. Mineralized intercepts average less than 0.05% Zn in the lower portion of the stockwork system, 0.1-0.2% Zn in the middle portion, about 0.6% Zn in the upper portion, and over 1.0% Zn in the strata-bound mineralization. Some sections through massive sulfide lenses average 6-7% Zn. The maximum concentrations of zinc within the strata-bound

mineralization surround a central region of lower values, and they generally reflect the distribution of massive sulfide bodies (Juhas and Gallagher, 1981).

Deposit-wide variations in the concentration of silver correspond to those of zinc, although neither silver minerals nor native silver were identified and preliminary microprobe analyses indicate that silver is not a significant constituent of sphalerite. Much of the silver in strata-bound mineralization may be contained in tetrahedrite. Silver averages approximately 0.2-0.4 oz/ton in the stockwork zone and over 1.0 oz/ton in the strata-bound zone with the highest average of 5-6 oz/ton in zones of massive sulfides.

Gold averages less than 0.01 oz/ton in stockwork mineralization and about 0.02 oz/ton in strata-bound mineralization. The distribution of gold generally mimics that of copper (Juhas and Gallagher, 1981).

With respect to the entire Red Ledge deposit, concentrations of zinc, silver, and gold increase, and that of copper decreases, upward and outward, which results in a zinc-silver enriched top and a copper-rich base. Individual cycles of strata-bound mineralization show higher Zn/Cu and Ag/Au ratios near their hangingwalls, which are identical to trends in these parameters throughout the deposit. Such variations in metal distributions are similar to those of other massive sulfide deposits associated with island arc felsic volcanics (Large, 1977; and Franklin et al., 1981). However, ratios of Zn/Cu and Ag/Au decrease upward through the stacked cycles of massive sulfide layers reflecting a general, but erratic, increase in the

concentrations of copper and gold and a decrease in those of zinc and silver with time (Texasgulf Inc., unpub. data).

Metamorphism

Two episodes of regional metamorphism overprinted the host rocks and ore minerals of the Red Ledge deposit. The younger episode represents the last major thermal event to affect the area prior to uplift and exposure in Late Tertiary time. The older episode commenced with deposition of the Lower Permian System and the formation of the Red Ledge deposit, and it probably culminated in Late Triassic to Early Jurassic time with the intrusion of numerous small plutons. Moreover, it is probable that diagenetic and metamorphic water-rock reactions during the older episode contributed many of the components to the convecting fluids and, ultimately, the mineral deposit (as previously discussed). Upon cessation of ore formation and subsequent burial, the deposit experienced maximum metamorphic conditions consistent with the greenschist facies. The presence of actinolite as an accessory phase, the absence of biotite in basaltic rocks of the Seven Devils Group (Vallier and Batiza, 1978), and the application of pertinent experimental work involving amphibole-bearing assemblages (Liou et al., 1974; Winkler, 1976; Mottl and Holland, 1978) to natural systems, indicate that peak temperatures were 400 to 450 °C and maximum pressures were 4kb. In this environment, the high temperature assemblages (>250 °C) of the Red Ledge deposit were stable whereas those inferred to be of the low temperature zeolite- and clay-bearing assemblages were converted to minerals of the greenschist metamorphic facies. A weak foliation and increase in grain size was imparted to the rocks during this

metamorphic event, particularly those with abundant hydrothermal chlorite and sericite. Metamorphism also imposed the addition of Na_2O, H_2O and CO_2 to most rocks in the Seven Devils Group and caused the mobilization of other elements (Vallier and Batiza, 1978). However, because of the stability of most mineral phases and the depleted concentrations of some highly mobile elements (e.g. Na_2O, CaO and CO_2), the compositions of intensely altered and mineralized rocks in the Red Ledge area were not greatly modified.

Paleomagnetic data from the region record a subsequent widespread but sporadically distributed thermochemical event associated with voluminous plutonism of Late Jurassic and Early Cretaceous age (Hillhouse et al., 1982). A diorite intrusion of this magmatic episode, the Deep Creek stock, is situated 3.5 miles southeast of the Red Ledge deposit. Samples of biotite from the Deep Creek intrusion have been dated by the K-Ar method at 117+/-4 and 121 m.y., whereas samples of comagmatic hornblende have been dated at 127 and 137+/-4 m.y. (White, 1973; Armstrong et al., 1977). These K-Ar dates are essentially identical to one of 125+/-5 m.y. for sericite (whole rock determination) from the Red Ledge deposit, as reported by Long (1975). The similarity of these dates suggest that temperatures in the Red Ledge deposit exceeded approximately 320 °C, or the blocking temperature for Ar in muscovite (L.W. Snee, 1984, pers. comm.), during this last major thermal event.

Fluid Inclusions

The results of a preliminary investigation of the petrographic features, thermometric properties, and hydrogen isotopic composition of fluid inclusions in vein minerals are presented and discussed in this chapter. The purpose of this study was to establish the depositional temperatures of the host minerals, the thermal history of the deposit, and the range and variations in the salinity of the mineralizing fluids. However, the record of primary fluid inclusions in the Red Ledge deposit has been obscured and partially destroyed by subsequent thermal and tectonic events related to regional metamorphism. As a result, the fluid inclusion data variably reflect the effects of these secondary processes.

Petrography

The milky white, fractured quartz of stages 2A through 2C contain abundant fluid and solid inclusions that impart a turbid appearance to the quartz when viewed in thin section. By contrast, the cores of some stage 1 or 2A quartz crystals, the terminations to quartz crystals projecting into vugs, and randomly dispersed aggregates of quartz are relatively clear and free of inclusions. The first (1 and 2A crystals) and second (terminations) occurrences represent early and late stages of hydrothermal quartz deposition, respectively, whereas the third (dispersed aggregates) type is a product of metamorphic recrystallization. The domains of metamorphic quartz locally disrupt trails of secondary inclusions or growth bands

which implies that the inclusion arrays were locally destroyed during the recrystallization process.

The fluid inclusions in the Red Ledge deposit consist solely of vapor and liquid. Estimated vapor/vapor + liquid ratios range from 0.05 to 0.30, as indicated by the data listed in Table 4. The majority of the fluid inclusions in vein quartz are less than 3 microns in their longest dimension and are commonly concentrated in distinct planes of both inter- and intragranular distribution. Inclusions of the intergranular set are clearly of secondary origin and represent fluids trapped after the deposition of the host crystal. Those of the intragranular set occur in randomly oriented planes that are either of secondary origin, possibly consisting of fluids trapped during metamorphic recrystallization, or of pseudosecondary origin, representing fluids trapped along fractures in the core of a crystal during the growth of its outer zones (see Roedder, 1979). However, fluid inclusions that form radiating planar arrays within discrete growth zones of stage 1 or 2A quartz are certainly of pseudosecondary origin. A minor number of the fluid inclusions in vein quartz are randomly distributed, isolated, and relatively large; ranging from 5 to 20 microns in their greatest dimension (Table 4). These are tentatively considered primary inclusions, or fluids trapped during the growth of their enclosing host. Primary inclusions exhibit both subrounded geometric and asymmetric forms (Table 4). Many display narrow protuberances which is suggestive of a "necking down" process resulting from the dissolution-reprecipitation of the host mineral (Roedder, 1979).

Table 4. Petrography and Homogenization Temperatures of Fluid Inclusions in Vein Minerals

Sample No.	Host/Stage	Type*	Form	Max. Dim (μ)	V/V+L	T_h °C
TG1-831	Dol 4A	P	ovoid	5	0.20	265
"	Dol 4A	P	ovoid	5	0.25	292
TG3-939-A	Qz 1	S	cylindroid	10	0.15	221
"	Qz 1	P	ovoid	5	?	264
TG3-939-B	Qz 1	S	irregular	8	0.10	134
"	Qz 2A	P	ovoid	5	0.10	104
TG3-939-C	Qz 1	S	ovoid	6	0.10	134
"	Qz 1	S	spheroid	7	0.10	107
"	Qz 1	P	cylindroid	9	0.10	120
"	Qz 1	S	spheroid	12	0.05	119
"	Qz 1	S	cylindroid	15	0.05	120
"	Qz 1	S	cylindroid	12	0.05	114
"	Qz 1	S	irregular	10	0.05	130
"	Qz 1	P	ovoid	20	0.20	256
"	Qz 1	P	cylindroid	10	0.15	270
"	Qz 1	P	ovoid	10	0.15	277
"	Qz 1	P	irregular	12	0.15	275
"	Qz 1	P	ovoid	5	0.25	185
"	Qz 1	P	ovoid	6	0.20	189
TG16-415-B	Qz 2C	S	cylindroid	7	0.15	169
"	Qz 2C	S	irregular	10	0.15	164
"	Qz 2C	P	spheroid	5	0.30	270
"	Qz 2C	P	cylindroid	8	0.25	270
"	Qz 2C	P	ovoid	5	0.10	160
"	Qz 2C	P	cylindroid	12	?	298

****

*Type of inclusion: P = primary; S = secondary;

Fluid inclusions in dolomite and anhydrite are typically subangular in cross section, tending towards negative crystal habits, and are concentrated along cleavage planes. In contrast, those in barite are of subrounded or irregular form and randomly distributed. Although these characteristics are not clearly diagnostic of either a primary or secondary origin, it is well-known that carbonates and sulfates are relatively susceptible to recrystallization during metamorphism, and thus the preservation of primary fluid inclusions in these phases may be unlikely.

Thermometric Properties

Thermometric determinations of phase transitions in the fluid inclusions were made on a gas flow heating-freezing stage that was designed by personnel at the U.S. Geological Survey. A description of this stage and a discussion of its operation, capabilities and advantages has been provided by Woods et al. (1981). The total precision for homogenization temperatures, based on the calibration of the thermocouple, control of heating rates and thermal gradients within the sample chamber, and positioning of the thermocouple, was +/- 2.0 °C . Fluid inclusion chips were either broken or cut on a low-speed wire saw from doubly polished sections of approximately 100 micron thickness.

The temperature at which the vapor phase homogenized into the fluid was measured for both secondary and primary inclusions in a few samples of vein material (Table 4). These determinations range from 104 to 298 °C and display a bimodal distribution that generally

corresponds to the type of inclusion (Figure 16). Homogenization temperatures for most secondary inclusions range between 104 and 134 °C and average 124 °C, whereas those of most primary inclusions range between 256 and 298 °C and average 274 °C. These data imply that the vein host minerals were deposited at temperatures comparable to those for ore and gangue minerals from other volcanogenic massive sulfide deposits (see Franklin et al., 1981). The determinations for secondary inclusions imply that later fluids were trapped at temperatures that averaged 150 °C lower than the depositional temperature of the host mineral.

Several attempts were made to freeze the fluid inclusions in order to ascertain the salinity of the liquid. However, ice or other solids did not form when the inclusions were maintained for several minutes at temperatures ranging between -175 and -88 °C and with gentle tapping of the stage. This phenomenon suggests that either the fluids were highly saline or unusually clean and free of solid particles (Roedder, 1963). A depression of the freezing point of a sodium chloride solution below -20.8 °C would correspond to NaCl concentrations greater than 23.3 wt. %, or the saturation limit of NaCl in the NaCl-H_2O system (Potter et al., 1978). Because neither halite nor other daughter minerals were observed in the fluid inclusions, it is unlikely that the fluid salinities were at or exceeded the saturation limit for NaCl or other salts. Rather, the salinity of the Red Ledge fluids was probably similar to that of the Kuroko fluids, or 3.5 to 6 wt. % NaCl equivalent (Pisutha-Arnond and Ohmoto, 1983). Roedder (1963) reported having to supercool some fluid inclusions for periods ranging from several hours to several days

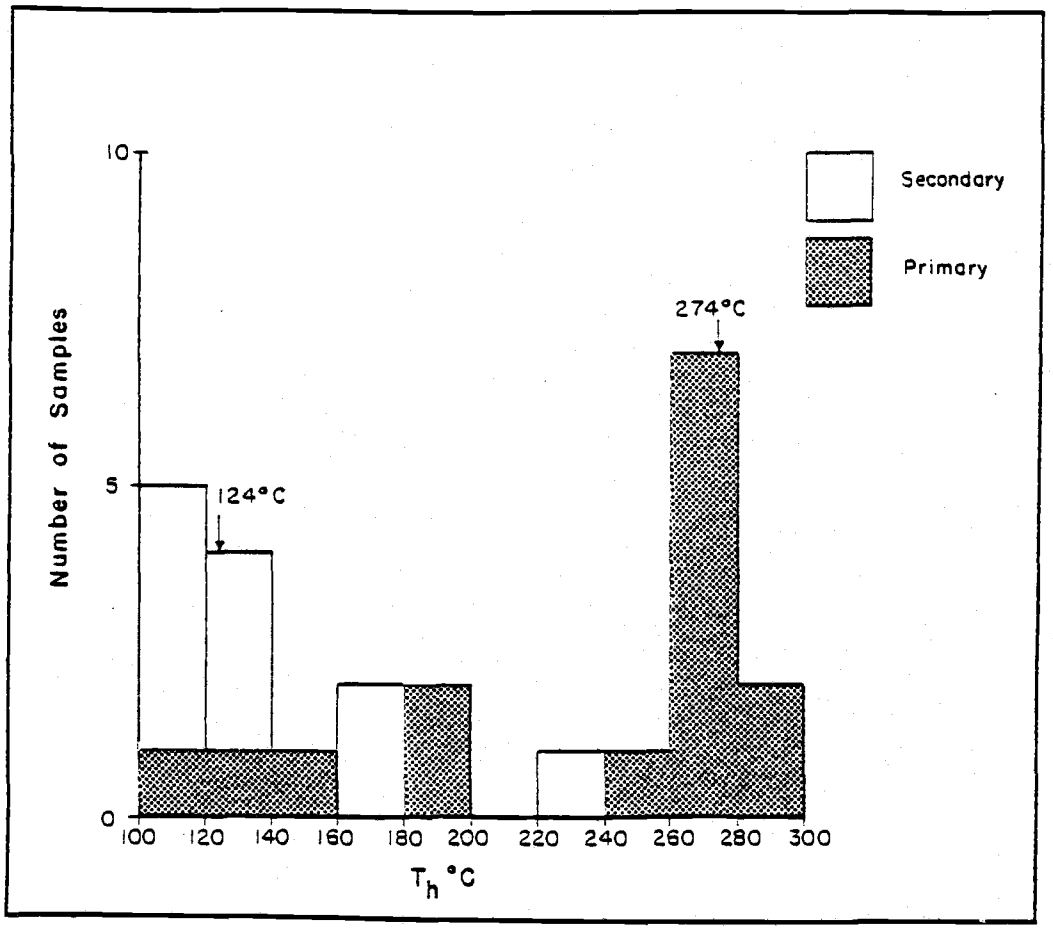

Figure 16. Histogram of vapor homogenization temperatures in fluid inclusions of vein minerals.

before the liquids would freeze. He attributed this phenomenon to a lack of suspended solids on which ice could nucleate and suggested that fluids of such high purity may have been entrapped during periods of extremely slow flow.

Hydrogen Isotopic Composition of Inclusion Fluids

The hydrogen isotopic composition of fluids extracted from vein quartz are presented in Table 5. Because the extraction method cannot specify the type of inclusion sampled, the fluids analyzed are representative of both primary and secondary varieties. Analytical precision and procedures are discussed in the following section entitled "Stable Isotope Geochemistry." The δD ratios range from -112 to -78 $^{o}/_{oo}$ and average -98 $^{o}/_{oo}$. These values essentially reflect the hydrogen isotopic composition of fluids trapped after the formation of the host mineral because the fluid inclusions in vein quartz are predominantly of secondary origin. The data indicate that these fluids are considerably depleted in ^{2}H relative to the -14 to -5 permil mineralizing fluids of the Red Ledge deposit (see subsequent discussion), the -30 to +15 permil ore fluids of the Kuroko deposits (Pisutha-Arnond and Ohmoto, 1983), and the -65 to -20 permil waters produced during regional metamorphism (Taylor, 1979). However, the hydrogen isotopic ratios of the secondary fluids are similar to those of modern meteoric water in the Red Ledge area (i.e. approximately -110 +/- 10 $^{o}/_{oo}$ according to Fig. 6.3 in Taylor, 1979).

Table 5. Hydrogen Isotopic Composition of Inclusion Fluids in Vein Quartz

Sample No.	Stage	δD ($^{o}/oo$)
TG1-682	2C	-91
TG3-939	1 + 2A	-95
TG10-259	2C	-112
TG11-115	2C	-105
TG15-808	2C	-108
TG18-261	2C	-78

Discussion of Results

Some quartz crystals in vugs exhibit a clear top and a fractured milky white base. This relationship suggests that deformation resulting in fractures took place prior to the end of hydrothermal activity. If so, the fracturing may have resulted from thermal shock caused by a sudden temperature change, abrupt pressure fluctuations produced by phreatic explosions, or mechanical stress during crystal growth caused by distortion of the vein wall. Thermal shock, in a submarine environment, could result from an influx of cold seawater or, if the deposit formed near shore, from an influx of cold meteoric groundwater that had moved laterally along aquifers from subaerial areas of recharge. Either of these alternatives is consistent with the observed homogenization temperatures of the secondary inclusions but not with the implication of highly pure fluids that resulted from slow movement. Additionally, the involvement of meteoric water might account for the apparent low salinities and depleted δD values. Fracturing by phreatic explosions and the subsequent incorporation of condensed steam in secondary inclusions is consistent with the entrapment temperatures, δD ratios, and the inferred paucity of

solids in the fluids. However, evidence for boiling is absent from the fluid inclusions, perhaps because the solutions did not boil or because the evidence was destroyed by subsequent thermal-tectonic events.

The effects of metamorphism and (or) deformation and uplift on the Red Ledge fluid inclusion record must also be considered. Features and textures exhibited by the quartz, such as undulatory extinction, sutured grain boundaries, granulation, and recrystallization domains (e.g. pressure shadows), indicate that the Red Ledge deposit was subjected to one or more metamorphic-tectonic events after its formation. Kerrich (1976) and Wilkins and Barkas (1978) have shown that intracrystalline deformation of quartz produces a decrease in the number of fluid inclusions and an increase in homogenization temperatures due to leakage. Recrystallization, in contrast to deformation, leads to the destruction of inclusion arrays in the interior of grains and a concentration of inclusions at crystal boundaries. Wilkins and Barkas (1978) have further proposed that the inclusion fluids may migrate during recrystallization by such mechanisms as leakage, attachment to dislocations which move under stress, dissolution-precipitation, and diffusion. These studies suggest the possibility that the homogenization temperatures of the primary-appearing inclusions in the Red Ledge vein minerals do not represent depositional temperatures of the host phase, but actually record a metamorphic overprint, and that many of the secondary inclusions were produced during metamorphism. Accordingly, the processes of fluid migration during recrystallization may have resulted in the formation of clean, low salinity and isotopically

fractionated fluids. Because relevant experimental data are lacking, it is difficult to assess accurately the effects of metamorphism on the Red Ledge fluid inclusions and the degree to which the inclusions may have been modified.

Finally, rapid unloading due to uplift and erosion is another potential mechanism by which quartz might be fractured and meteoric waters allowed to reach the site of the Red Ledge deposit.

In summary, the fluid inclusion record in the Red Ledge stockwork zone exhibits petrographic features that are diagnostic of both hydrothermal and metamorphic environments. Unfortunately, the evidence is unclear as to which event was largely responsible for the chemical and isotopic characteristics of the fluids. Nonetheless, homogenization temperatures between 250 and 300 °C may be representative of vein mineralization because they form a well-defined population which is distinct from that of the secondary inclusions, and because they are consistent with results from analagous deposits.

Stable Isotope Geochemistry

Sulfur, carbon, oxygen and hydrogen isotopic ratios were determined for minerals and rocks from the Red Ledge deposit and from the Seven Devils Group in Hells Canyon. The Red Ledge suite is representative of the various mineralization styles and their facies (distal vs. proximal, top vs. bottom), paragenetic stages, and alteration assemblages (including hangingwall and footwall samples) that have been recognized in the deposit. Samples analyzed from the Seven Devils Group provide a preliminary isotopic characterization of the greenschist metamorphic rocks within the region and a comparative population for the Red Ledge data. The purpose of this study was to establish the mineralization temperatures, sources of carbon and sulfur, origin of the mineralizing fluids, and role of fluid mixing in the formation of the deposit.

Analytical Procedures

The samples were prepared and analyzed at the laboratory of Robert O. Rye, U.S. Geological Survey, Branch of Isotope Geology, Lakewood, Colorado. Most of the samples analyzed were chosen from splits of diamond drill core located below the zone of oxidation. Mineral separates were typically handpicked from coarsely crushed and sieved (-20 to +60 mesh) material. If necessary, carbonate and sulfide contaminants in quartz were dissolved in boiling HNO_3 acid. Individual sulfide aggregates from fine-grained specimens were drilled out with a dental drill or, in the case of sphalerite,

converted quantitatively to H_2S by acid treatment and precipitated as Ag_2S in a AgCl solution. Gypsum that was intermixed with barite was dissolved in gently boiling 0.6N HCl and precipitated as barite with the addition of 0.1N BaCl. The majority of the minerals separated by these methods were visually estimated or, for the chemical precipitates, assumed to be pure. Up to 5% of noncritical contaminants were present in some samples. Fine-grained, pervasively disseminated, sericite and chlorite were sequentially concentrated by ultrasonic disaggregation of crushed rock, decantation, and heavy liquid separation. Diffraction patterns of X-rays indicated that these samples were 80 to 95% pure chlorite or sericite. Inclusion fluids were extracted from quartz that had been electrostatically cleaned and dried at approximately 120 °C for 24 to 36 hours. The extraction was accomplished under vacuum by crushing the host mineral in a stainless steel tube and heating the sample to 1200 °C.

Sulfide sulfur was converted to SO_2 by combustion with cupric oxide at 1025 °C (Fritz et al., 1974). Natural and synthetic barite was reduced to SO_2 in the presence of quartz powder at approximately 1200 °C (Bailey and Smith, 1972). Barite oxygen was converted to CO_2 by roasting at temperatures of 800-1100 °C in the presence of admixed graphite (Nehring et al., 1977). Oxygen was released from silicate minerals and rocks by reaction with BrF_5 at about 520 °C and then converted to CO_2 by reaction with a carbon rod at 720-780 °C (Taylor and Epstein, 1962; Clayton and Mayeda, 1963). Carbon dioxide gas was evolved from dolomite and calcite separates and from disseminated calcite in rock powder by dissolution in 100% H_3PO_4 (orthophosphoric acid) at 25 °C (McCrea, 1950). Sericite and chlorite were outgassed

for 12-18 hours at 120 °C to drive off adsorbed water and then heated to 1200 °C to extract the structurally bound water. This latter water and that from fluid inclusions was converted to H_2 over uranium metal heated to 800 °C (Freidman, 1953; Godfrey, 1962).

The SO_2 and most of the CO_2 gasses were analyzed on a modified Nuclide Corporation RMS-60, 6-inch, 60 degree magnetic sector mass spectrometer. Fourteen CO_2 gas samples were analyzed on a Finnigan MAT-251 mass spectrometer. Analyses of H_2 gasses were made on a Nuclide Corporation RMS-60, 3-inch, 60 degree magnetic sector mass spectrometer. Relevant instrumental, isotopic abundance, and reference standards corrections were routinely applied to raw analyses during computer reduction of the data.

All stable isotope analyses reported in this investigation follow conventional notation:

$$\delta A_{spl} \ (^{o}/oo) = [(R_{spl} - R_{std}) / R_{std}] \times 1000 \qquad (1)$$

where A = D (^2H or deuterium), ^{18}O, ^{13}C, and ^{34}S, in permil, and R = D/H, $^{18}O/^{16}O$, $^{13}C/^{12}C$, and $^{34}S/^{32}S$. R_{std} represents the isotopic ratio of the standard SMOW (Standard Mean Ocean Water) for hydrogen and oxygen (Craig, 1961), PDB (PeeDee Belemite) for carbon (Craig, 1957), and CDT (troilite from the Canyon Diablo meteorite) for sulfur (Ault and Jensen, 1963). Analytical precision, reported as +/- 1s, is 0.1 permil for sulfide sulfur, carbonate carbon and oxygen, and silicate oxygen; 0.2 permil for sulfate sulfur and oxygen; and 1 permil for hydrogen.

Sulfates and Sulfides

The $\delta^{34}S$ compositions of 93 sulfides and 40 sulfates from the Red Ledge deposit are presented in Table 6 and summarized in Figures 17 and 18. The sulfides range from -9.5 to -0.6 permil and are distinguishable based on the style of mineralization and stage of paragenesis (Fig. 17). Vein sulfides average -2.8 $^{o}/oo$ whereas those of stringer (-5.1 $^{o}/oo$) and massive sulfides (-5.1 $^{o}/oo$) are isotopically indistinct. Pyrite of stages 2C, 3, and 4A (-1.4 $^{o}/oo$) is enriched in ^{34}S relative to pyrite of stages 2A (-2.7 $^{o}/oo$) and 2B (-2.9 $^{o}/oo$). The $\delta^{34}S$ ratios of disseminated pyrite in intensely altered rocks range from -7.9 to -1.1 permil and average -3.3 permil.

The $\delta^{34}S$ values of the analyzed sulfates (largely barite) vary from 11.1 to 19.0 permil. Anhydrite, gypsum and barite are isotopically indistinguishable. Vein sulfates average 15.2 $^{o}/oo$ but display an isotopic distribution that is strongly skewed toward heavy values (Fig. 18B). In contrast, the $\delta^{34}S$ ratios of stringer and bedded barite (massive barite and barite in massive sulfide lenses) average 14.5 and 12.7 permil, respectively, and are more uniformly distributed. The $\delta^{18}O$ ratios of sulfates range from 6.8 to 11.2 permil, are not distinguishable based on the environment of sulfate deposition (Fig. 18A). However, the two varieties of bedded barite are apparently distinct in that massive barite is relatively depleted in ^{18}O (6.8 and 7.1 permil).

These isotopic results indicate that the Red Ledge mineralization is characterized by: 1) sulfides and sulfates anomalously depleted in ^{34}S relative to their counterparts in other volcanogenic

Table 6. Isotopic Composition of Sulfides and Sulfates

Sample No.	Min/Stage	$\delta^{34}S$ (°/oo)	$\delta^{18}O$ (°/oo)	Comments
		Vein Mineralization		
TG1-508	py, 2B	-4.2		
TG1-584	ba, 3	14.2	8.6	assoc. w/sp-gn-td-(sr);
	cp, 2A	-3.9		blebs in 2A qz;
TG1-640A	py, ?	-1.9		clast in lapilli tuff;
TG1-640B	py, 2B	-4.0		vein in lapilli tuff;
TG1-682	ba, 3	17.7	9.4	crystals in vugs of 3c qz;
	py, 2B	-3.2		
	cp, 3	-3.3		crystals in vugs of 3c qz;
TG1-726	py, 2A	-2.2		
	cp, 2A	-3.0		marginally replaced py;
TG1-755	py, 3-4A	-0.7		vug filling in 2C qz;
TG1-831	cp, 2A	-1.3		
TG1-1701	ah, 4B	17.6	8.3	after 4A dol in vug of 2C qz; cuts stringer minz;
TG1-1814	gp, 4B?	14.9	9.8	qz-gp-sp-cp vnlt in stringer minz;
TG2-259	ba, 3		10.2	vnlts cut by py vnlts;
TG2-1853	gp, ?	16.7	9.6	hangingwall vein; fibrous habit;
TG3-460	py, 2A	-3.2		assoc. w/cp;
TG3-538	py, 2A	-3.7		
	cp, 2A?	-2.8		
	cp, 2B	-3.2		
TG3-810	py, 2B	-2.3		
	cp, 2B	-2.9		replaced margins of py granules;
TG3-949	py, 2B	-3.2		1-2 mm cubes;
TG3-1003	py, 2C-4A	-0.6		cavity lining followed by 4A dol;
TG4-846A	ba, 2C-3	13.7	9.2	qz-ba-(cp) vein in hematitic wallrock;
TG4-846B	py, 4A	-1.4		dol-py vein in hematitic wallrock;
TG5-1305	py, 2B	-1.8		
	cp, 2B	-3.5		
TG5-1311	ba, 2B-C	16.1	9.8	assoc. w/py-cp-gray qz;
	py, 2B	-2.6		
	cp, 2B	-3.0		
TG8-88	cp, &2C	-4.0		crystals in vugs of 2C qz;
TG9-1409	ba, 4A?		9.8	py-cp-sp(dark)-ba-sp (amber) in vugs of 2C qz;
TG10-1107	py, 2C	-0.7		
TG10-1334	cp, 2B	-1.9		stringers in 2B qz;
TG10-1678	ba, 3	14.2	8.7	crystals in vug of 2C qz which cuts massive minz;

Table 6. (continued)

TG10-1761	gp, 4A		10.1	qz-cal-gp veins in mafic flow;
TG11-599	py, 2A	-2.9		
TG11-994	py, 2A	-2.0		locally replaced by cp;
TG11-1837	gp, 4B-C	13.7	10.5	vug deposition after 4A dol;
TG14-1731	py, 2C	-0.6		cubic habit;
TG15-808	py, 3-4A	-3.2		vug filling; coexisting w/ba, dol, sp, cp;
	sp, 3-4A	-4.1		inclusions of cp, py, td;
	cp, 3-4A	-6.1		after py, sp, gn;
TG16-415	ba, 2B-C?	14.1	9.8	vug and fracture filling in 2A qz;
	py, 2A	-2.1		
	cp, 2A	-2.8		
	ba, 3	19.0	8.7	cavity filling in 2C qz;
	cp, 3-4A	-3.0		deposited in 2C qz vugs;
TG16-1483	ba, 3	14.0	9.2	vug deposition in 2C qz;
TG17-406	ba, 3	13.6	9.1	vnlts in 2A qz;
	cp, 2B	-2.8		
TG17-563	py, 2A	-3.5		after syngenetic py sediment;
	py, 2C	-2.6		after 2A qz vein;
	cp, 2C	-4.8		after 2A qz vein;
TG17-799	cp, 2B	-4.2		
TG18-286	ba, 2B-C	14.6	10.1	vnlts in 2A qz, cut by 2C qz;
	py, 3-4A	-1.1		vug filling in 2C qz, overlaps 4A dol. deposition;
	cp, 3-4A	-2.4		same as above;
TG18-331	py, 2B	-2.7		
	cp, 2B	-3.5		after 2B py;
	ba, 3	14.3	10.2	crystals in 2C qz, followed by 4A dol;
	py, 2C	-1.4		hosted by 2C qz;
	cp, 2C	-3.6		same as above;
TG18-722	py, 2A	-1.8		
H4-220	ba, 3	14.1	7.8	followed by 4A dol-sp-py;
	gp, 3		8.8	intermixed w/ba;
H4-360	ba, 3		9.9	in 2C qz vugs, followed by 4A dol;
SS105-310				
360A	py, 2B	-2.3		
	cp, 2B	-2.7		
SS151-200*	py	-3.5		
	sp	-5.0		
SS151-715*	py	-2.6		
	cp	-2.5		

Disseminated Mineralization

TG3-239	py	-3.6	QFP, SC;
TG7-408	py	-1.6	sr-ch-cly interm. tuff;
TG11-1816	py	-2.6	qz-sr-py felsic tuff;

Table 6. (continued)

TG14-472	py	-3.2		QFP, PR;
TG17-182	py	-7.9		QFP, SC;
RL72-96	py	-1.1		
		Stringer Mineralization		
TG1-1741	py	-6.6		
	sp	-5.3		assoc. w/disseminated ba;
	cp	-5.7		surrounds and infills py;
TG1-1742	ba	15.1	8.3	ba-(py) cement;
TG1-1788	ba	14.4		py-sr stringers;
TG2-130	ba	15.4	7.9	
	py	-6.9		
TG4-1086	sp	-5.4		
TG4-1129	ba	13.8	8.7	after qz-py;
TG6-751	ba	14.9	9.9	w/sp blebs;
	py	-2.0		
TG7-45	ba	12.6	10.6	clot;
TG7-220	ba	14.4	8.3	
	py	-3.9		w/qz, before cp;
TG8-88	ba	14.6	7.8	
TG9-1341	py	-2.2		in silicified rk, followed by hm;
TG9-1471	ba	15.9	11.2	clot;
	py	-5.9		
TG9-1624	py	-4.5		stringers in felsic tuff;
TG10-1787	ba	13.4	7.3	
TG14-2050	py	-4.7		py band;
TG16-1386	py	-9.5		
TG16-1407	py	-4.1		
	sp	-5.4		
	cp	-4.8		in aggregates after py;
TG18-923	py	-1.5		
RLC2-700-800A	py	-5.3		
RLC2-700-800B	ba	14.5	9.7	
	py	-8.1		
		Massive Mineralization		
TG1-1895	py	-4.4		py-sp-(cp)-qz-ba;
	sp	-3.6		assoc. w/ba;
	cp	-4.4		
TG4-838	ba	12.1	10.2	w/sp after py-sp-qz;
	py	-5.1		
TG7-161	ba	14.0	7.1	massive w/finely dissem. py;
TG9-1247	ba	12.7	8.5	ba-py-sp-(gn) and hm-ba-ch layers;
TG10-1697	ba	13.3	9.7	qz-ba-(py);
TG10-1758	py	-4.4		py-ba-sp-cp w/qz clast;

Table 6. (continued)

TG12-1428	ba	12.3	9.3	
TG12-1438	py	-4.1		sp-ba-py-gn w/jasper clast;
	sp	-2.7		
	gn	-4.2		
TG12-1440	ba	12.5	9.1	laminated sp-ba-py;
TG15-873	ba	11.1	9.2	distal; ba-sp-py-chl-sr;
TG16-1433	py	-5.2		
TG16-1599	py	-9.0		py-qz-(sr);
TG17-563	py	-4.7		footwall; py sediment;
RL1	ba	13.0	6.8	
RL2800	ba	13.1	9.6	py-qz-ba-cp-(sp);
	py	-5.5		
	sp	-4.2		
RLUT	ba	12.9	10.0	
	sp	-6.6		
RLM-2*	py	-6.5		
RLM-1*	cp	-6.5		

****

* Data from R. C. Long (1975).

Abbreviations: ah-anhydrite; ba-barite; cal-calcite; ch-chlorite; cly-clay; cp-chalcopyrite; dol-dolomite; gp-gypsum; gn-galena; hm-hematite; minz-mineralization; PR-propylitic alteration; qz-quartz; SC-sericite-chlorite alteration; sp-sphalerite; sr-sericite; td-tetrahedrite; vnlt-veinlet;

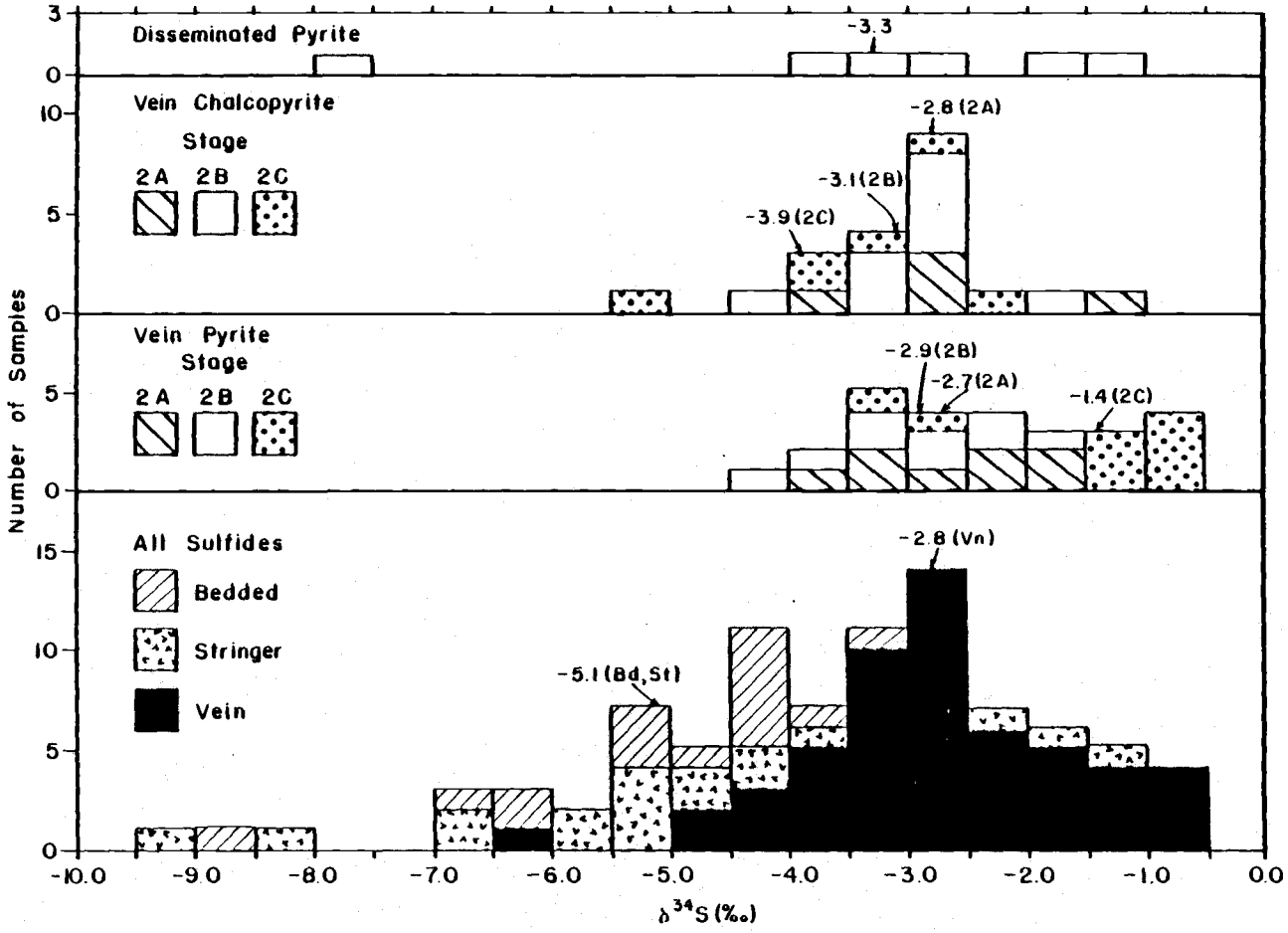

Figure 17. Histograms of sulfide $\delta^{34}S$ ratios for the principal types of mineralization and paragenetic stages.

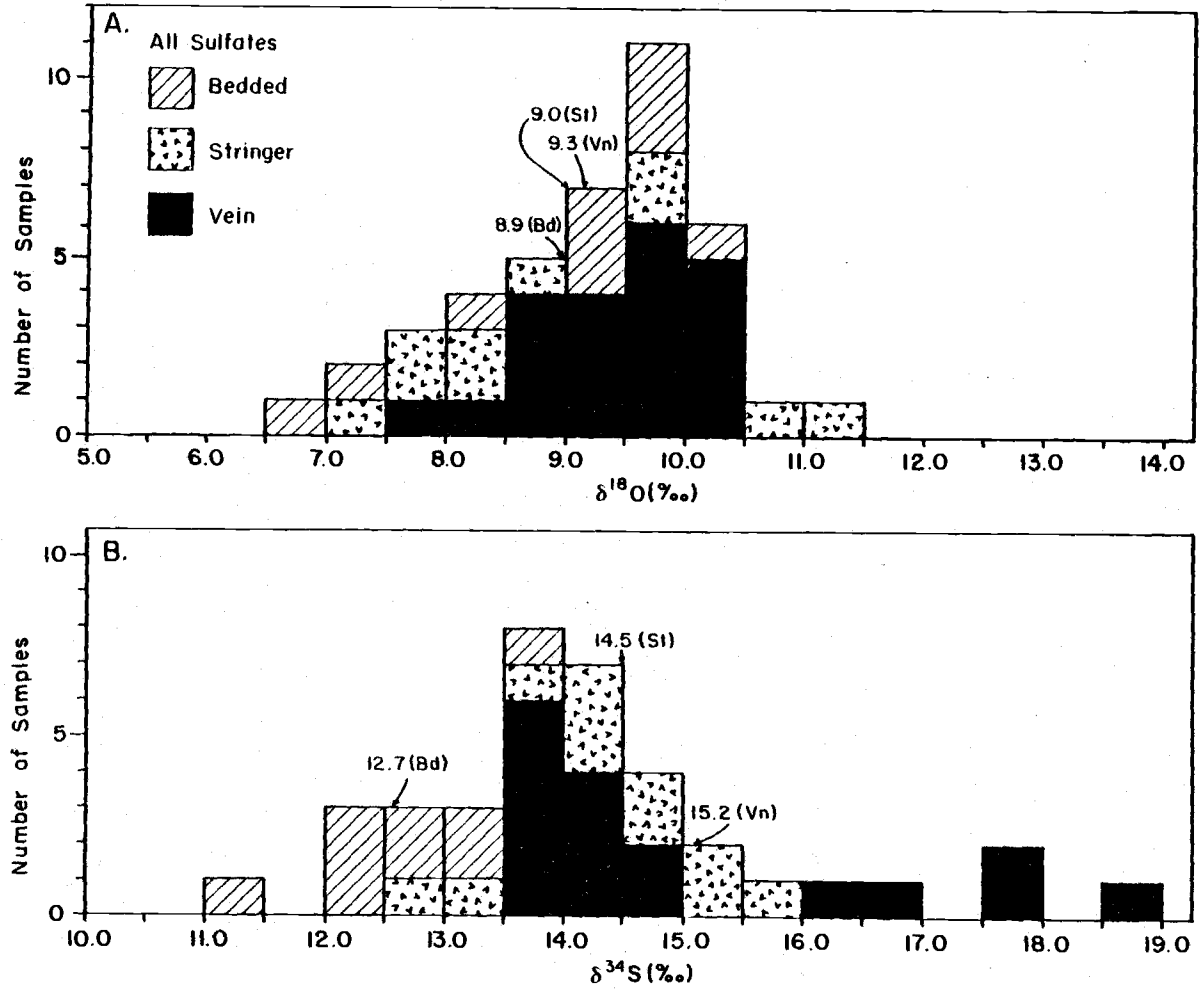

Figure 18. Histograms of oxygen (A) and sulfur (B) isotopic composition of sulfate from vein, stringer, and massive mineralization.

massive sulfide deposits (e.g. see Ohmoto and Rye, 1979, Fig. 10.13; and Franklin et al., 1981, Fig. 73); 2) an abrupt decrease in the $\delta^{34}S$ composition of both sulfides and sulfates at or near the paleo-seafloor; and 3) an increase in the $\delta^{34}S$ of vein pyrite during the latter stages of vein deposition. The spatial and temporal variations (2 and 3) are discussed in the following sections, whereas an interpretation of the anomalous range of $\delta^{34}S$ values is presented in a later section concerned with "Source of Hydrothermal Sulfur".

The potential causes of the isotopic variability in the Red Ledge sulfides and sulfates can be constrained by examining two limiting cases of cooling a Red Ledge-like fluid. The first case considers the chemical and isotopic effects of cooling a hydrothermal fluid under equilibrium conditions and by mechanisms other than fluid mixing. This equilibrium model would pertain to those Red Ledge fluids that were confined to veins and cooled adiabatically or by conductive heat loss during their ascent through the conduit system. The second case involves the effects of mixing hydrothermal fluids and seawater with and without the attainment of chemical and isotopic equilibrium. This nonequilibrium model would apply to mixing above the vent orofice, within permeable volcaniclastics around the vent, and possibly in the upper portion of the conduit system.

Simple Equilibrium Cooling

The equilibrium sulfur isotopic composition of a hydrothermal sulfide or sulfate mineral is a function of fluid temperature (T), hydrogen ion activity (pH), fugacity of oxygen (fO_2), ionic strength

(I), and isotopic composition of the total sulfur in the system ($\delta^{34}S_s$) (Sakai, 1968; Ohmoto, 1972). Thus, in the case of simple equilibrium cooling, variations in any one of these parameters, except $\delta^{34}S_s$, during formation of the Red Ledge deposit might have resulted in the observed $\delta^{34}S$ variations. It is likely that the temperature of the Red Ledge fluids decreased during their ascent from deep within the stockwork zone to the seafloor. However, the magnitude of this temperature decrease may have varied markedly (10's to 100's of degrees) depending on the extent of contact with cold seawater. Moreover, the thermal history of the Red Ledge fluids was possibly similar to that of the Kuroko deposits; that is, the temperature increased rapidly, reached a maximum temperature near 325 °C, and then decreased gradually to ambient values.

The pH of the Red Ledge fluids can be estimated from the phyllic alteration assemblage that envelops the stockwork mineralization. This assemblage in felsic rocks contains abundant quartz and sericite, but lacks potassium feldspar (an assumed primary phase of the dacites and rhyolites). Therefore, the pH of the vein fluids was between an upper limit determined by the hydrolysis of potassium feldspar,

$$3KAlSi_3O_8 + {}^2H^+ = KAl_3Si_3O_{10}(OH)_2 + 6SiO_2 + K^+ \quad (2),$$

and a lower limit controlled by the hydrolysis of sericite,

$$2KAl_3Si_3O_{10}(OH)_2 + {}^2H^+ + 3H_2O = 3Al_2Si_2O_5(OH)_4 + 2K^+ \quad (3).$$

Utilizing the equilibrium constants for reactions 2 and 3 (Ohmoto, 1972), and assuming the K^+ concentration was similar to that of the Kuroko fluids, or 0.08 molal (m) (Pisutha-Arnond and Ohmoto, 1983), the pH of the Red Ledge vein fluids is calculated to have been in the range 3.8 to 5.4 at 300 °C and 4.2 to 5.7 at 250 °C.

Because barite, pyrite and chalcopyrite are constituents of the phyllic alteration assemblage, the fO_2 of the early vein fluids can be estimated from a pH-fO_2 representation of the stability fields of these and related phases, as depicted in Figure 19. At 250 °C and within the determined range of pH, this critical assemblage defines a stability field confined to log fO_2 values between -33 and -35.

Figure 19 also portrays the $\delta^{34}S$ contours for pyrite and barite based on a total sulfur concentration of 0.01 m and a $\delta^{34}S_s$ ratio of 10.5 permil. In the pH-fO_2 range of the Red Ledge fluids, both oxidized and reduced aqueous sulfur species (e.g SO_4^{--}, HSO_4^-, KSO_4^-, $NaSO_4^-$, $CaSO_4$ (aq), H_2S, and HS^-) are present in significant quantities and a small change (e.g. ~0.5 units) in pH or fO_2 causes a considerable shift (several permil) in the $\delta^{34}S$ compositions of coprecipitating sulfides and sulfates. However, variations of pH or fO_2 in the range where either oxidized or reduced sulfur species predominate produces isotopic shifts generally less than 0.5 permil. Similarly, changes of I within the range 0.5 to 3 (considered typical for ore-forming fluids) result in isotopic variations of 0.5 permil or less (Ohmoto, 1972).

The simple cooling (without mixing) of a Red Ledge-type fluid will result in a decrease in pH because of the dissociation of acid species and a decrease in fO_2 (Ohmoto et al., 1983; Reed, in

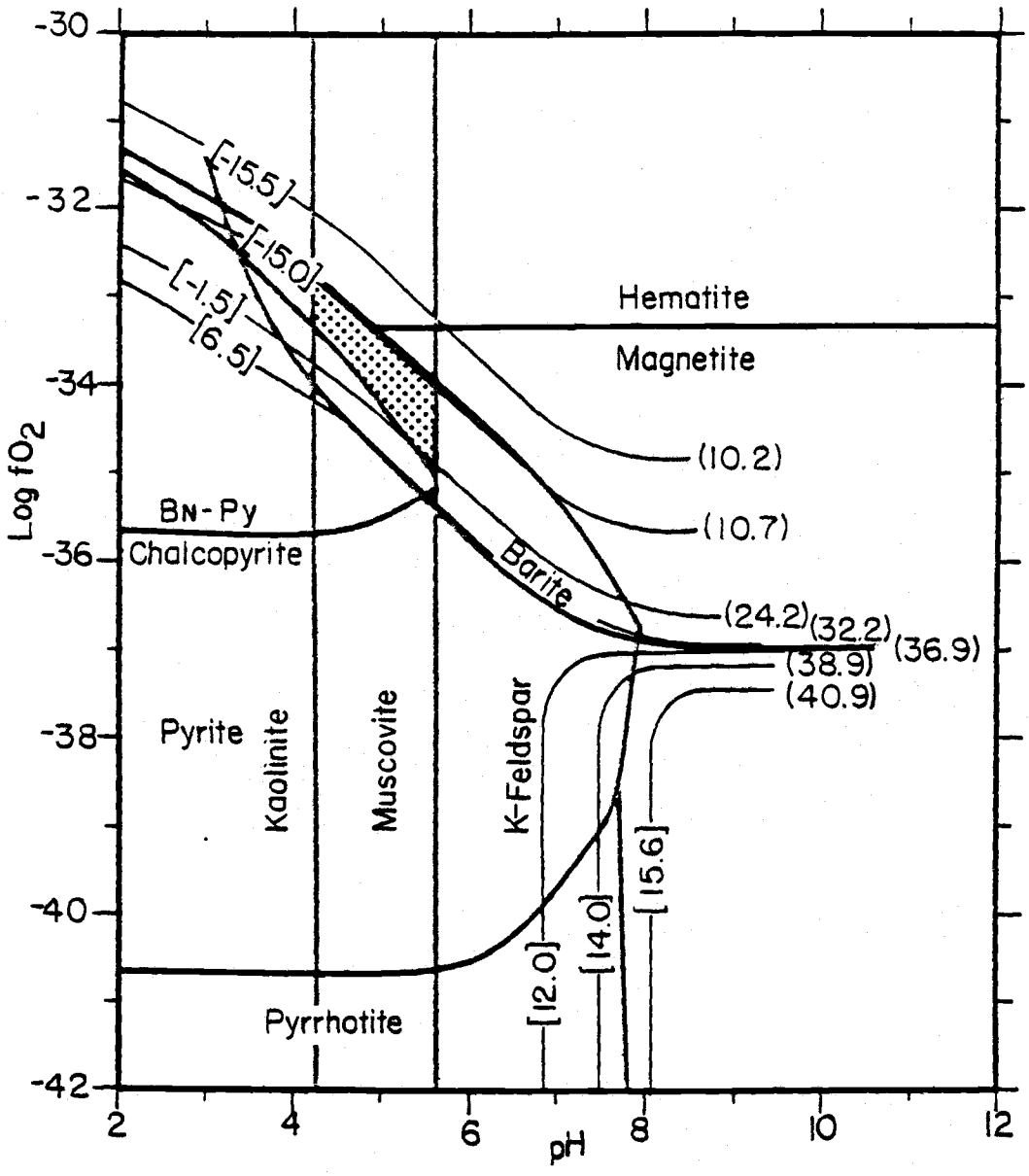

Figure 19. Log fO_2-pH diagram (modified after Rye and Ohmoto, 1974) relating the stability fields of phases potentially in equilibrium with the Red Ledge fluids to the $\delta^{34}S$ ratios of pyrite (brackets) and barite (parentheses). The stippled area represents the probable fO_2 and pH of the early vein fluids. T=250 °C; I=1; m k^+=0.08; m Ba^{++}=0.001; m ΣS=0.01; $\delta^{34}S_{\Sigma S}$=10.5 °/oo;

review.). For instance, a decrease from 300 to 200 °C causes the pH to drop by approximately 0.5 units and the fO_2 to decrease from approximately -30 to -40 log units (ibid.). A decrease in pH or fO_2, at constant temperature, produces a decrease in the total SO_4/H_2S ratio and, in turn, a sympathetic increase in the $\delta^{34}S$ values of equilibrated sulfides and sulfates (Fig 19). However, a decrease in temperature, at a constant total SO_4/H_2S ratio, produces an antipathetic trend of $\delta^{34}S$ ratios in which the sulfides become depleted in ^{34}S and the sulfates concomitantly enriched in ^{34}S. Regardless of whether T, pH, or fO_2 exerted the predominant isotopic effect, it is clear that the average 2 to 3 permil upward decrease in the $\delta^{34}S$ compositions of the Red Ledge sulfides and sulfates cannot be explained solely by the simple cooling of the hydrothermal fluid under equilibrium conditions.

By contrast, the average temporal increase in $\delta^{34}S$ of 1.5 permil for vein pyrite may have resulted from a slight increase in temperature or a decrease in pH and (or) fO_2 by approximately 0.2 to 0.4 units. Although a modest rise in temperature is possible during the period between stages 2 and 4 of pyrite deposition, it is contrary to the probable overall trend of falling temperatures during the later stages of mineralization. The initiation of wallrock chloritization and an increase in sulfide precipitation are two potential mechanisms that could cause a slight decrease in pH and (or) fO_2 and thereby result in an increase in the $\delta^{34}S$ value of vein pyrite.

Mixing of Seawater and Hydrothermal Fluids

The mixing of cold seawater and a Red Ledge-like hydrothermal fluid in the vicinity of a submarine hot springs vent can result in the precipitation of a variety of minerals because of effects such as a decrease in temperature and an increase in pH, fO_2 and total SO_4/H_2S ratio (Large, 1977; Ohmoto et al., 1983; Reed, in review.). In this section, the isotopic variations of aqueous sulfide and sulfate are modeled as a function of the extent of seawater-hydrothermal fluid mixing under conditions of equilibrium and nonequilibrium isotopic exchange. The model assumes that the isotopic effects of sulfide and sulfate mineral precipitation are negligible and that the inorganic reduction of sulfate to sulfide is insignificant because of the general lack of potential reductants in the vent environment (e.g. reduced rocks). Three hypothetical hydrothermal fluids (HF-1, HF-2, HF-3) were utilized in the model calculations. These fluids represented the potential range in temperature, concentration of sulfate and sulfide species, and isotopic composition of sulfate and total sulfur in the hydrothermal end member. Their specific temperature and composition, as well as those of seawater, are presented in Table 7, along with the equations utilized in the model. The temperature and $\delta^{18}O$ of the solution mixtures were calculated from the temperature, $\delta^{18}O$ composition, and mass fraction of the end member fluids (Table 7, eq. a and b). Using these values, the $\delta^{18}O$ ratio of the sulfate was computed by applying the pertinent sulfate-water fractionation factor. The $\delta^{34}S$ value of total sulfur in the mix was calculated as a function of the mole fractions and

Table 7. End Member Fluids and Equations Utilized in Model Calculations of Seawater-Hydrothermal Fluid Mixing

Fluids	T°C	$m\Sigma SO_4$	$\delta^{34}S_{SO_4}$	$\delta^{18}O_{SO_4}$	$m\Sigma H_2S$	$\delta^{34}S_{H_2S}$	$\delta^{34}S_S$	$\delta^{18}O_{H_2O}$
HF-1	350	0.032[1]	14.0[4]	8.3[7]	0.0250[1]	-3.2[3]	6.5[8]	5.0[6]
HF-2	300	0.010[1]	17.0[4]	9.7[7]	0.0040[1]	-3.2[3]	11.2[8]	5.0[6]
HF-3	250	0.004[1]	21.0[4]	11.4[7]	0.0005[1]	-3.2[3]	18.3[8]	5.0[6]
SW	0	0.028[2]	10.5[5]	9.0[5]	----	----	10.5[8]	0.0

Equations

(a) $T_{mix} = T_{HF}\,(1-F) + T_{SW}\,(F)$

where F = SW/(SW + HF) or the mass fraction of SW in the mixture;

(b) $\delta^{18}O_{mix} = F(\delta^{18}O_{SW}) + 1\text{-}F(\delta^{18}O_{HF})$

(c) $\delta^{34}S_{S,mix} = X_{S,SW}(\delta^{34}S_{S,SW}) + X_{S,HF}(\delta^{34}S_{S,HF})$

where $X_{S,SW} = F(m\Sigma S_{SW}) \,/\, F(m\Sigma S_{SW}) + 1\text{-}F(m\Sigma S_{HF})$,

and $X_{S,HF} = 1\text{-}F(m\Sigma S_{HF}) \,/\, 1\text{-}F(m\Sigma S_{HF}) + F(m\Sigma S_{HF})$;

(d) $\delta^{34}S_{H_2S,mix} = \delta^{34}S_{\Sigma S,mix} - \Delta_{SO_4\text{-}H_2S}(R/1+R)$

where $R = \Sigma SO_4/\Sigma H_2S$,

$\Sigma SO_4,mix = F(m\Sigma SO_4,SW) + 1\text{-}F(m\Sigma SO_4,HF)$,

and $\Sigma H_2S,mix = 1\text{-}F(m\Sigma H_2S,HF)$.

****

1. From Table 2 in Ohmoto et al., (1983);
2. Assumed equivalent to modern seawater (see Holland, 1978);
3. Approximately equivalent to average $\delta^{34}S$ value of vein chalcopyrite.
4. Calculated from SO_4 - H_2S fractionation equation given by Ohmoto and Lasaga (1981).
5. Estimated from isotopic composition of Early Permian evaporites (Claypool et al., 1980).
6. See "Hydrothermal Fluids" section of this investigation.
7. Calculated from SO_4 - H_2O fractionation equation given by Mizutani and Rafter (1969).
8. Calculated from equation 10.5 in Ohmoto and Rye (1979).

isotopic compositions of seawater and hydrothermal total sulfur (Table 11, eq. c). The sulfur isotopic compositions of the total sulfate and total sulfide species were then calculated from $\delta^{34}S_{\Sigma s,mix}$, the ratio of sulfate to sulfide species, and the appropriate fractionation factor between oxidized and reduced sulfur species (Table 7, eq. d). In the case of disequilibrium mixing, the isotopic ratios of the sulfate and sulfide species in the mix are a linear function of the mole fraction and isotopic composition of total sulfate and sulfide in the hydrothermal fluids and in seawater.

The results of these model calculations are depicted in Figure 20 as variations in the $\delta^{34}S$ ratio of aqueous sulfate and sulfide with respect to the extent of seawater-hydrothermal fluid mixing expressed as T,mix. Equilibrium $\delta^{34}S$ values of H_2S decrease dramatically from -3.2 permil to less than -46 permil with the progressive addition of seawater to the hydrothermal fluid to the extent that the final temperature of the solution is 50 °C (Fig. 20). By contrast, the equilibrium $\delta^{34}S$ ratios of the SO_4 either increase or decrease over a relatively narrow range, 11 to 22 permil, respectively, depending on whether or not the $\delta^{34}S$ composition of sulfur in seawater is greater than or less than that of the hydrothermal fluid (HF-1, and HF-2 or HF-3, resp.). The isotopic variations produced by disequilibrium mixing closely follow those resulting from equilibrium mixing, and in the case of HF-3 are essentially identical (Fig. 20). These trends are a function of mixing cold sulfate-rich and sulfide-poor seawater with a sulfate-sulfide hydrothermal fluid. The sulfur isotopic composition of the sulfide, with disequilibrium mixing,

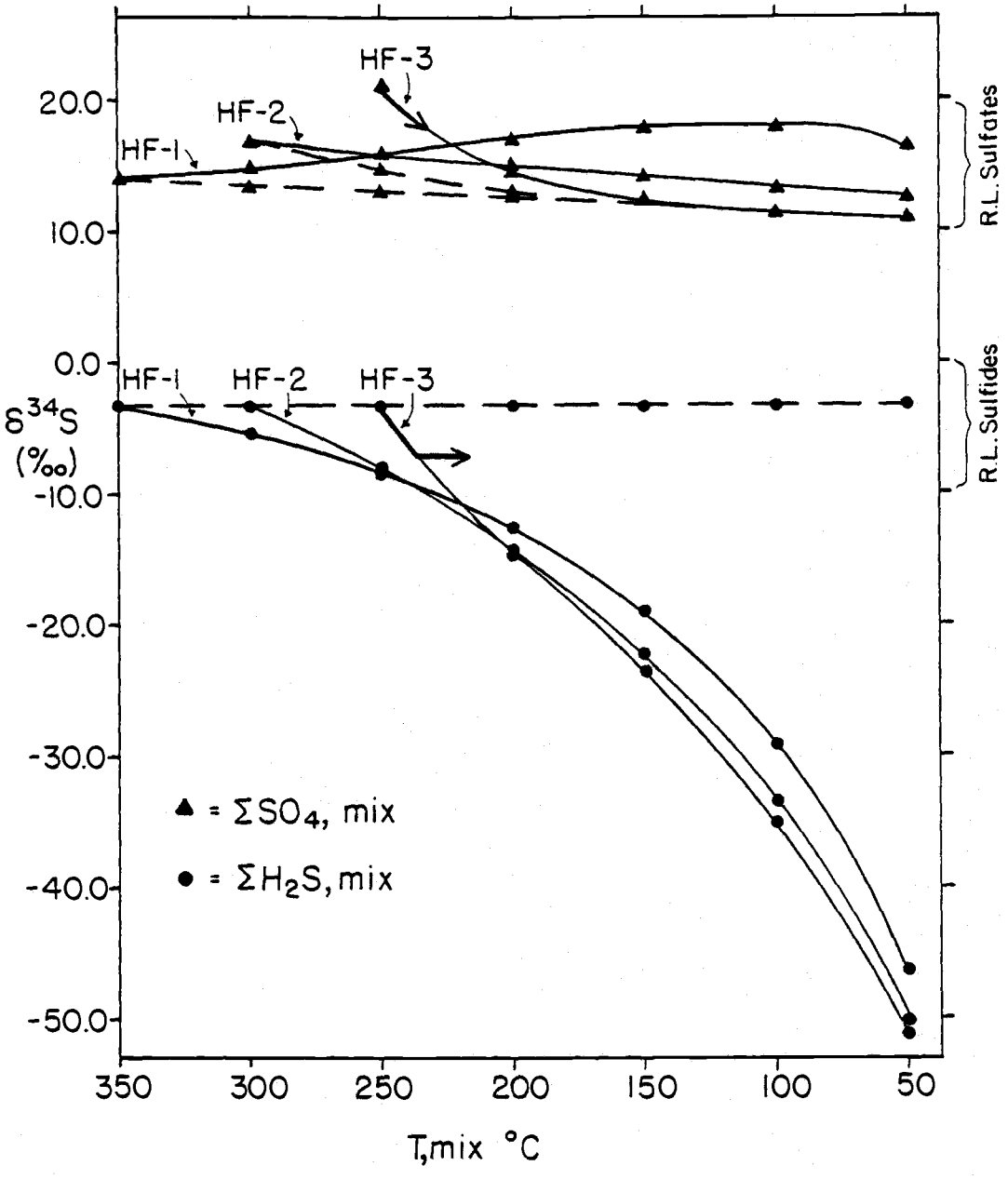

Figure 20. Variations of $\delta^{34}S$ in total aqueous sulfate (SO_4) and sulfide (H_2S) species resulting from the equilibrium (solid lines) and disequilibrium (dashed lines) mixing of seawater and three hypothetical hydrothermal fluids (HF-1, -2, -3). The extent of mixing is expressed as the temperature of the mix (T_{mix}). Probable mixing path for the Red Ledge system is shown by the arrows.

remains constant at -3.2 permil, because isotopic exchange is precluded in this model (Fig. 20).

The range of aqueous sulfide $\delta^{34}S$ values (-3.2 to -50 permil) predicted for cooling to 50 °C by seawater mixing is five times that recorded by the Red Ledge sulfides (-9.5 to -0.6 permil). This more restricted range and the average upward decrease in the sulfide mineral compositions, from -2.8 to 5.1 permil, may have been produced by equilibrium isotopic exchange accompanying the addition of only minor amounts of seawater to any of three end member hydrothermal fluids, and that with the influx of additional seawater, isotopic exchange between reduced and oxidized sulfur species essentially ceased. By contrast, the model calculations suggest that the total range of $\delta^{34}S$ ratios for the Red Ledge sulfates (11.1 to 19.0 permil) could have resulted from the mixing of seawater and HF-1 or HF-3 (but not HF-2) over a wide range of proportions and under conditions of either equilibrium or disequilibrium isotopic exchange (Fig. 20). However, the involvement of a fluid similar to HF-1 requires the mixture of large amounts of seawater (>40%) and isotopic equilibration to produce the ^{34}S-enriched sulfates (>17 $^{o}/_{oo}$). Such conditions are unlikely because a corresponding ^{34}S-depletion (<-12 permil) among sulfides has not been recorded.

The model which best fits the Red Ledge sulfate and sulfide data involves a hydrothermal fluid between 250 and 275 °C with a total SO_4/H_2S ratio of 3 to 8 and a $\delta^{34}S$ composition of total sulfur in the range 14 to 18 permil. Sulfur isotope exchange between aqueous sulfate and sulfide species may have taken place during the mixing of up to 10 percent seawater and down to temperatures of approximately

240 °C (Fig. 20) Rising hydrothermal fluids probably first encountered seawater in the permeable volcaniclastics around the vent with the result that the stringer sulfides and sulfates would have been depleted in ^{34}S by an average of 2 to 3 permil relative to their counterparts in the stockwork zone. The infusion of more than ~10 percent seawater into the hydrothermal fluid within a short distance above and below the seafloor would have caused cooling below 240 °C and thus inhibited significant isotopic exchange between sulfate and sulfide species (refer to Isotopic Equilibria). Nevertheless, the $\delta^{34}S$ composition of the total SO_4 would have continued to decrease through the addition of isotopically light seawater sulfate, but the composition of total H_2S would have remained close to the value of final equilibration because only negligible amounts of reduced sulfur were added to the mixture from seawater or from the reduction of seawater sulfate (Fig. 20).

A comparison of the sulfur and oxygen isotopic compositions of the Red Ledge sulfate minerals to those of Early Permian seawater sulfate and hydrothermal sulfate (HF-1,-2,-3) corroborates and further refines the previously described model. These data are portrayed in Figure 21, as are the curves representing equilibrium and nonequilibrium mixing between hydrothermal and seawater sulfate. The estimated composition of seawater sulfate ($\delta^{34}S$ = 10.5 $^{o}/_{oo}$, $\delta^{18}O$ = 9.0 $^{o}/_{oo}$) was derived from the isotopic composition of evaporites of Leonardian to Early Guadalupian age (both $\delta^{34}S$ and $\delta^{18}O$ = 12.0 $^{o}/_{oo}$; Holser and Kaplan, 1966; Claypool et al., 1980) by assuming the evaporitic anhydrite or gypsum was enriched by 1.5 and 3.0 permil for sulfur and oxygen, respectively, relative to the seawater sulfate at

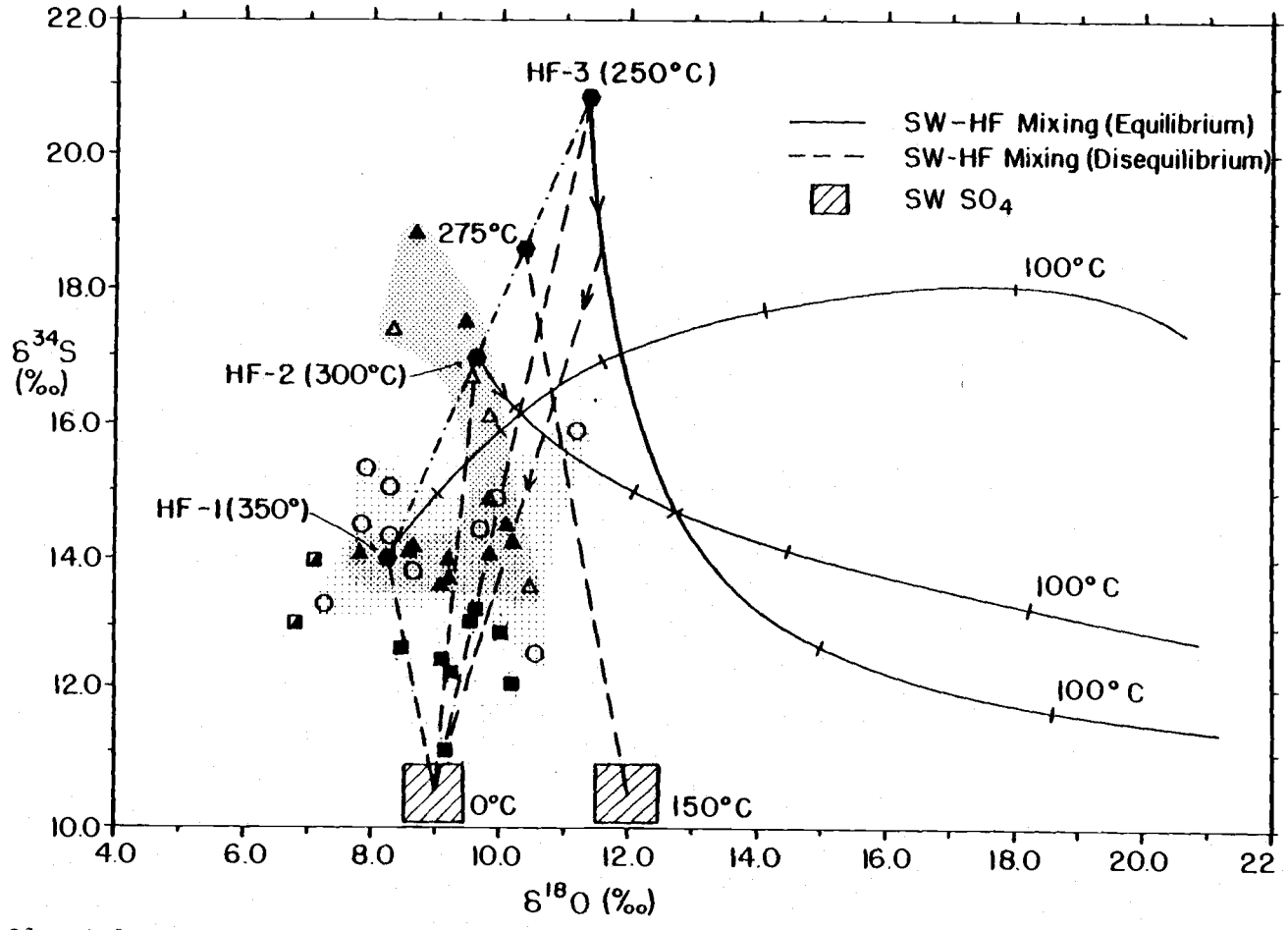

Figure 21. Sulfur and oxygen isotopic composition of the Red Ledge sulfates, seawater sulfate during Early Permian time, and hydrothermal sulfate (HF-1, -2, -3). Symbols represent: barite in massive sulfide (squares); massive barite (half filled squares); stringer barite (circles); vein barite (filled triangles); and vein anhydrite and gypsum (open triangles);

25 °C (Thode and Monster, 1965; Holser and Kaplan, 1966; Lloyd, 1968; Mizutani and Rafter, 1969; Chiba et al., 1981).

As illustrated by Figure 21, the Red Ledge sulfates from the massive sulfide lenses, massive barite lenses, and stockwork zone occupy distinct fields in terms of their sulfur and oxygen isotopic compositions. Stringer barite forms a compositional field that partially overlaps those of sulfate from the stockwork system and massive sulfide lenses. In general, these data form a spectrum between the compositions of seawater sulfate and hydrothermal sulfate that is in equilibrium with aqueous sulfide and water at temperatures between 250 and 350 °C. Furthermore, the samples plot on or near the lines representing the nonequilibrium mixing of these sulfate end members and overlap the portion of the mixing curves that represent the equilibrium mixing of hydrothermal sulfate and minor seawater sulfate. However, the sample compositions do not exhibit a tendency to follow these latter curves.

Barite has the same sulfur isotopic composition, within the analytical uncertainty, as the aqueous sulfate with which it has equilibrated, but is enriched in $\delta^{18}O$ by 1.8 to 2.1 permil relative to the aqueous species at temperatures of 350 to 250 °C, respectively (Kusakabe and Robinson, 1977). Therefore, those samples with a $\delta^{18}O$ ratio at least one permil lighter than that of the hydrothermal sulfate at an equivalent $\delta^{34}S$ value may contain a high proportion of hydrothermal sulfate to seawater sulfate (Fig. 21). This is particularly plausible for the two vein sulfates which have $\delta^{34}S$ ratios >17 permil, but it is less certain for the stringer and massive barite samples in question because of their lower $\delta^{34}S$ values

(14-15.5 permil) and the uncertainty concerning the isotopic composition of the hydrothermal sulfate.

The majority of the Red Ledge sulfates have isotopic compositions that are consistent with various unequilibrated mixtures of seawater sulfate and a hydrothermal sulfate similar to HF-2 or HF-3. A portion of the "hydrothermal" sulfate incorporated in stringer and syngenetic barite may, in fact, be an equilibrated mixture of HF-2 or HF-3 and a small amount of seawater sulfate, as suggested previously for the upward decrease in sulfide $\delta^{34}S$ values. Moreover, the possible involvement of seawater sulfate that has undergone oxygen isotopic exchange with heated (~150 °C) seawater is suggested by the linear trend of decreasing $\delta^{18}O$ values with increasing $\delta^{34}S$ ratios that is evident from the isotopic distribution of some vein samples (Fig. 21).

According to the interpretation presented above, the Red Ledge sulfates are essentially unequilibrated mixtures of hydrothermal and seawater sulfate. If the hydrothermal sulfate had a $\delta^{34}S$ composition of ~19.0 permil (i.e. similar to the most ^{34}S enriched sample), then the barite in massive sulfide lenses is characterized by high ratios of seawater sulfate to hydrothermal sulfate (.67-.93), massive barite by moderate ratios (.59-.66), stringer barite by moderate to high ratios (.37-.75), and vein sulfates by low to moderate ratios (~0-.64). These changing compositions and ratios are generally consistent with the deposition of bedded barite on the seafloor, and stringer barite at shallow to moderate depths (<100 m), and vein sulfates at variable depths (0- +300 m) below the seafloor. The presence of seawater sulfate in vein barite indicates that seawater

infiltrated the stockwork zone during the late stage of hydrothermal activity and rapidly mixed with rising hydrothermal fluids. However, the incursion of seawater into the stockwork zone apparently was not uniform because the ratios of seawater to hydrothermal sulfate for vein sulfates do not correlate with the depth below the seafloor. Finally, the restriction of the compositions of vein sulfates and barite in massive sulfide lenses to $\delta^{34}S$ values higher and lower than 13.5 permil, respectively, implies that the limits of mixing may have been determined by the physical and chemical parameters of the depositional environment. For example, in the stockwork system, constraints on the ingress of seawater may have been imposed by the hydraulics of mixing two fluids in a network of fractures. In the seafloor environment, the control on the amount of hydrothermal sulfate may be related to the minimum mixture of Ba-rich and sulfate-rich fluids required for barite saturation. An interplay of these fundamental controls possibly operated in the permeable rocks on the seafloor where stringer barite was precipitated.

Isotopic Equilibria

Sulfur isotopic disequilibrium between sulfide and sulfate species is critical to the interpretation of the Red Ledge $\delta^{34}S$ systematics, as discussed in the foregoing section. The extent to which isotopic equilibrium was attained in the Red Ledge system may be constrained by examining the conformity of mineralization temperatures, calculated from the $\delta^{34}S$ fractionations between coeval phases, to those determined by other means for the same deposit or for

analagous deposits, the order of isotopic enrichment among phases, and the variablility of the fractionations within specific populations.

Mineralization temperatures calculated from probable equilibrium pairs of sulfides and listed in Table 8 are generally variable, ungrouped, and internally inconsistent with respect to the same sample (based on mineral triplets) or equivalent pairs representing the same paragenetic stage. Reversals in the equilibrium order of ^{34}S enrichment between coeval sulfides are prevalent in stringer and massive mineralization, but are uncommon in stockwork mineralization. Nevertheless, many of the temperature calculations based on the fractionation of sulfur isotopes between vein sulfides (mostly pyrite-chalcopyrite pairs) are improbably high (338 to 786 °C) for this type of deposit. These results indicate that isotopic equilibrium among the Red Ledge sulfides either was not achieved, or if established, was not preserved.

By contrast, the calculated depositional temperatures based on barite-sulfide pairs are relatively uniform ranging from 251 to 343 °C (Table 8). This distinction may be partially related to the differences in temperature sensitivity between the two types of geothermometers. For example, a decrease from 300 to 250 °C corresponds to an increase of 3.69 $^{o}/_{oo}$ in the barite-pyrite fractionation factor but to only a 0.27 $^{o}/_{oo}$ increase in the pyrite-chalcopyrite fractionation factor. Accordingly, the fractionation of sulfur isotopes between pyrite and chalcopyrite is particularly sensitive to analytical and experimental uncertainties, sample impurities, and

Table 8. Sulfur Isotopic Temperatures

Sample No.	A-B	Stage	$\delta^{34}S_A$ (°/₀₀)	$\delta^{34}S_B$ (°/₀₀)	ΔA-B	T°C
			Vein Mineralization			
TG5-1311	Ba-Py	2B	16.1	-2.6	18.7	305
	Ba-Cp	2B	16.1	-3.0	19.1	320
	Py-Cp	2B	-2.6	-3.0	0.4	786
TG1-682	Ba-Cp	3	17.7	-3.3	21.0	291
TG16-415	Ba-Cp	3	19.0	-3.0	22.0	278
	Py-Cp	2A	-2.1	-2.8	0.7	528
TG1-726	Py-Cp	2A	-2.2	-3.0	0.8	476
TG3-538	Py-Cp	2A	-3.7	-2.8	-0.9	diseq
TG3-810	Py-Cp	2B	-2.3	-2.9	0.6	592
TG5-1305	Py-Cp	2B	-1.8	-3.5	1.7	241
TG15-808	Py-Cp	3-4A	-3.2	-6.1	2.9	120
	Py-Sp	3-4A	-3.2	-4.1	0.9	307
	Sp-Cp	3-4A	-4.1	-6.1	0.4	diseq
TG17-563	Py-Cp	2C	-2.6	-4.8	2.2	179
TG18-286	Py-Cp	3-4A	-1.1	-2.4	1.2	338
TG18-331	Py-Cp	2B	-2.7	-3.5	0.8	476
	Py-Cp	2C	-1.4	-3.6	2.2	179
SS105-310 -360A	Py-Cp	2B	-2.3	-2.7	0.4	786
SS151-715	Py-Cp	?	-2.6	-2.8	-0.2	diseq
SS151-200	Py-Sp	?	-3.5	-5.0	1.5	176
			Stringer Mineralization			
TG2-130	Ba-Py		15.4	-6.9	22.3	255
TG6-751	Ba-Py		14.9	-2.0	16.9	336
TG7-220	Ba-Py		14.4	-3.9	18.3	311
TG9-1471	Ba-Py		15.9	-5.9	21.8	261
RLC2-700-800B	Ba-Py		14.5	-8.1	22.6	251
TG16-1407	Py-Cp		-4.1	-4.8	0.7	528
	Py-Sp		-4.1	-5.4	1.3	209
	Sp-Cp		-5.4	-4.8	-0.6	diseq
TG1-1741	Py-Cp		-6.6	-5.7	-0.9	diseq
	Py-Sp		-6.6	-5.3	-1.3	diseq
	Sp-Cp		-5.3	-5.7	0.4	339

Table 8.(continued)

Massive Mineralization

TG4-838	Ba-Py	12.1	-5.1	17.2	330
RL2800	Ba-Py	13.1	-5.5	18.6	307
	Ba-Sp	13.1	-4.2	17.3	343
	Py-Sp	-5.5	-4.2	-1.3	diseq
TG1-1895	Py-Cp	-4.4	-4.4	0.0	diseq
	Py-Sp	-4.4	-3.6	-0.8	diseq
	Sp-Cp	-3.6	-4.4	0.8	160
TG12-1438	Py-Sp	-4.1	-2.7	-1.4	diseq
	Py-Gn	-4.1	-4.2	0.1	+1000
	Sp-Gn	-2.7	-4.2	1.5	421
RLUT	Ba-Sp	12.9	-6.6	19.5	306

****

Temperatures calculated from SO_4-H_2S fractionation equations given by Ohmoto and Lasaga (1982) and sulfide-H_2S equations presented by Ohmoto and Rye (1979). diseq - disequilibrium;

small amounts of disequilibrium relative to the fractionation of sulfur isotopes between barite and sulfides.

The barite-sulfide temperatures for vein deposition (278-320 °C, av. = 298 °C) are comparable to fluid inclusion homogenization temperatures for Kuroko stockwork mineralization (see summary in Hydrothermal Fluids). Barite-pyrite temperatures for stringer mineralization are also plausible (251-336 °C, av. = 283 °C), whereas barite-pyrite and barite-sphalerite temperatures for massive sulfide mineralization (307-343 °C, av. = 323 °C) are demonstrably high relative to those determined for analagous Kuroko mineralization (250 +/- 25 °C; Kajiwara, 1971; Mukaiyama et al., 1974; Marutani and Takenouchi, 1978; Hattori and Muehlenbachs, 1980). Although many determinations are comparable to those for equivalent Kuroko mineralization, the calculated temperatures and isotopic fractionations for some barite-sulfide pairs are notably variable. For instance, the range in temperatures for stringer mineralization is 85 °C and the range in fractionations among barite-pyrite, -chalcopyrite, and -sphalerite pairs is 5.7 $^{o}/_{oo}$ (1s = 2.3 $^{o}/_{oo}$), 2.9 $^{o}/_{oo}$, and 2.2 $^{o}/_{oo}$, respectively. The variability in the sulfur isotopic fractionations among the vein barite-sulfide pairs is largely caused by differences in the $\delta^{34}S$ composition of barite (range of 2.9 $^{o}/_{oo}$), whereas that among the stringer barite-sulfide pairs is a function of differences in the $\delta^{34}S$ composition of sulfides (range of 6.1 $^{o}/_{oo}$).

Experimental studies have established that sulfate-sulfide isotopic equilibration rates decrease markedly at temperatures below about 300 °C. For example, Ohmoto and Lasaga (1982) reported that a 90% exchange of sulfur isotopes between oxidized and reduced aqueous

sulfur species was attained in 17 days at 350 °C, 140 days at 300 °C, and 4.4 years at 250 °C in solutions having a pH range of 4 to 7. The more sluggish equilibrations with diminishing temperature imply that if rates of cooling are greater than rates of isotopic equilibration, then sulfate-sulfide fractionations will be variably smaller than the equilibrium fractionation factor at the temperature of deposition. If rapid cooling results from the mixing of seawater, then the sulfate-sulfide fractionation factor of final equilibration may be further reduced by the addition of isotopically light seawater sulfate. For example, the range of barite-sulfide isotopic temperatures for late stage vein mineralization can be explained by final SO_4-H_2S equilibration near 275 °C and a 3 permil reduction in the $\delta^{34}S$ ratio of the sulfate through the nonequilibrium mixing of Early Permian seawater sulfate. Similarly, the barite-sulfide temperatures for stringer mineralization could have resulted from final equilibration between sulfate and sulfide species at temperatures varying between 240 and 275 °C and a 1.5 to 5 permil nonequilibrium decrease in the $\delta^{34}S$ composition of total sulfate. An additional 1.5 to 4 permil decrease in the sulfate value via the rapid influx of seawater sulfate, without isotopic equilibrium, would explain the improbably high temperatures calculated for massive sulfide mineralization. Consequently, the same model used to explain the $\delta^{34}S$ variations in the Red Ledge sulfates and sulfides can also be employed to reproduce the observed sulfate-sulfide fractionations. However, models invoking combinations of simple cooling, equilibrium seawater-hydrothermal fluid mixing, and variable temperatures of final SO_4-H_2S equilibration are incapable of explaining completely the vertical

temperature profile calculated from the barite-sulfide fractionations, the sympathetic upward decrease in barite and sulfide $\delta^{34}S$ compositions, and the variations in the fractionation factors among mineral pairs representing equivalent types of mineralization.

Sulfur isotopic disequilibrim among the Red Ledge sulfides may have been produced by several mechanisms during the formation of the deposit. If there was isotopic disequilibrium between aqueous sulfate and sulfide, then isotopic disequilibrium between pyrite and chalcopyrite, and between these phases and other sulfides, was likely because pyrite and chalcopyrite typically form by redox reactions involving both SO_4 and H_2S (Ohmoto and Rye, 1979). Thus, the unreasonably small isotopic fractionations among the Red Ledge sulfides may have resulted from SO_4-H_2S isotopic disequilibrium produced by rapid cooling which, near the seafloor, was caused by the mixing of seawater and the hydrothermal fluid.

The textural relationships among sulfides also suggest some possible reasons for isotopic disequilibrium. Chalcopyrite in the stockwork zone replaces pyrite along grain boundaries and occupies the interstices of pyrite aggregates. This textural relationship implies that the nonequilibrium pyrite-chalcopyrite fractionations result from sequential paragenesis caused by the partial and variable incorporation of pyrite sulfur in chalcopyrite during replacement. In massive and stringer mineralization, pyrite precedes and chalcopyrite succeeds sphalerite, galena and tetrahedrite. If this represents the paragenesis of primary sulfides, then the preponderance of ^{34}S reversals and improbable fractionations between massive and

stringer sulfides may have resulted from small temporal shifts in the $\delta^{34}S$ composition of H_2S.

The sulfur isotopic fractionations and sulfide textures in the Red Ledge deposit may be partly attributable to metamorphism. Sulfides during metamorphism tend to rapidly equilibrate (cf. silicates and oxides) under the ambient conditions and modify their primary features (Barton and Skinner, 1967). Indeed, those textures and compositional heterogeneities that characterize unmetamorphosed massive sulfide ores, such as framboids, colloform banding, "chalcopyrite disease" and sphalerite growth zones, have not been observed in the Red Ledge mineralization. However, only local domains of equilibrium were established because microscopic criteria for intergranular equilibrium are also absent (e.g. see Spry, 1976; Vernon, 1975). These features suggest that reaction rates were sluggish and that chemical diffusion, rather than reconstruction (breaking and reforming bonds), was the dominant mode of recrystallization. Therefore, the nonequilibrium isotopic fractionations among sulfides are possibly the result of limited isotopic exchange by solid diffusion between adjacent phases, disequilibrium exchange between solids and a minor intergranular fluid, and variable equilibration rates. Isotopic fractionations between sulfides from several other metamorphosed volcanogenic sulfide deposits exhibit features similar to those from the Red Ledge deposit (see discussion in Franklin et al., 1981). Moreover, sulfides in the Raul volcanogenic deposit apparently attained chemical and structural (polymorphic), but not isotopic, equilibrium during retrograde metamorphism (Ripley and Ohmoto, 1977).

In summary, the establishment of the equilibrium order of ^{34}S enrichment between vein pyrite and chalcopyrite and a general lack of sulfur isotopic equilibrium in some unmetamorphosed Kuroko deposits (see Eldridge et al., 1983) implies that the sulfides from the Red Ledge veins achieved only partial isotopic equilibrium during deposition. The cause most likely relates to isotopic disequilibrium among aqueous sulfide and sulfate species, and (or) to the variable incorporation of pyrite sulfur in chalcopyrite during replacement. However, it is uncertain whether even partial isotopic equilibrium was established among stringer and massive sulfides. Furthermore, sulfide textures in the Red Ledge mineralization and isotopic data from similar metamorphosed deposits suggest that the sulfur isotopic systematics of the Red Ledge sulfides were disturbed during metamorphism, although the major $\delta^{34}S$ variations were clearly preserved.

Sulfides and Sulfates from Similar Deposits

In this section sulfur isotopic data for other volcanogenic massive sulfide deposits in the western Cordillera are presented and discussed. These results are then compared with isotopic data on analagous deposits of various locations throughout the world and with variations in the sulfur isotopic composition of seawater sulfate during Phanerozoic time.

The Cordilleran deposits under consideration include the Lynx Mine and Seneca in British Columbia, the Blue Jacket, Iron Dyke, and Peck Mtn. in western Idaho, the Keating District (Balm Creek and occurrences near Clover and Tucker Creeks) in northeastern Oregon,

the Banfield-Rowley, Silver Peak, Waite Barite, Almeda, Turner Albright, and Queen of Bronze and Cowboy of the Takilma-Waldo District, in southwestern Oregon, and Grey Eagle, and Iron Mtn., Balaklala, and Mammoth of the West Shasta District, and Afterthought, Bully Hill, and Rising Star of the East Shasta District, in northern California. The location of these deposits, except that of the Lynx Mine and Seneca, is shown in Figures 2 and 22. Published investigations, theses, private reports, and a reconnaissance field evaluation by the author provided the geologic basis for the geochemical intrepretations. The principal, detailed geologic studies (in the public domain) of the individual deposits or districts include those by Juhas et al. (1981) for the Iron Dyke, Mangham (in prep) and Wracher (1969) for Peck Mtn., Gilluly (1933) for the Keating Dist., Derkey (1982) for the Silver Peak, Fifarek (1982) for the Banfield-Rowley, Koski (1981) and Shenon (1933a) for the Almeda, Cunningham (1979) for the Turner Albright, Shenon (1933b) for the Takilma-Waldo District, Sorensen (1983) for the Queen of Bronze, Koski (1981) for the Grey Eagle, Kinkel et al. (1956) and Reed (1984) for the West Shasta District, and Albers and Robertson (1961) for the East Shasta District. A regional tectonic framework for volcanogenic massive sulfide deposits was presented by Albers (1981) for occurrences in California and by Koski (1981) for occurrences in the Klamath Mountains province.

Volcanogenic massive sulfide deposits in the western Cordillera formed in three principal geologic settings, as inferred from their associated host rocks: 1) volcanic arc, 2) near-arc basin, and 3) oceanic crust. Most of these deposits formed near active volcanic

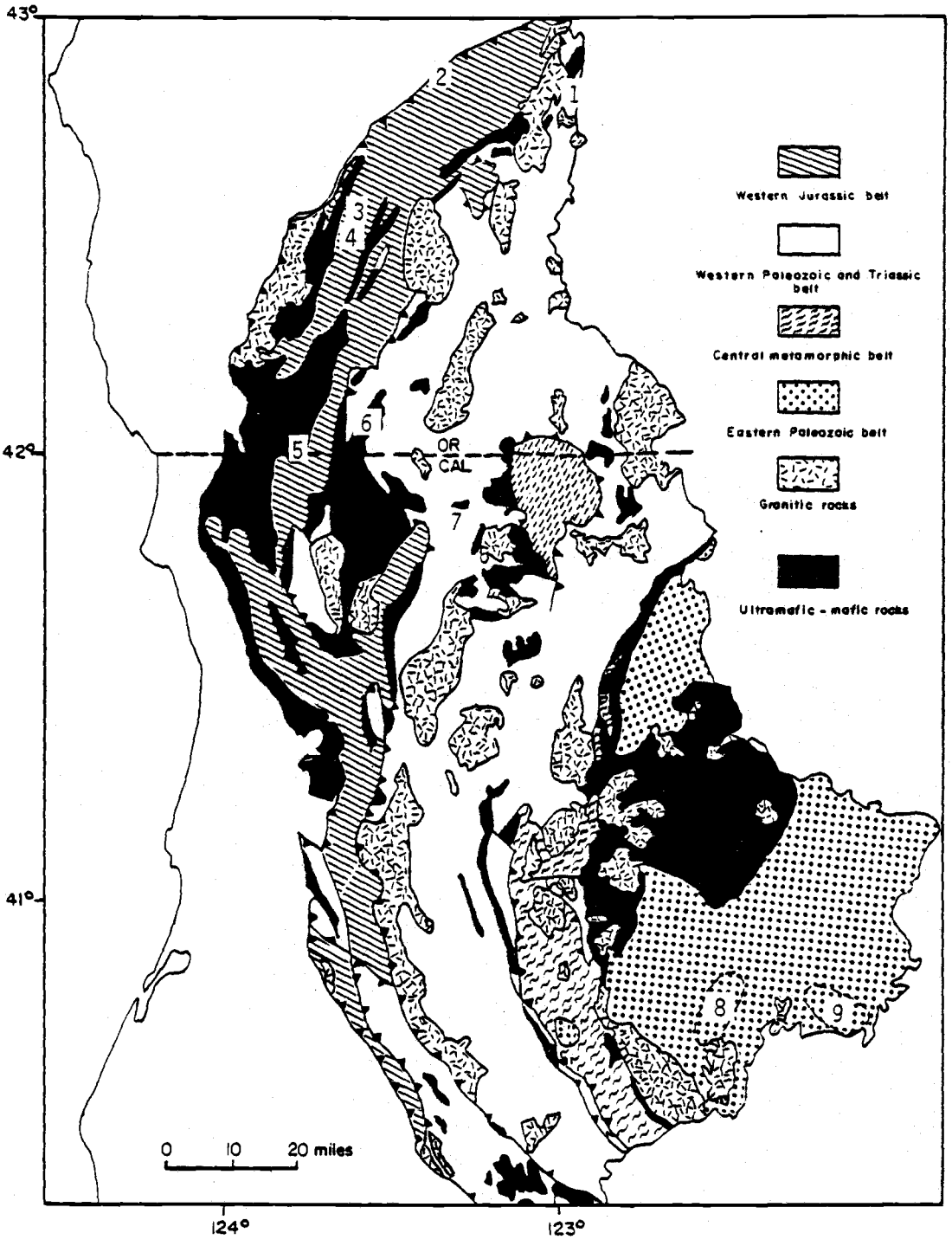

Figure 22. Geology of the Klamath Mountains Province (modified from Hotz, 1971, and Irwin, 1972) and location of principal volcanogenic massive sulfide deposits. 1-Banfield-Rowley; 2-Silver Peak; 3-Waite Barite; 4-Almeda; 5-Turner Albright; 6-Takilma-Waldo Dist; 7-Grey Eagle; 8-West Shasta Dist; 9-East Shasta Dist;

vents in a volcanic arc setting. They are typically hosted by felsic tuffs and breccias, and are spatially associated with flows and domes of quartz-(feldspar) porphyry or felsite. Massive mineralization consists of abundant pyrite, minor chalcopyrite, and variable amounts (trace to ~25%) of sphalerite. Galena and tetrahedrite are minor constituents, and barite a common gangue, in sphalerite-rich mineralization. Accordingly, metal associations range from Cu-(Zn) to Zn-Cu-(Pb) types. Silver and cadmium are enriched in the Zn-Cu deposits, whereas gold is commonly, but not consistently, enriched in the Cu-rich end members.

The Grey Eagle deposit formed in an interarc basin at a site that was distal to centers of volcanism. It is hosted by tuffs and tuffaceous epiclastics of mafic to intermediate composition that are overlain and underlain by fine-grained carbonaceous phyllites (siltstones). Mineralization is typically banded and consists of variable mixtures of pyrite, chalcopyrite, sphalerite, and quartz. Variations in trace element abundances and sulfur isotopic ratios suggest the deposit formed over a hydrothermal vent.

The Queen of Bronze, Cowboy, and Turner Albright deposits formed in oceanic crustal rocks that are part of ophiolitic suites. Host rocks include basalt, diabase, and fine-grained gabbro. Geologic relationships suggest that the Turner Albright developed on and immediately below the seafloor, whereas the Queen of Bronze formed entirely in open spaces at somewhat greater depths within the crust. Mineralization at these deposits contains abundant copper, minor zinc, and economically important concentrations of gold and cobalt.

The deposits under consideration apparently formed during four distinct intervals: 1) Middle Devonian (West Shasta Dist.), 2) Early Permian (e.g. Red Ledge, Iron Dyke), 3) Middle to Late Triassic, and 4) Middle to Late Jurassic (e.g. Seneca, Turner Albright, Silver Pk., Almeda). The age determinations for specific deposits are based on the ages of fossils or fossil suites found in the stratigraphic section near the horizon of mineralization. However, the paleontologic age of many deposits has not been established because of the general paucity of fossils in proximal volcanic arc assemblages. In these cases, regional stratigraphic relationships were used to constrain the age of mineralization.

The sulfur isotopic results, isotopic temperatures, age, and geologic setting for most of the regional deposits under consideration are listed in Table 9. Additionally, all the sulfur isotopic data for bedded sulfide and barite that have been presented in this investigation (Tables 6 and 9) and data for comparable mineralization in the Seneca (Urabe et al., 1983), Turner Albright (Cunningham, 1979), Grey Eagle (Cramer and Taylor, 1983), and West Shasta District (Casey and Taylor, 1981) deposits are depicted in Figure 23. This portrayal indicates that the sulfur isotopic composition of bedded sulfides and barite varies considerably between deposits (up to 10 and 11 $^{o}/oo$). The range in $\delta^{34}S$ ratios among the sulfides analyzed from individual deposits is also significant (e.g. 7.3 $^{o}/oo$ for Red Ledge sulfides) and typically greater than that of associated barite. Some of the variability among the sulfide data results from computing the range for all the sulfide phases analyzed because pyrite is generally enriched in ^{34}S relative to the other sulfides, as would be

Table 9. Sulfur Isotopic Data for Selected Volcanogenic Massive Sulfide Deposits in the Western Cordillera.

Deposit (Type,Age) Sample No.	Min	$\delta^{34}S$ (°/₀₀)	A-B	T°C[6]	Description
British Columbia					
Lynx Mine (VA, M.-L. Paleoz)					
LM83-1[1]	Ba	22.6			mass. ba;
LM83-2[1]	Py	4.0	Py-Sp	342	mass. sp-cp-py-ba;
" "	Sp	3.2			" "
WM74-1	Cp	3.1			cp-sp-py vnlt;
N.E. Oregon-W. Idaho					
Blue Jacket (VA, E. Per or M.-L. Tr)					
BJ-1-79	Ba	18.6	Ba-Sp	347	mass. sp-cp-py-(ba);
" "	Sp	1.1			" "
BJ-3-79	Ba	15.2			mass. ba;
BJ-1-81	Py	2.5			mass. py-qz;
BJ-2-81	Ba	16.0			mass. ba;
BJ-6-81	Ba	16.0			mass. ba;
Iron Dyke (VA, E. Per)					
ID-650-1	Py	-2.9	Py-Cp	674	py-cp-qz stngr;
" "	Cp	-3.4	Ba-Py	366	" "
" "	Ba	12.0	Ba-Cp	389	ba clot;
ID-650-2	Ba	11.4	Ba-Py	320	py-cp-qz stngr;
" "	Py	-6.4			" "
ID-V-2	Py	-2.7	Py-Cp	366	py-cp-qz stngr;
" "	Cp	-3.8			" "
Peck Mtn. (VA, L. Tr)					
PM-80-149	Ba	17.3			mass. ba;
PM-150	Ba	18.7			ba vein;
PM-1-992[3]	Py	-5.3			mass. py;
PM-72-143[2]	Py	2.9			diss. in volcanics;
PM-72-144[2]	Py	0.0			diss. in QD pluton;
Keating Dist. (VA, E. Per or M.-L. Tr)					
CCR-8	Ba	14.9			mass. ba; Clover Ck;
CCR-8313[4]	Ba	14.6			mass. ba; Tucker Ck;
BC-3	Py	-2.7	Py-Sp	162	cp-py-sp; Balm Ck;
" "	Sp	-4.3	Py-Cp	diseq	" "
" "	Cp	-1.7	Sp-Cp	diseq	" "
S.W. Oregon-N. California					
Banfield-Rowley (VA, M.-L. Tr)					
BF-2[2]	Cp	4.6			bleb in Fe-form.;
BU-1-ST	Py	5.5	Py-Cp	786	py-cp bleb, Fe-form;
" "	Cp	5.1			" "
BU-1-46	Py	5.4	Py-Cp	786	py-cp bleb, Fe-form;
" "	Cp	5.0			" "
BU-4-F1	Cp	6.6			py-cp bleb, Fe-form;

Table 9. (continued)

RW-2[2]	Py	2.4			mass. py-sp-cp;
" "	Sp	-0.9			" "
RS-11	Py	-0.5	Py-Sp	597	mass. py-sp-cp;
" "	Sp	0.9			" "
Silver Peak (VA, M.-L. Jr)					
LU-1-H	Py	2.4	Py-Cp	274	cp-sp-py-qz clasts;
" "	Cp	0.9			" "
LU-4-S	Ba	17.3	Ba-Py	344	mass. ba-py-cp;
" "	Py	0.8			" "
LU-10	Ba	18.1			mass. ba-py;
LSP-4-S	Py	0.7			mass. py;
" "	Py	2.1			" "
Waite Barite (VA, M.-L. Jr)					
WB-4	Ba	17.4			mass. ba-sp-py;
Grey Eagle (NAB, M.-L. Jr)					
GEU-1	Py	-2.4	Py-Cp	diseq	mass. py-cp bands;
" "	Cp	0.5			" "
Almeda (VA, M.-L. Jr)					
AL-5	Ba	18.2			mass. ba-(py);
AL-41	Ba	16.6			mass. ba-(py);
A-4-118	Ba	17.7			mass. ba-cp;
AL-28	Ba	18.0			mass. ba;
Takilma-Waldo Dist. (OC, M.-L. Tr)					
Queen of Bronze					
QB-M-1	Py	-0.9	Py-Cp	430	mass. py-cp;
" "	Cp	-1.8			" "
QB-C-1	Py	-1.5			mass. py-cp;
QB-LCH-C	Cp	-3.2			cp-py stngr;
Cowboy					
CB-1	Po	-4.9			mass. po w/cp blebs;
W. Shasta Dist. (VA, M. Dev)					
Iron Mtn.					
79-WS-1[5]	Py	5.1			mass. py-(cp);
79-WS-2[5]	Py	3.5			mass. py-(cp);
79-WS-3B[5]	Py	5.1			mass. py-(cp);
79-WS-7B[5]	Py	5.6			qz-py vn;
Balaklala					
79-WS-15[5]	Py	5.6			mass. py-(cp);
Mammoth Mine					
79-WS-20[5]	Py	2.9			200 level;

Table 9. (continued)

E. Shasta Dist. (VA, Per or M.-L. Tr)					
Afterthought					
AFT-1	Sp	6.2	Sp-Cp	diseq	laminated sp-cp;
" "	Cp	7.1			" "
Rising Star					
RS-1[2]	Gn	-4.3			mass. blk ore;
RS-2[2]	Sp	0.2			mass. blk ore;
Bully Hill					
BH-1[2]	Py	1.8	Ah-Py	496	vn;
BH-2[2]	Ah	12.6			vn;
BH-4[2]	Cp	2.3			

1. Sample from A.E. Soregaroli;
2. Unpublished data from C.W. Field
3. Sample from J. R. Mangham;
4. Sample from R. Willden;
5. Samples collected by B.R. Doe;
6. Calculated from SO_4-H_2S fractionation equations given by Ohmoto and Lasaga (1982) and sulfide - H_2S equations presented by Ohmoto and Rye (1979).

Abbreviations: Ah-anhydrite; Ba-barite; Cp-chalcopyrite; diseq-disequilibrium; Gn-galena; Po-pyrrhotite; qz-quartz; Sp-sphalerite; vn-vein;

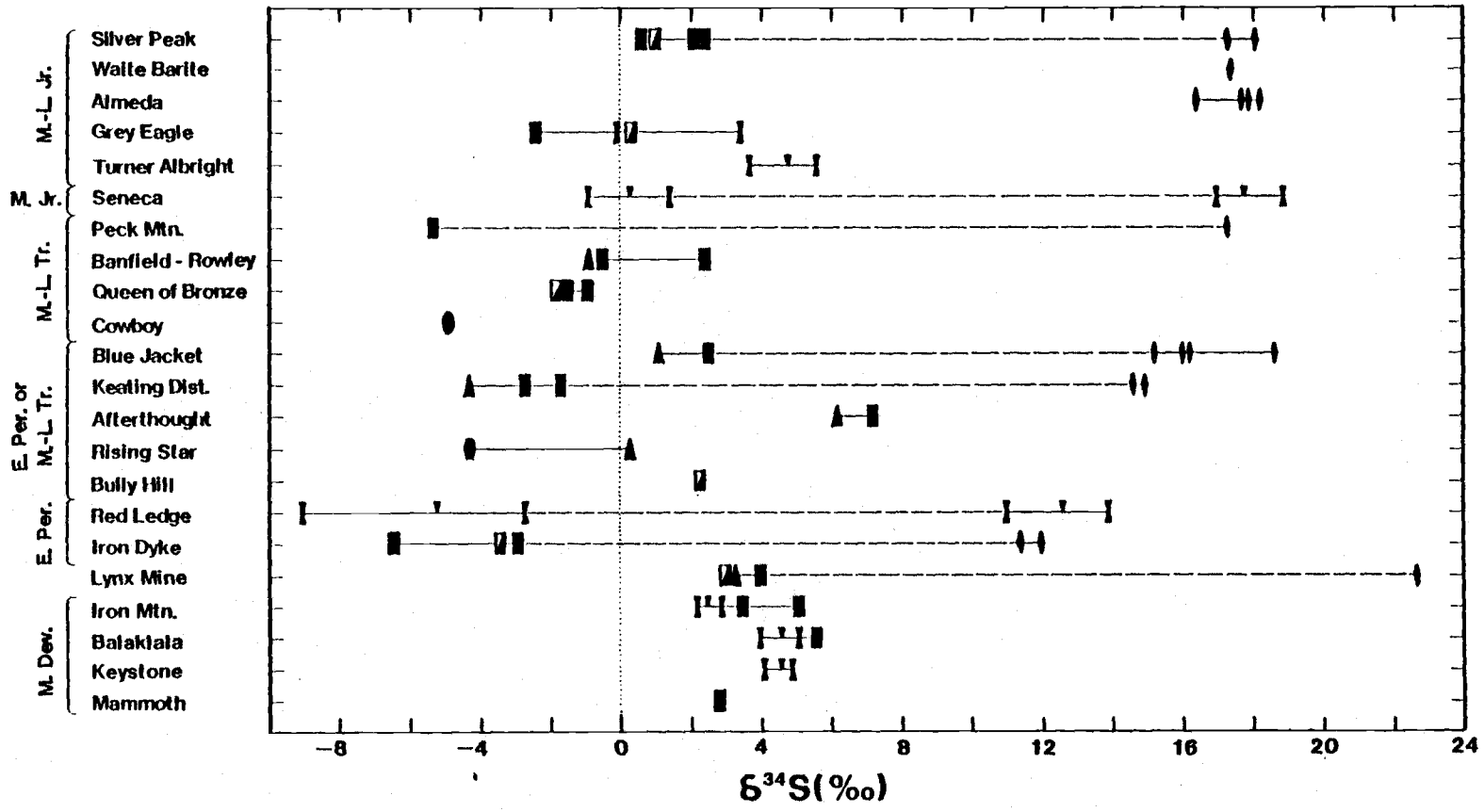

Figure 23. Sulfur isotopic ratios of massive mineralization in selected volcanogenic massive sulfide deposits of the western Cordillera. Symbols: barite (diamond); pyrite (rectangle); chalcopyrite (half-filled rectangle); sphalerite (triangles); galena (hexagon); and pyrrhotite (oval); average (inverted triangle) and endpoints of range (hourglass) for analyses other than those reported in Tables 6 and 9 (see text);

expected if the sulfides coprecipitated under equilibrium conditions. However, the sulfur isotopic temperatures are variable and skewed to implausibly high values. These are the same characteristics exhibited by the isotopic temperatures determined from the Red Ledge sulfides and sulfates (refer to Isotopic Equilibria) and, thus, the data imply that only partial isotopic equilibrium was established and retained in the sulfur-bearing minerals of these deposits.

In contrast to the sulfide $\delta^{34}S$ values, those for bedded barite from the various deposits define four isotopic populations: group I, 11.1 to 14.0 $^{o}/oo$, from Red Ledge and Iron Dyke; group II, 14.6 to 16.0 $^{o}/oo$, from Blue Jacket (3 of 4 samples analyzed) and the Keating District; group III, 16.6 to 18.6 $^{o}/oo$, from Silver Peak, Waite Barite, Almeda, Seneca, and Peck Mtn.; and group IV, ~22 to 23 $^{o}/oo$, from the Lynx Mine. Although the sulfide $\delta^{34}S$ ratios are not readily divisible into distinct groups, those sulfides that are coextensive with the isotopically lightest and heaviest barite (groups I and IV, resp.) tend to be among the isotopically lightest and heaviest sulfides, respectively.

Differences in the average isotopic composition of sulfur between volcanogenic deposits of different ages are correlative with temporal variations in the isotopic composition of seawater sulfate; a phenomenom first noted by Sangster (1968). Such a correlation is illustrated by Figure 24 where the average and range in $\delta^{34}S$ values for bedded pyrite and barite from the volcanic arc massive sulfide deposits considered in this investigation, and from several other analagous deposits, are compared with the average $\delta^{34}S$ value of contemporaneous oceanic sulfate. The analagous deposits and sources

Figure 24. Average and range of $\delta^{34}S$ values for bedded pyrite (squares) and barite (diamonds) from volcanogenic massive sulfide deposits of the same age compared with the $\delta^{34}S$ composition of coeval seawater sulfate (circles). Deposits of known age (left margin and closed symbols): K-Kuroko; SP-Silver Pk; AL-Almeda; WB-Waite Barite; S-Seneca; RL-Red Ledge; ID-Iron Dyke; WS-West Shasta District; WL-Woodlawn; BU-Buchans; HS-Heath Steele; RB-Roseberry; Deposits of uncertain age (right margin and open symbols): PM-Peck Mtn., KD-Keating District; BJ-Blue Jacket; LM-Lynx Mine;

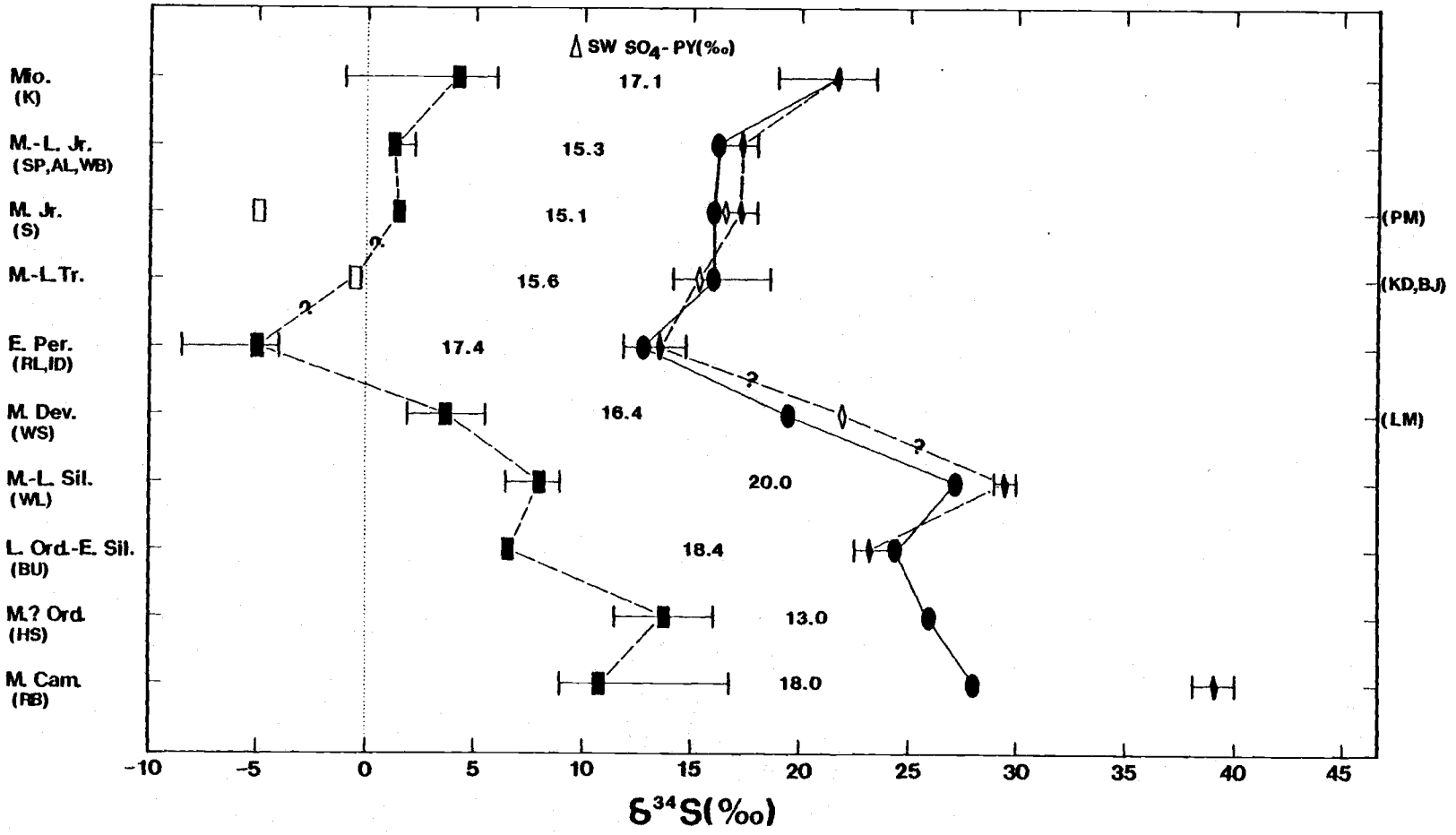
Δ SW SO4- PY(‰)
Mio. (K)
M.-L. Jr. (SP,AL,WB)
M. Jr. (S)
M.-L.Tr.
E. Per. (RL,ID)
M. Dev. (WS)
M.-L. Sil. (WL)
L. Ord.-E. Sil. (BU)
M.? Ord. (HS)
M. Cam. (RB)
17.1
15.3
15.1
15.6
17.4
16.4
20.0
18.4
13.0
18.0
(PM)
(KD,BJ)
(LM)
?
?
?
?
-10
-5
0
5
10
15
20
25
30
35
40
45
δ34S(‰)

Figure 24.

of data include: Kuroko, Japan (Kajiwara, 1971; Yamamota, 1974; Kuskabe and Chiba, 1983; Watanabe and Sakai, 1983); Woodlawn, Australia (Ayers et al., 1979); Buchans, Canada (Kowalik et al., 1981); Heath Steele, Canada (Lusk and Crocket, 1969); and Rosebery, Tasmania (Solomon et al., 1969; Green et al., 1981). Figure 24 illustrates that the average $\delta^{34}S$ ratio of bedded barite is typically within 2.5 $^{o}/oo$ of that of oceanic sulfate, whereas the average $\delta^{34}S$ ratio of bedded massive pyrite ranges from 13.0 to 20.0 $^{o}/oo$, and averages 16.6 $^{o}/oo$, less than that of oceanic sulfate. The general consistency of these relationships throughout the Paleozoic era, when the isotopic composition of seawater sulfate varied by more than 20 $^{o}/oo$, has several implications:

1. The major source of sulfur in volcanogenic massive sulfide deposits is seawater sulfate. Thus, sulfur from other isotopically distinct sources, such as that leached from country rocks (~0 $^{o}/oo$) or expelled from crystallizing intrusions (~0 $^{o}/oo$), is limited to a minor component in the hydrothermal fluids.

2. Because seawater contains only negligible quantities of sulfide species, much of the reduced sulfur incorporated in the bedded sulfides was produced through the inorganic reduction of seawater sulfate. For the reduced sulfur to maintain a seawater signature, at least one or more of three conditions must have prevailed: a) seawater sulfate was quantitatively reduced to sulfide sulfur, b) isotopic equilibration between sulfate and sulfide species was limited, even at sites below the seafloor, and c) the ratio of total sulfate to total sulfide species and the isotopic fractionation between them was relatively constant for volcanogenic massive sulfide

deposits, regardless of age. Estimates of fluid temperatures in excess of 300 °C and sulfate/sulfide ratios of approximately one for the Kuroko deposits (Ohmoto et al., 1983; Pisutha-Arnond and Ohmoto, 1983) suggest that the latter condition (c) is the most probable.

3. The average sulfur isotopic composition of bedded barite in volcanogenic deposits may be utilized to establish the approximate age of a deposit, particularly if the age constraints imposed by geological relationships provide a choice between intervals when the average $\delta^{34}S$ composition of seawater sulfate differed by several permil. Accordingly, the Blue Jacket and Keating District deposits are probably Middle to Late Triassic in age, and the Lynx deposit may be Middle Devonian in age (as suggested by Figure 24). However, the Peck Mtn. deposit is inferred to be Middle to Late Jurassic in age by this method, whereas the geologic constraints suggest a Middle to Late Triassic age. Furthermore, the previously described isotopic populations of barite $\delta^{34}S$ ratios are consistent with barite sedimentation during different geologic Periods: Group I, Early Permian; Group II, Middle to Late Triassic; Group III, Middle to Late Jurassic; and Group IV, Middle Devonian.

Exceptions to the correlation between the $\delta^{34}S$ ratio of oceanic sulfate and that of bedded pyrite and barite in volcanogenic deposits may indicate unusual environmental factors. For example, the Rosebery and Peck Mtn. deposits are characterized by average isotopic compositions of barite and pyrite that are enriched and depleted in ^{34}S, respectively, relative to their expected compositions. This variance could have been produced by equilibrium isotopic exchange between sulfate and sulfide at temperatures below which

exchange normally occurred. If correctly interpreted, such a condition implies unusally low fluid velocities, long residence times for the fluids near the seafloor, and low permeablities in the sulfide blankets. Finally, exceptions to the correlation in isotopic compositions may not be related to environmental conditions, but rather to uncertainties in the age of evaporites and (or) metamorphosed volcanogenic massive sulfide deposits.

Source of Hydrothermal Sulfur

Sulfur isotopic data presented in the previous section suggest that seawater is the prime source of sulfur for volcanogenic massive sulfide deposits and, by corollary, that sulfur from other sources is limited to minor quantities. According to this interpretation, the $\delta^{34}S$ composition of total sulfur in the Red Ledge hydrothermal fluids, prior to mixing with seawater, was similar to that of Early Permian seawater sulfate, or 10 to 12 permil. In contrast, if the sulfur was derived from the country rocks (i.e. mafic volcanic rocks of the Hunsaker Creek Formation) by leaching, then the sulfur isotopic composition of the fluids would have been about 0 permil or slightly less (neqative $\delta^{34}S$ values would result from the incorporation of minor bacteriogenic sulfide sulfur). Similarly, the derivation of sulfur from a crystallizing felsic magma would result in $\delta^{34}S_{fluid}$ values in the range of -3 to +7 $^{o}/oo$, with the higher $\delta^{34}S$ values characteristic of initially high oxidation states in the fluids (Ohmoto and Rye, 1979).

The sulfur isotopic composition of total sulfur in the Red Ledge hydrothermal system can be estimated from the relationship of sulfide $\delta^{34}S$ compositions to the pH, fO_2, T, and $\delta^{34}S_{fluid}$, as previously discussed and portrayed by Figure 19. Accordingly, the range in $\delta^{34}S$ ratios for vein pyrite (-4.2 to -0.6 permil) is consistent with a $\delta^{34}S$ composition of total sulfur between 9 and 23 permil at 250 °C and within the pH-fO_2 field estimated for the vein fluids. Moreover, the $\delta^{34}S$ composition of the Red Ledge fluids may be computed from equation d in Table 7, which relates the $\delta^{34}S$ of the total sulfur to that of H_2S, the ratio of total sulfate to total sulfide species, and the appropriate SO_4-H_2S fractionation factor. Based on the fractionation factors of 24.2 $^{o}/_{oo}$ for SO_4-H_2S (Ohmoto and Lasaga, 1982) and 1.5 $^{o}/_{oo}$ for FeS_2-H_2S (Ohmoto and Rye, 1979) at 250 °C, the range of vein pyrite $\delta^{34}S$ values (-4.2 to -0.6 permil), and assumed total SO_4/H_2S ratios between 1 and 100, the isotopic composition of sulfur in Red Ledge fluids is calculated to have been in the range 6 to 22 permil. Estimates by both of these methods are similar to that (14 to 18 $^{o}/_{oo}$) determined by assuming the sulfate/sulfide ratios in the Red Ledge fluids were equivalent to those in the Kuroko fluids (refer to Mixing of Seawater and Hydrothermal Fluids). Therefore, the calculated isotopic composition of total sulfur in the Red Ledge system is consistent with a sulfur derived mainly from seawater. An oceanic source of sulfur would account for the anomalously low $\delta^{34}S$ values of Red Ledge sulfides and sulfates because the $\delta^{34}S$ composition of seawater sulfate during Permian time was at a minimum for the Paleozoic era.

As previously mentioned, the derivation of hydrothermal sulfide sulfur from seawater must involve the inorganic reduction of seawater sulfate. Ohmoto et al., (1983) have modeled this process for seawater convection in the vicinity of a subseafloor intrusion. They suggested that seawater sulfate is first precipitated as disseminated anhydrite in volcanic rocks during diagenesis (<150 °C), and it is then partially or completely converted to H_2S during the hydrothermal stage (150 to +300 °C) via redox reactions involving Fe^{+2} and carbon in the wallrocks:

$$CaSO_4 + 8(Fe^{+2})_{rk} + 10H^+ \text{ --- } H_2S + 8(Fe^{+3})_{rk} + Ca^{+2} + H_2O \quad (4)$$

and

$$CaSO_4 + 2(C)_{rk} + 2H^+ \text{ --- } H_2S + 2CO_2 + Ca^{+2} \quad (5).$$

A minor amount of pyrite was also presumably leached from the country rocks during the hydrothermal stage. This model is supported by a variety of evidence including: the precipitation of anhydrite at temperatures as low as 25 °C during the experimental reaction of seawater and tuffaceous rocks (Mizukami and Ohmoto, 1983), and at temperatures of >150 °C in seawater-basalt experiments (see refs. in Mottl, 1983); the generally retrograde solubility of anhydrite (Holland and Malinin, 1979); and the presence of anhydrite in the outer Kuroko alteration zones (Ohmoto et al., 1983); and an increase in the Fe^{+3}/Fe^{+2} ratio of the country rocks towards the Kuroko deposits (ibid). This model implies that the majority of the H_2S in the Red Ledge fluids was produced in a restricted shallow zone,

approximately equivalent to the area of propylitic alteration, that surrounds the Red Ledge intrusion and where the rocks reached temperatures of 200 to 300 °C.

Carbonates

The isotopic compositions of 59 carbonates from the Red Ledge deposit and two from Hells Canyon are given in Table 10 and portrayed in Figure 25. The $\delta^{13}C$ and $\delta^{18}O$ ratios vary from -10.8 to 0.8 and 9.1 to 22.6 permil, respectively. The ranges in carbon and oxygen values differ according to the environment of carbonate deposition and are, respectively: -10.8 to -0.8 and 9.1 to 20.1 permil for vein dolomite and calcite; -10.0 to -3.9 and 9.4 to 11.3 permil for disseminated calcite in propylitized rocks; -4.5 to 0.0 and 9.7 to 17.6 permil for disseminated calcite associated with hematite alteration; and -2.7 and 0.8 and 15.7 and 22.6 permil for disseminated calcite in greenstone from Hells Canyon.

The distribution of $\delta^{13}C$ and $\delta^{18}O$ ratios for vein carbonates is strongly skewed, as is evident in Figure 25. A majority of the analyses are concentrated in a field defined by $\delta^{13}C$ values ranging from -7 to -11 permil and $\delta^{18}O$ values ranging from 9 to 11 permil, whereas the remainder are uniformly distributed over heavier values and display a general positive correlation between $\delta^{18}O$ and $\delta^{13}C$. This variability is apparently unrelated to the mineral paragenesis, although the difficulty in determining the specific temporal relationships among most carbonate samples may have obscured such a correlation. However, carbonate of relatively depleted isotopic

Table 10. Isotopic Composition of Carbonates, Red Ledge Deposit, Idaho, and Hells Canyon, Oregon-Idaho

Red Ledge Deposit

Sample No.	Min/ Stage	$\delta^{18}O$ (‰)	$\delta^{13}C$ (‰)	Comments
		Vein Mineralization		
TG1-523	dol 4A	9.7	-9.8	vug filling in 2C qz;
TG1-584	dol 4A	19.1	-0.8	vug filling in 2A qz, after ba crystals;
TG1-636	dol 4A	9.8	-9.2	vug filling in 2C qz, followed by 4C cal;
TG1-682	dol 4A	9.2	-7.5	vug filling in 2C qz, after ba;
TG1-726	dol 4A?	16.8	-1.4	
TG1-755	dol 4A	9.2	-9.5	vug filling in 2C qz, followed by 4B dol;
TG1-831	dol 4A	10.8	-6.0	medial cavity filling in 2A qz;
TG1-851	dol 4A	18.7	-2.1	medial cavity filling in 2C qz, after qz druse;
TG1-1094	dol 4A	9.6	-10.2	surrounds qz crystals;
TG1-2028	cal 4B	9.9	-10.4	hw; cal-ch vug filling;
	cal 4B	11.0	-9.2	orange cal-py;
TG3-548	dol 4A	9.9	-10.0	medial cavity filling in 2C qz, followed by 4B dol;
TG3-810	dol 4A	15.9	-1.0	
TG3-1003	dol 4A	18.2	-3.1	cavity filling after py druse;
TG4-846B	dol 4A	10.1	-9.7	vn w/py in hematitic wallrock;
TG8-223	dol 4A	9.8	-7.6	vug filling in 2C qz;
TG9-1071	dol 4A	19.6	-1.8	cuts stringer minz;
TG10-535	dol 2C	9.5	-8.8	intergrown? w/qz;
TG10-1086	dol 4A	13.5	-1.3	cavity and vnlt filling in 2A qz;
TG10-1330	dol 4A	9.9	-7.2	white dol vug filling in 2C qz;
	dol 4A	13,2	-6.9	orange dol-sp after white dol;
TG10-1334	dol 4A	12.7	-5.3	gray dol-hm at margin of 2B qz vn;
TG10-1949	cal 4A?	17.3	-3.4	cal-qz vn in hw;
TG11-115	dol 4A	9.8	-8.7	vug filling in 2C qz followed by 4B dol;
TG11-599	dol 4A	20.1	-2.3	vug and fracture filling, after ba crystals;
TG11-994	dol 4A	9.7	-9.8	vug filling in 2C qz;
TG11-1837	dol 4A	9.9	-9.1	vug filling in 2C qz, followed by 4B-C gp;

Table 10. (continued)

TG12-931	dol 4A	9.6	-7.9	vug filling in 2C qz;
TG13-1926	dol 4A	10.1	-10.0	vug filling in 2C qz;
TG14-1193	dol 4A	17.1	-5.6	assoc. w/minor qz;
TG14-1780	dol 4A	17.7	-3.5	dol-sp-cp cavity filling after qz druse;
TG15-808	dol 4A	10.0	-7.1	vug filling w/ba, py, sp, cp and gn;
TG16-130	dol 4A	10.5	-7.5	dol-cp medial cavity filling, followed by 4B dol;
TG16-415	dol 4A	9.9	-8.0	vug and fracture filling, after ba;
	dol 4A	9.6	-8.1	vug filling in 2C qz, after ba;
TG16-1069	dol 4A	20.1	-1.4	dol-ch-sp-cp cavity and fracture filling;
TG16-1483	dol 4A	9.1	-8.0	vuggy, cuts stringer minz;
TG17-364B	dol 4A	13.7	-1.8	dol-py vnlts in 2A qz, after ba;
TG17-563	dol 4A	10.9	-3.6	medial cavity filling in 2A qz;
	dol 2C	9.4	-10.0	marginally replaced qz;
TG18-261	dol 4A?	13.8	-5.6	vuggy;
	dol 2B-C	9.6	-9.7	cuts 2A qz-py-sr;
TG18-286	dol 4A	10.0	-8.8	on 2C qz crystals, followed by 4C cal;
TG18-331	dol 4A	14.7	-1.2	vug filling in 2C qz;
TG18-523	dol 4A	9.7	-9.6	vug filling in 2C qz;
TG18-722	dol 4A	17.6	-2.6	vnlts in 2A qz;
TG19-622	cal 4A?	9.1	-4.4	qz-cal vnlt in Cordwood Rhyolite;
TG20-1986	cal 4A	11.1	-1.7	amygdules and veins in hw flow;
H4-220C	dol 4A	16.7	-1.0	dol-sp-py after ba crystals;
H4-360	dol 4A	9.6	-9.3	vug filling after ba in 2C qz;
RLC1-442	dol 4A	9.6	-9.4	after? ba in vugs of 2A qz;
		Disseminated		
TG4-937	cal	12.7	-3.7	hm-cal altered clast;
TG9-1201	cal	17.6	-0.8	hm-cal altered clast;
TG9-1208	cal	9.7	-4.5	
TG9-1339	cal	12.7	0.0	
TG10-1761	cal	9.4	-5.6	propylitized mafic flow;
TG13-597	cal	10.2	-4.1	propylitized QFP;
TG20-570	cal	11.0	-6.1	propylitized QFP;
RL4-79	cal	11.3	-10.0	propylitized QFP;
RL2-81	cal	9.8	-3.9	propylitized mafic flow;

Table 10. (continued)

Hells Canyon[1]

VC-224	cal	22.6	-2.7	Triassic spilite;
VC-265	cal	15.7	0.8	Triassic spilite;

****

[1]Samples from Tracy Vallier, U. S. Geological Survey, described in Vallier and Batiza, 1978.

Abbreviations: ba-barite; cal-calcite; ch-chlorite; cp-chalcopyrite; dol-dolomite; gp-gypsum; hm-hematite; hw-hangingwall; py-pyrite; QFP-quartz-feldspar-porphyry; qz-quartz; sp-sphalerite; sr-sericite; vn-vein; vnlt-veinlet;

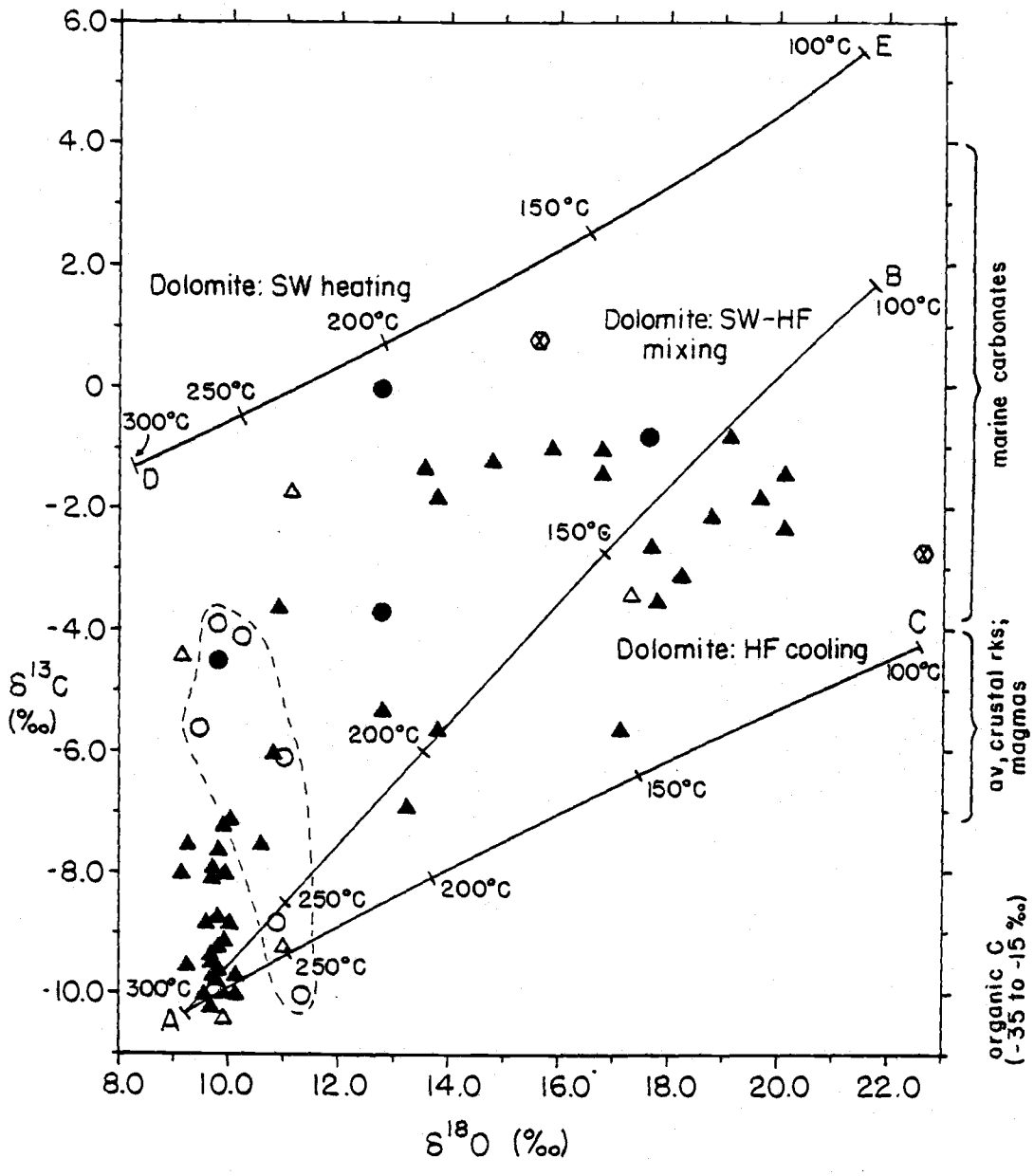

Figure 25. Isotopic composition of carbonates in the Red Ledge deposit and in volcanics of the Seven Devils Group, Hells Canyon. Lines A-B, A-C, and D-E represent the calculated composition of dolomite for three limiting cases (refer to text). vein dolomite (solid triangles); vein calcite (open triangles); calcite in propylitized QFP (open circles); calcite associated with hematitic alteration (dots); calcite in Hells Canyon greenstone (hexagons);

composition ($\delta^{13}C < -7$ $^{o}/_{oo}$ and $\delta^{18}O < 11$ $^{o}/_{oo}$) is largely restricted to the central portion of the stockwork system, whereas the carbonate distinguished by more enriched compositions is present in both the central and peripheral areas of the stockwork zone. Consequently, the admixture of carbonate with distinct isotopic compositions implies that the $\delta^{13}C$ and $\delta^{18}O$ ratios of the carbonate varied with time.

Models of Isotopic Variations

The $\delta^{13}C$ ratios of hydrothermal carbon-bearing minerals may vary because of changes in T, pH, fO_2, and I, and in a manner analagous to variations in the $\delta^{34}S$ ratios of sulfur-bearing minerals (Ohmoto, 1972). This relationship results from the effects of the physiochemical parameters on the proportion of oxidized to reduced carbon species and the large fractionation factors between oxidized and reduced species. Additionally, variations in mineral $\delta^{13}C$ compositions may be produced by mixing carbon from isotopically distinct reservoirs.

If the pH and fO_2 of the fluids in equilibrium with the Red Ledge carbonates were similar to those of the early vein fluids, or 4.2 to 5.7 and -33 to -35 log units, respectively (Fig. 19), then oxidized carbon species (CO_2, H_2CO_3, HCO_3^-, and CO_3^{2-}) comprised 90% or more of the total carbon species in the fluids (see Fig. 10 in Ohmoto, 1972). Furthermore, thermochemical calculations by Reed (1983; 1984, pers. comm.) indicate that seawater in equilibrium with basalt at 300 °C and a water/rock ratio of 18 contains $10^{-2.44}$ m of

H_2CO_3 (ap) (or $H_2CO_3 + CO_2$), the most abundant oxidized carbon compound, and $10^{-11.35}$ m of CH_4, the most abundant reduced carbon compound. These theoretical results are consistent with the presence of abundant CO_2, and undetectable quantities of CH_4, in vapor-liquid inclusions of Kuroko stockwork minerals (Pisutha-Arnond and Ohmoto, 1983). Consequently, both thermochemical considerations and data from analagous deposits suggest that H_2CO_3 (ap) was the most abundant carbon species in the Red Ledge fluids and that CH_4 was present in negligible amounts. Thus, the isotopic variability that characterizes the vein carbonates was largely produced by changes in the $\delta^{13}C$ ratio of total carbon and (or) T, rather than by fluctuations in pH, fO_2, or I.

In the geologic setting of the Red Ledge deposit, appreciable variations in $\delta^{13}C_{\Sigma C}$ might be reasonably ascribed to the mixing of hydrothermal fluids (HF) and seawater (SW), and variations in T might have resulted from either mixing or nonmixing mechanisms. In order to identify the probable cause(s) of the isotopic variability among the vein carbonates, the range in the isotopic composition of dolomite was calculated for three limiting cases: SW-HF mixing, the cooling of HF, and the heating of SW. The method of calculation first involved estimating the concentration and isotopic composition of the carbon species in SW during Early Permian time and in HF during stage 4 carbonate precipitation. Then, the $\delta^{13}C$ and $\delta^{18}O$ ratios of the dolomite were computed from the $\delta^{13}C$ composition of H_2CO_3 (ap) and the $CaMg(CO_3)_2$-CO_2 fractionation curve for carbon isotopes (Ohmoto and Rye, 1979), and from the $\delta^{18}O$ composition of the fluid and the $CaMg(CO_3)_2$-H_2O fractionation curve for oxygen isotopes

(Northrop and Clayton, 1966), respectively. In the case of fluid mixing, the T of the solution was calculated from equation a in Table 7 , and the $\delta^{18}O$ of the fluid mixture and the $\delta^{13}C$ of the H_2CO_3 (ap) $_{mix}$ were calculated from equations analagous to b and c in Table 7, respectively.

The concentration of carbon in the Early Permian oceans was assumed to have been similar to that of the modern oceans, or 0.0024 m of oxidized species (primarily HCO_3^-) and a negligible amount of reduced species (Holland, 1978). Furthermore, isotopic studies of ancient limestone and carbonate fossils indicate that the $\delta^{13}C$ value of oceanic carbon and the $\delta^{18}O$ ratio of ocean water have remained relatively constant at 0 +/- 4 $^{o}/oo$ through at least the Mesozoic and Cenozoic Eras (Taylor, 1979; Ohmoto and Rye, 1979). The calculations by Reed suggest that the Red Ledge hydrothermal fluids contained approximately $10^{-2.44}$ (0.0036) m of H_2CO_3 (ap). The large proportion of vein carbonates with isotopic compositions limited to $\delta^{13}C$ values between -10.5 and -8.5 permil, and $\delta^{18}O$ values between 9 and 10 permil, suggests that these carbonates may have equilibrated with H_2CO_3 (ap) of essentially hydrothermal origin. Thus, if the sample with the most depleted isotopic composition best represents hydrothermal dolomite, then the hydrothermal H_2CO_3 (ap) had a $\delta^{13}C$ value of about -9.0 $^{o}/oo$ at 300 °C.

The results of the computations regarding the potential causes of isotopic variability among the Red Ledge carbonates are portrayed in Figure 25 along with the analytical results. The variation in the isotopic composition of dolomite resulting from SW-HF mixing is depicted by line A-B, that resulting from HF cooling is represented

by line A-C, and that resulting from SW heating is expressed by line D-E. From the relationships portrayed in Figure 25, it is apparent that the progressive mixing of seawater and hydrothermal fluids can account for the range and overall trend in the isotopic composition of the Red Ledge vein carbonates. By contrast, cooling the hydrothermal fluids from 300 to 100 °C and heating seawater from 100 to 300 °C can result in dolomite with $\delta^{13}C$ values that are respectively depleted and enriched in ^{13}C relative to Red Ledge vein carbonates with a comparable $\delta^{18}O$ ratio. Thus, the mixing of seawater and hydrothermal fluids was the predominant cause of the isotopic variability among the Red Ledge carbonates.

Because the differences between the $\delta^{13}C$ ratios of seawater and hydrothermal H_2CO_3 (ap) (9 $^{o}/oo$) was appreciably larger than the difference in $\delta^{18}O$ values of seawater and hydrothermal fluid (1.0 $^{o}/oo$), the extent of mixing was primarily recorded by the $\delta^{13}C$ composition of carbonate. As a corollary relationship, the temperature of carbonate deposition was primarily expressed in the $\delta^{18}O$ ratio of the carbonate because fractionation of oxygen isotopes between carbonate and water varies (antipathetically) with temperature. Therefore, the scatter of analytical data about the mixing curve in Figure 25 may indicate that the SW-HF solutions were locally heated or cooled after fluid mixing and prior to carbonate precipitation. For example, an increase in T would have produced a shift to lower $\delta^{13}C$ and $\delta^{18}O$ ratios along a trend parallel to line D-E in Figure 25, and a decrease in T would have resulted in a shift to higher ratios along a trend parallel to line A-C.

The interpretation that the isotopic variability of the vein carbonates resulted primarily from the mixing of seawater and hydrothermal fluid provides three important inferences.

1. Seawater infiltrated the stockwork system to depths of at least 1000 feet below the seafloor during the last major stage of hydrothermal mineral deposition. This ingress of seawater was probably related to the waning of the thermal anomaly. If so, the collapse of the convection cell resulted in the overprinting of the isotopically heavy and paragenetically late carbonate, which contains a significant amount of seawater H_2CO_3 (ap), on the isotopically light and paragenetically early carbonate, which consists of a high proportion of hydrothermal H_2CO_3 (ap). Furthermore, those vein barites which contain a considerable amount of seawater sulfate were probably coeval with the isotopically enriched vein carbonates and, thus, the interval of vein barite deposition may have overlapped that of the vein carbonates to a greater extent than shown in Figure 15.

2. The maximum fraction of seawater in the SW-HF solutions was 60%, and the minimum temperature of dolomite precipitation was 115 °C.

3. The local heating of the SW-HF mixtures may have been an important mechanism for the deposition of vein carbonate, as inferred from the preponderance of samples with $\delta^{18}O$ values less than those predicted by the mixing model (line A-B). Such a mechanism is consistent with the strong retrograde solubilities of dolomite and calcite (Holland and Malinin, 1979). However, the absence of carbonate in strata-bound mineralization suggests that the effect of cooling on the solubilities of dolomite and calcite was greater than

those of an increase in Ca^{++}, Mg^{++}, and HCO^{-}_{3} activities as a result of seawater-hydrothermal fluid mixing in the vicinity of the sea-floor.

Disseminated calcite in propylitized rocks is characterized by a wide range of $\delta^{13}C$ ratios (-10.0 to -3.9 $^{o}/_{oo}$) but a relatively limited range of $\delta^{18}O$ ratios (Figure 25). Two samples have $\delta^{13}C$ compositions that are similar to those of "hydrothermal" vein dolomite. These light values and the variability of the $\delta^{13}C$ data imply that the disseminated calcite consists of different proportions of "hydrothermal" carbon and carbon of probable seawater derivation (see discussion under Source of Hydrothermal Carbon). Moreover, the consistency of the $\delta^{18}O$ ratios suggests that the disseminated calcite precipitated over a restricted range of temperatures, most likely between 250 and 300 °C. Thus, fluid mixing in the zone of propylitic alteration did not involve cold pristine seawater but seawater that had been heated during its convection through hot crustal rocks (the origin and isotopic evolution of fluids in the propylitic zone is discussed further in a subsequent section on Origin of Fluid and Rock Compositions.

Unlike their counterpart in propylitized rocks, disseminated calcite in hematitically altered rocks and in greenstone do not exhibit a distinct trend with respect to their isotopic compositions. However, most of the samples analyzed have $\delta^{13}C$ ratios between -4 and +1 permil and $\delta^{18}O$ ratios between 12 and 23 permil. Such relatively heavy ratios may indicate a seawater influence and depositional temperatures in the range of 100 to 200 °C.

Source of Hydrothermal Carbon

The oxidized carbon in the Red Ledge hydrothermal fluids may have been originated from: 1) a magmatic source, 2) the oxidation and leaching of carbon in the country rocks, and (or) 3) the dissolution of limestone. The typical ranges of $\delta^{13}C$ compositions for carbon (Ohmoto and Rye, 1979) from these reservoirs are depicted in Figure 25. The $\delta^{13}C$ ratio of carbon in the Red Ledge hydrothermal fluids (-9 $^{o}/_{oo}$) is intermediate between that of organic carbon and carbon in magmas or in average crustal rocks. This comparison suggests that the hydrothermal carbon was probably leached from rocks of the Hunsaker Creek Formation, which consists primarily of volcanic and epiclastic sedimentary lithologies. The contribution of carbon from organic matter to the fluids is inferred to have been minor, but significant relative to that from igneous rocks, because the $\delta^{13}C$ composition of the dissolved carbon is slightly less (by 2 to 5 $^{o}/_{oo}$) than the $\delta^{13}C$ composition of igneous carbon. Such an inference is consistent with the paucity of organic-rich sedimentary rocks in the Hunsaker Creek Formation and in stratigraphic assemblages near modern volcanic island arcs.

Reduced carbon may be incorporated into hydrothermal fluids through either oxidation or hydrolysis reactions (Ohmoto and Rye, 1979). The former mechanism would probably result in CO_2 with an $\delta^{13}C$ composition similar to that of the reduced carbon, whereas the latter process may yield CO_2 at temperatures between 350 and 600 °C that is 3 to 12 $^{o}/_{oo}$ heavier than that of the reduced carbon (Ohmoto and Rye, 1979). Both types of reactions probably contributed

oxidized carbon species to the Red Ledge hydrothermal system. For example, the redox reaction represented by equation 7, the reduction of $SO_4^=$ to H_2S and the oxidation of C_{rk} to CO_2, probably operated in a restricted, shallow zone around the Red Ledge intrusive complex and at temperatures generally between 200 and 300 °C. Both oxidation and hydrolysis reactions were presumably important at deeper levels within the volcanic pile where temperatures in the 350-450 °C range prevailed.

It is possible that the hydrothermal carbon in the Red Ledge fluids was derived from a crystallizing magma with a slightly unusual $\delta^{13}C$ composition (e.g. -9 $^{o}/_{oo}$). For instance, magmas generated through the partial melting of graphitic source rocks may have a $\delta^{13}C$ composition different from those of magmas formed by the partial melting of "average" crustal rocks (Ohmoto and Rye, 1979). Such a magma would have an oxidation state slightly below the quartz-fayalite-magnetite (QFM) buffer (Ohmoto and Rye, 1979). However, if the sulfur in the Red Ledge system ($\delta^{34}S_{fluid}$ = 6-23 $^{o}/_{oo}$) were also derived from a magma, then an oxidation state slightly above the QFM buffer is required.

Silicates and Whole Rocks

The oxygen isotopic composition of 69 separates of hydrothermal quartz are presented in Table 11 and the $\delta^{18}O$ and δD compositions of 5 sericite and 4 chlorite separates are listed in Table 12. The oxygen isotope ratios of sulfates and carbonates were presented and

Table 11. Oxygen Isotopic Composition of Quartz

Sample No.	Stage	$\delta^{18}O$ (‰)	Comments
		Vein Mineralization	
TG1-523	2C	12.2	
TG1-579	1	8.1	amethyst clots in 2A-B minz;
TG1-584	2A	11.8	
TG1-682	2C	10.6	cuts 2A qz;
TG1-726	2A	9.6	
TG1-831	2A	11.4	
TG1-1701	2C	11.8	cuts stringer minz;
TG1-2028	2C?	13.3	
TG3-460	2A	11.4	vugs filled by 4A dol-py and 4C cal;
TG3-548	2C	11.6	
TG3-810	2B	11.1	
TG3-939	1	7.0	amethyst-white qz in 2B minz;
	1&2A	8.9	
TG4-846A	2C	12.5	qz-ba-cp cutting hematitic wallrock;
TG5-1148	2C	10.0	
TG5-1305	2B	12.4	abundant py-cp;
TG5-1311	2A	10.8	
TG8-88	2C	12.3	vuggy, cutting stringer minz;
TG8-223	2C	12.6	vuggy, cutting weak stringer minz;
TG9-643	2C	11.6	vuggy w/trace dol.
TG9-1409	3-4A?	14.0	clear terminations in vugs, cutting stringer minz;
TG10-259	2C	11.9	vuggy;
TG10-535	2A	11.3	
	2C	12.3	
TG10-1086	2A	11.5	
TG10-1107	2C	12.1	
TG10-1334	2B	12.1	
TG10-1678	2C	12.0	cuts massive minz;
TG11-115	2C	12.7	vuggy;
TG11-599	1	9.1	amethyst w/minor 2A qz;
	2A	11.5	
TG11-994	2A	12.1	
	2C	11.9	cuts 2A minz;
TG11-1436	2C	11.9	some vugs filled w/4A dol;
TG11-1837	2C	12.2	
TG12-931	2C	11.7	cuts hematitic wallrock;
TG13-1926	2C	12.6	
TG14-1731	2C	12.2	
TG15-808	2C	12.4	
TG16-130	2A	11.2	
TG16-415	2A	11.6	w/blebs of py and cp;
	2C	12.1	

Table 11. (continued)

TG16-1386	2C?	11.9	
TG17-364B	2A	11.1	cut by 2B minz and 4A dol;
TG17-406	2A	10.9	
TG17-563	2A	10.9	
	2C	11.6	
TG18-261	2C	11.6	vuggy, cuts dol vein;
TG18-286	2A	11.7	cut by 2B cp-py stringers;
	2C	11.7	open vuggy, capped by dol, py, cp, and cal;
TG18-331	2A	11.2	
	2C	10.1	cuts 2A qz vein;
TG18-523	2B	11.3	gray qz-py-cp;
	2C	12.1	cuts 2B minz;
TG18-722	2A	11.3	
H4-360	2C	11.7	
H4-637	2A	10.3	
SS105-310 360B	2A	10.8	
SS105-310 360C	1&2A	9.0	
SS105-310 360E	2C	11.8	vuggy;
SS151-707	2C	12.0	dol in vugs; cuts hematitic alteration;
RLC1-442	2C	12.4	
RL-UT-D4B	2C	12.1	hangingwall;
RL-FZ	2B	11.3	cuts QFP intrusion;
		Stringer Mineralization	
TG6-751		10.6	
TG9-1471		13.6	
TG16-1386		11.1	
		Massive Mineralization	
TG10-1678		11.8	qz-ba and ba-sp-py layers;
TG12-1438		13.0	chert fragment in sulfide minz;
TG16-1518		11.6	chert;

****

Abbreviations: ba-barite; cal-calcite; cp-chalcopyrite; dol-dolomite; minz-mineralization; py-pyrite; qz-quartz; sp-sphalerite;

discussed previously in the sections on Sulfides and Sulfates, and Carbonates, respectively.

The $\delta^{18}O$ ratios of hydrothermal quartz range from 7.0 to 14.0 permil. A paragenetic effect is evident in the data for vein samples, as shown in Figure 26: stage 1 quartz averages 8.4 $^{o}/oo$, stage 2A quartz 11.2 $^{o}/oo$, stage 2B quartz 11.6 $^{o}/oo$, and stage 2C quartz 11.9 $^{o}/oo$. This temporal influence is supported by analyses of crosscutting quartz veins from the same hand specimen. Eight of nine such comparisons yielded either identical values, within the uncertainty of the analytical techniques, or a positive shift up to 2.4 $^{o}/oo$ in $\delta^{18}O$ with increasing relative time (Table 11). Stringer quartz and syngenetic chert average 11.8-11.9 permil and, therefore, are isotopically indistinguishable from vein quartz of stage 2C. Because of this similarity and the superposition of vein quartz with distinct isotopic signatures, there is little evidence for the zonation of $\delta^{18}O$ values in hydrothermal quartz throughout the Red Ledge deposit.

The oxygen isotopic compositions of chlorite and sericite from hydrothermally altered rocks, as listed in Table 12, are uniform (7.4 - 8.5 $^{o}/oo$) and similar to that of chlorite associated with chert (7.5 $^{o}/oo$), but distinct from those of vein chlorite (5.8 $^{o}/oo$), exhalitive chlorite (4.5 $^{o}/oo$), and chlorite from a post-mineralization dike (9.4 $^{o}/oo$). However, sericite is isotopically enriched in deuterium (δD = -56 to -52 permil) relative to chlorite (δD = -72 to -63 permil), irrespective of the environment in which the phyllosilicate formed.

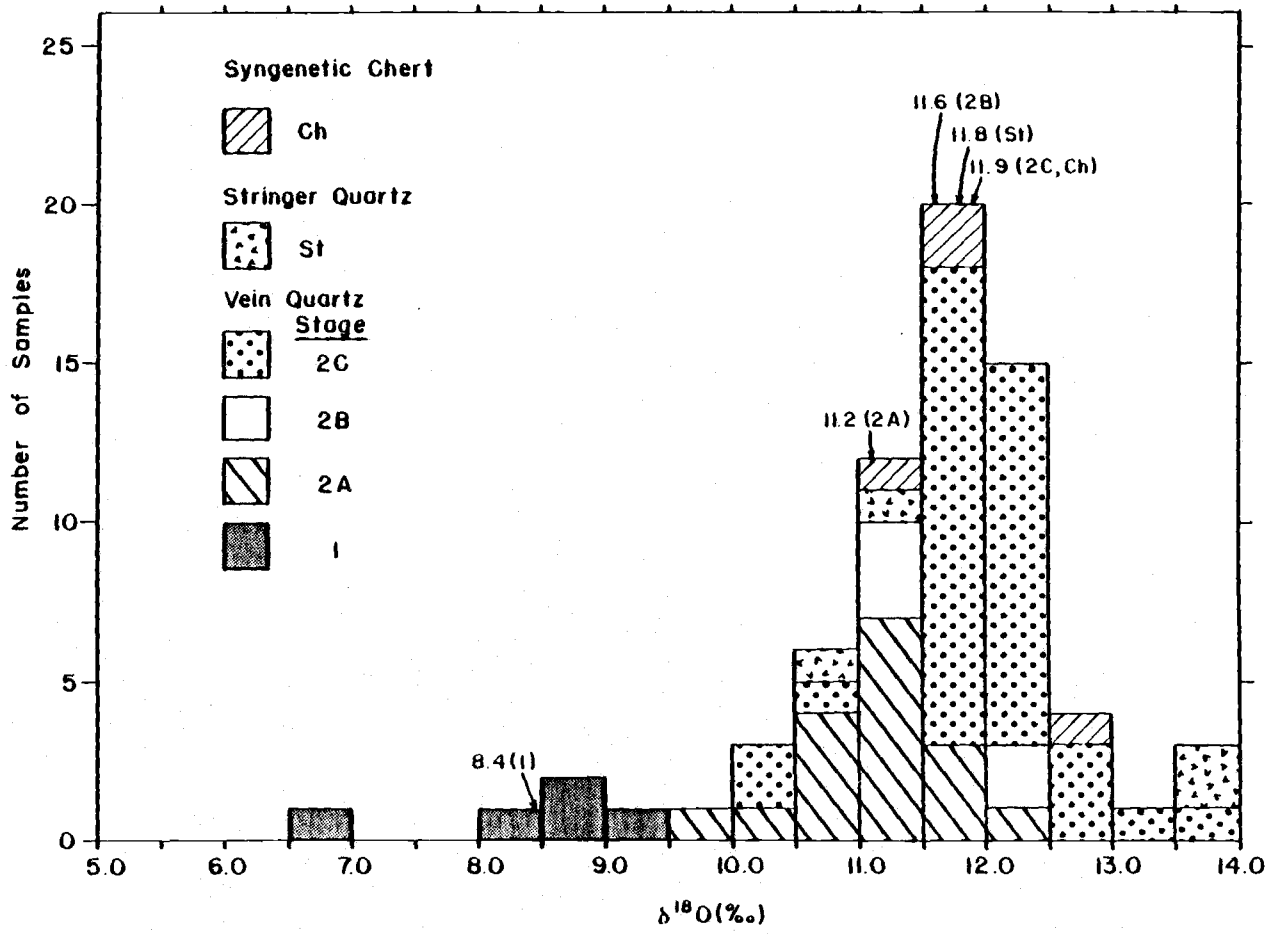

Figure 26. Distribution of $\delta^{18}O$ ratios for hydrothermal quartz as distinguished by mineralization type and paragenetic stage.

****

Table 12. Oxygen and Hydrogen Isotopic Composition of Phyllosilicates

Sample No.	Min	$\delta^{18}O$ (‰)	δD (‰)	Comments
TG2-1519	sr	8.5	-52	felsic tuff, SR
TG7-284	ch	7.8	-66	chert exhalite
TG9-1332	ch	7.4	-69	chloritized tuff
TG10-259	sr	8.5	-53	QFP, SR
TG11-115	sr	9.4	-72	post-minz. dike
TG11-1816	sr	8.3	-56	felsic tuff, SR
TG17-779	sr	7.8	-52	felsic lapilli tuff, SR
RLC1-262	ch	5.8	-63	chlorite in vein quartz
RL5-79	ch	4.5	-65	ch-qz-hm-ba exhalite

Abbreviations: ba-barite; ch-chloride; hm-hematite; qz-quartz; sr-sericite; SR-sericite alteration;

****

Hydrothermal Fluids

The $\delta^{18}O$ and δD values of a hydrothermal fluid can be estimated from the isotopic ratios of precipitated phases, mineral depositional temperatures, and relevant equations that express mineral-H_2O fractionations as a function of temperature. Furthermore, variations in the isotopic composition of the fluids can be estimated if the appropriate sample coverage and paragenetic data are available. This procedure implicitly assumes that equilibrium isotopic exchange occurred in an open system (such as a convecting fluid cell) and that the original isotopic ratios were preserved in the material analyzed.

By this method, the $\delta^{18}O$ and δD values were calculated for fluids in equilibrium with the various mineralization, alteration, and paragenetic assemblages in the Red Ledge deposit. The results are presented in Table 13, along with the parameters and uncertainties involved in the calculations and depicted in Figure 27. The

Table 13. Isotopic Composition of the Hydrothermal Fluids Responsible for the Red Ledge Mineralization and Alteration

Mineral(A) Stage	T°C	$\delta^{18}O(A)$ x (1s)	$\delta^{18}O(H_2O)^4$ x (+/-)[5]	$\delta D(A)$ x	$\delta D(H_2O)^4$ x
		Vein Mineralization			
Quartz 1	268[1]	8.1 (0.6)	0.0 (1.7)		
Quartz 2A	300[3]	11.2 (0.6)	4.3 (1.5)		
Quartz 2B	290[3]	11.6 (0.6)	4.2 (1.6)		
Quartz 2C	279[1]	11.9 (0.7)	4.2 (1.7)		
Chlorite	275[3]	5.8 (0.6)	5.3 (1.0)	-63	-16
H. Barite 3	275[2]	8.7 (0.6)	4.9 (1.4)		
E. Dolo 4A	279[1]	9.8 (0.4)	0.7 (1.4)		
L. Dolo 4A	250-100[3]	12.7 to 20.1	2.4 to -1.4		
		Stringer Mineralization			
Quartz	250[3]	11.8 (0.6)	2.8 (1.8)		
		Massive Mineralization			
Quartz	250[3]	11.9 (0.6)	2.9 (1.8)		
		Wallrock Alteration			
Sericite	300[3]	8.3 (0.6)	4.9 (1.2)	-53	-5
Calcite	250[3]	10.4 (0.8)	3.1 (1.8)		

1. Fluid inclusion data; 2. Sulfur isotopic geothermometry; 3. Analogy to equivalents in Kuroko ore; 4. Mineral-water (A-H_2O) fractionations for quartz (Matsuhisa et al., 1979), chlorite (Wenner and Taylor, 1971 for $\delta^{18}O$; Taylor, 1974, Fig. 4 for δD), dolomite (Northrop and Clayton, 1966), barite (Kusakabe and Robinson, 1977), anhydrite (Chiba et al., 1981), sericite (O'Neil and Taylor, 1969 for $\delta^{18}O$; Suzuoki and Epstein, 1976 for δD), and calcite (O'Neil et al., 1969); 5. Total uncertainty expresses range of values resulting from an assumed uncertainty of ±25°C for T plus ±1s for $\delta^{18}O(A)$ (0.6 denotes an assumed value for populations of four or less).

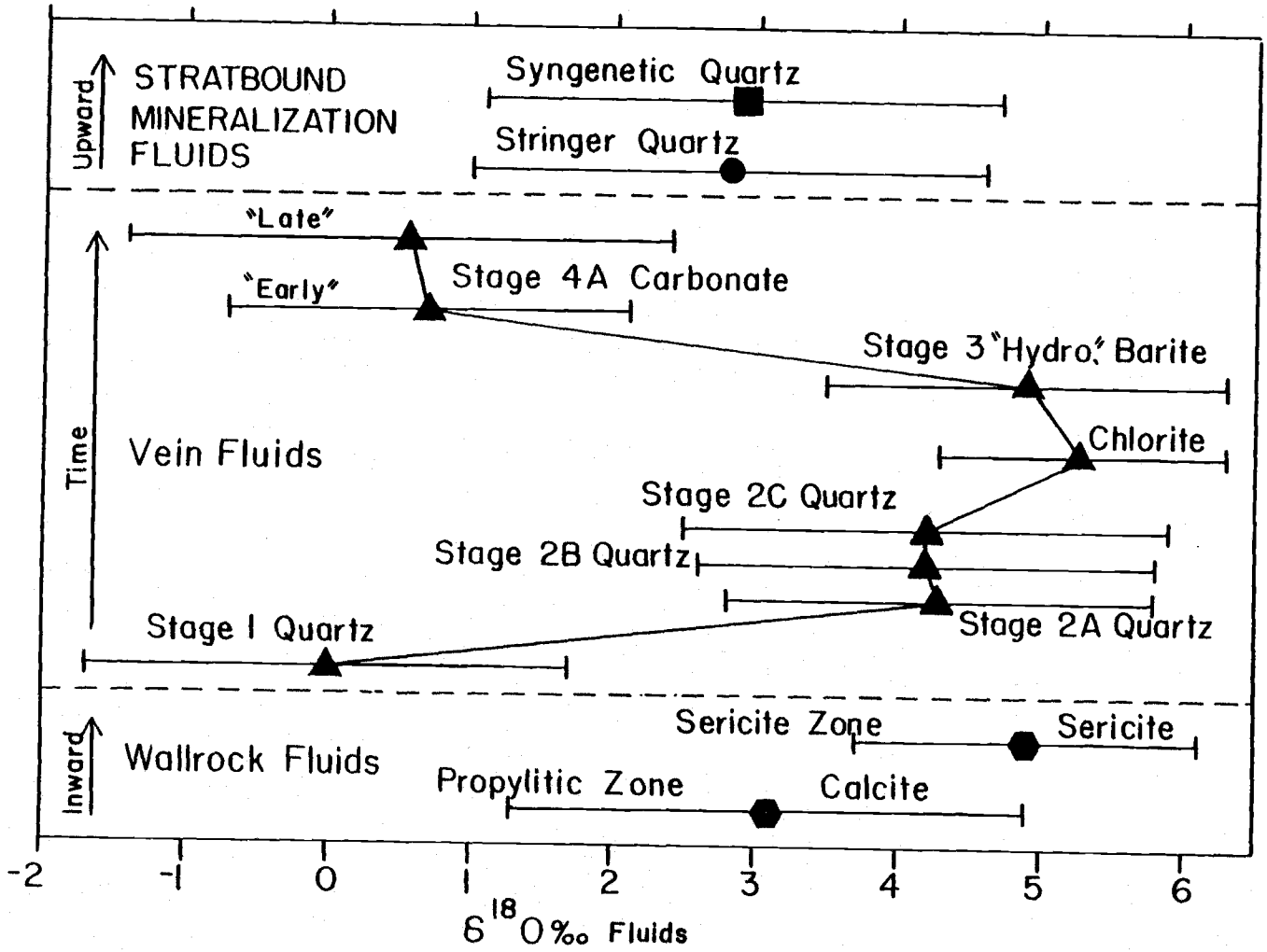

Figure 27. Oxygen isotopic composition of the fluids in equilibrium with various alteration, paragenetic, and mineralization assemblages.

oxygen isotopic composition of the fluids was derived from the average $\delta^{18}O$ ratio for the various occurrences and stages of quartz, dolomite, calcite, sericite and chlorite, and from the $\delta^{18}O$ value of the vein barite sample which isotopically approximates "hydrothermal" barite (see Mixing of Seawater-Hydrothermal Fluid). The mineral depositional temperatures listed in Table 13 are based on fluid inclusion and isotopic geothermometric data from the Red Ledge deposit (see Fluid Inclusions and Isotopic Equilibria) and by analogy to depositional temperatures for equivalent Kuroko mineralization. Pisutha-Arnond and Ohmoto (1983) described a generalized four-stage thermal history for Kuroko mineralization that was based on a fluid inclusion and paragenetic study of stockwork phases from several deposits. Stage 1 (minor quartz-pyrite) deposition occurred at 200 +/-50 °C, Stage 2 (sphalerite-pyrite-galena+/ -barite+/-quartz) at 290 +/- 50 °C, Stage 3 (quartz-chalcopyrite) at 330 +/- 30 °C, and Stage 4 (minor sphalerite-anhydrite-calcite) at 280 +/- 20 °C. Sulfide and quartz in massive Kuroko ore were deposited at approximately 250 °C, whereas phyllic alteration of the wallrocks occurred at about 300 °C (Kajiwara, 1971; Mukaiyama et al., 1974; Tokunaga and Honma, 1974; Marutani and Takenouchi, 1978; Kusakabe and Chiba, 1979, 1983; Hattori and Muelenbachs, 1980). The total uncertainty in the $\delta^{18}O$ ratios for the Red Ledge fluids is based on an assumed uncertainty of +/-25 °C in the depositional temperatures plus an uncertainty of +/- one standard deviation (1s) about the mean $\delta^{18}O$ value for the mineral. A standard deviation of 0.6 was assumed for populations of 4 isotopic analyses or less.

Average ^{18}O ratios of the Red Ledge vein fluids show a marked temporal variation from 0 permil during early (stage 1) amethyst quartz deposition, up to 4 to 5.5 permil during intermediate (stages 2-3) quartz-sulfide, quartz-chlorite-(dolomite), and barite precipitation, and finally to values near 0 permil during late (stage 4) carbonate formation (Fig. 27). The hydrogen isotopic composition of the vein fluids was approximately -14 $^{o}/_{oo}$ (Table 13). It is possible that the temporal variation in the fluid $\delta^{18}O$ ratios was, at least partially, induced by the assumed mineral depositional temperatures. However, the trend of ^{18}O enrichment and depletion is apparent even when plausible uncertainties are included in the calculations (Fig. 27). Furthermore, if stage 1 quartz formed between 270 and 300 °C, as suggested by fluid inclusion data, and the fluids remained constant at 0 $^{o}/_{oo}$, then the minerals of stages 2 and 3 must have precipitated around 200 °C. According to Pisutha-Arnond and Ohmoto (1983), this temperature trend and value are in the opposite direction and improbably low for major quartz-pyrite-chalcopyrite deposition in the stockwork system of Kuroko deposits. Similarly, if the fluid composition remained constant at 4 to 5 permil throughout the period of carbonate formation, then early dolomite deposition occurred at a temperature of about 400 °C. Such a temperature is unusually high for carbonate precipitation in most hydrothermal deposits. Conversely, if the temperature was approximately 275 °C over the interval of early and late dolomite deposition, then the $\delta^{18}O$ values of the fluids must have increased from 1 to 11 permil. However, the addition of a 10 $^{o}/_{oo}$ fluid (e.g. magmatic) is unlikely during the waning phase of hydrothermal activity

at the Red Ledge deposit. Therefore, it is probable that both a depletion of ^{18}O in the fluids and a decrease in temperature produced the range of $\delta^{18}O$ values in vein dolomite and calcite.

Wallrock fluids in the phyllic alteration zone had an approximate composition of $\delta^{18}O$ = 4.9 °/oo and δD = -5 °/oo and, thus, isotopically resembled those vein fluids associated with mineral deposition of stages 2 and 3 (Fig. 27). Fluids in the propylitic alteration zone, and those associated with stringer and syngenetic quartz deposition, were characterized by $\delta^{18}O$ ratios of about 2.5 to 3.5 permil (Fig. 27), implying that they were of different origin than the bulk of the vein fluids.

The isotopic composition of the Red Ledge fluids and the trend of ^{18}O enrichment and depletion is similar to those of the Kuroko fluids: $\delta^{18}O$ = -3 +/- 3 °/oo during Stage 1, 1 +/- 2 °/oo throughout Stages 2 and 3, and -4 +/- 4 °/oo during Stage 4, and δD = -30 to +15 permil (Pisutha-Arnond and Ohmoto, 1983). Isotopically, the Red Ledge fluids most closely resemble seawater ($\delta^{18}O$ and δD = 0 °/oo) but are different than magmatic water ($\delta^{18}O$ = 5 to 10 °/oo and δD = -85 to -40 °/oo), metamorphic water ($\delta^{18}O$ = 5 to 25 °/oo and δD = -65 to -20 °/oo) and most meteoric water ($\delta^{18}O$ < -5 °/oo and δD < -30 °/oo) (Taylor, 1979).

Whole Rocks

The $\delta^{18}O$ ratios of 27 rocks from the Red Ledge area and various localities in Hells Canyon range from 5.3 to 12.2 permil (Table 14).

Table 14. Oxygen Isotopic Composition of Samples of Whole Rocks and Phenocryst Phases

Sample No.	$\delta^{18}O$ (‰) wh rk	qz ph	pl ph	Alt Facies	Comments
		Red Ledge Area			
TG1-1494	10.2			PR	interm. volcaniclastic;
TG2-1519	9.6			SR	felsic tuff w/qz-(py) vns;
TG3-239	9.8			SC	QFP intrusion;
TG4-937	12.4			S	QP cut by py stringers;
TG7-55	12.2			S	QP in stringer minz;
TG7-220		8.6		S	QP in stringer minz;
TG8-529	8.3			SC	mafic flow;
TG9-1332	7.6			SC	interm. tuff;
TG10-259	9.6			SR	QFP intrusion;
TG10-820	8.4			SR	QP tuff;
TG10-1761	8.3			PR	mafic flow;
TG11-115	8.9	8.6	8.6	PR	post-minz dike;
TG13-597	10.4	9.3	11.8	PR	QFP intrusion;
TG14-472	10.7			PR	QFP intrusion;
TG15-808	11.9			S	QFP volcaniclastic;
TG17-182	10.8			SC	QFP intrusion;
TG19-622	10.5			PR	Cordwood Rhyolite Intr.;
TG20-570	10.3	7.8	9.8	PR	QFP flow;
RL4-79	11.2			PR	QFP intrusion;
RL5-79	5.3			EX	ch-qz-hm-ba exhalite;
RL2-81	8.5			PR	mafic flow;
		Hells Canyon Inlier[1]			
LS9-12	9.1				Permian spilite;
VC-197	10.0				" "
VC-79	10.7				Triassic spilite;
VB-87	10.5				" "
VC-224	8.8				" "
VC-265	9.8				" "
VS3-1	9.8				" "
VS3-6	10.6				Triassic keratophyre;

[1]Samples from Tracy Vallier, U.S. Geological Survey, described in Vallier and Batiza (1978).

Abbreviations: ba-barite; ch-chlorite; Ex-exhalite; hm-hematite; ph-phenocryst; pl-plagioclase; PR-propylitic alteration; py-pyrite; SC-sericite-chlorite alteration; SR-sericite alteration; vns-veins;

Hydrothermally altered rocks near the Red Ledge have $\delta^{18}O$ compositions that correlate with the alteration assembages and rock clans as illustrated by Figure 28. Felsic and mafic rocks respectively average 10.6 °/oo and 9.0 °/oo in the propylitic alteration zone, and 9.6 °/oo and about 8.0 °/oo in the phyllic zone, whereas silicified felsic rocks in mineralized areas average 12.2 °/oo and are isotopically indistinguishable from vein quartz (Fig. 28). The mafic and intermediate volcanic rocks from Hells Canyon proper average 9.9 permil. Two samples of highly chloritic rocks exhibit the isotopically lightest compositions at 5.3 and 7.6 permil.

These results indicated that the Red Ledge mineralization is encompassed by a halo of slightly ^{18}O-depleted rocks that corresponds to the zone of phyllic alteration. An ^{18}O-depleted halo is characteristic of most volcanogenic massive sulfide deposits (Addy and Ypma, 1977; Heaton and Sheppard, 1977; Beaty and Taylor, 1980, 1982; Green et al., 1983; Urabe et al., 1983). The magnitude of the ^{18}O-depletion generally ranges from 4 to 15 permil for deposits hosted by metamorphic rocks of the zeolite facies (e.g. Kuroko, Cyprus, and Seneca), but ranges from 1 to 5 permil for those deposits hosted by rocks of greenschist or higher metamorphic grade (e.g. Amulet A, Corbet, Ducktown, and Red Ledge). This relationship implies that the oxygen isotopic composition of the outer, low temperature, ^{18}O-rich hydrothermal-metamorphic assemblages (e.g. zeolite facies) are homogenized to lower values during recrystallization to the greenschist facies, whereas that of the inner, high temperature, relatively ^{18}O-poor assemblages (e.g. quartz-sericite) is preserved because the assemblages are generally stable over a

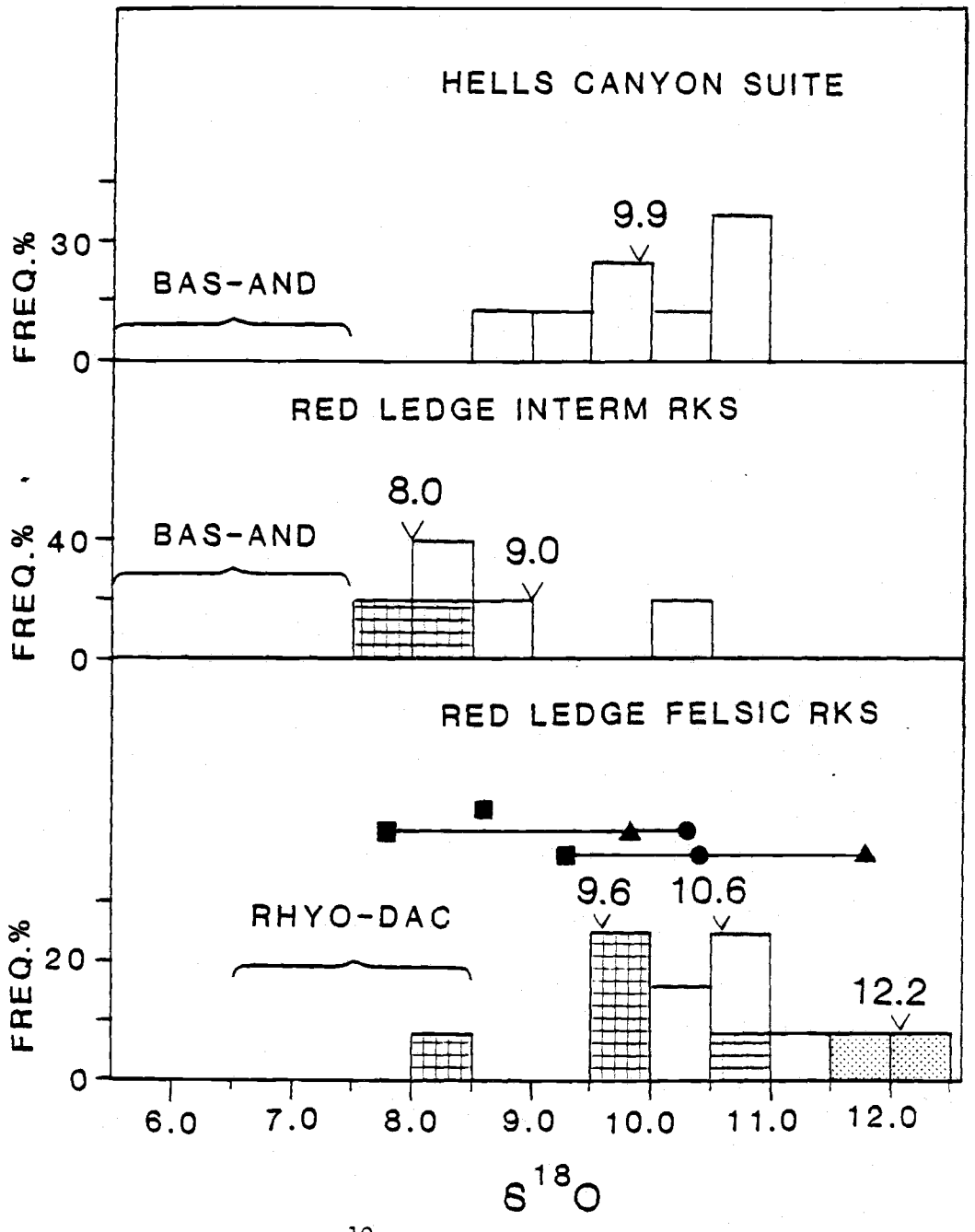

Figure 28. Histogram of $\delta^{18}O$ ratios for whole rocks from the Red Ledge and Hells Canyon areas as distinguished by secondary assemblages: silicified (stippled); phyllic (cross hatch); propylitic (R.L.) or greenschist facies (unpatterned); Also shown are ranges for fresh basalt -andesite (BAS-AND) and rhyolite-dacite (RHYO-DAC), and analyses of quartz (square) and plagioclase (triangle) phenocrysts compared to whole rock values (circles).

wider range of P-T conditions. The preservation of isotopic signatures is evident through multiple metamorphic events and at least up to P-T conditions represented by the kyanite-staurolite isograd (5 kbars, 540-690 °C), as at Ducktown, Tennessee. Thus, regional metamorphism to the greenschist facies apparently diminishes the areal extent of the ^{18}O-depletion halo and reduces the range of whole rock ^{18}O values around volcanogenic massive sulfide deposits. This relationship to metamorphic grade implies that oxygen isotopic analyses of whole rocks are less useful in the exploration for volcanogenic deposits (e.g. see Green et al., 1983) hosted by metamorphic rocks of greenschist and higher facies than they are for deposits in rocks of the zeolite facies.

Quartz phenocrysts from the Red Ledge QFP are depleted in ^{18}O compared to coexisting plagioclase feldspar phenocrysts and the parent whole rock value (Table 14 and Fig. 28). Because the quartz phenocrysts display only minor alteration and are resistant to post-crystallization isotopic exchange, their $\delta^{18}O$ values can be utilized to approximate primary mineral and whole rock $\delta^{18}O$ compositions. Quartz phenocrysts in granodiorite intrusions, and in dacite and rhyolite flows, are enriched in ^{18}O by 1.0 to 1.5 permil, whereas plagioclase feldspar is depleted by 0.0 to 2.0 permil relative to the parent melt (Taylor and Epstein, 1962; Taylor, 1968). Therefore, the $\delta^{18}O$ ratios of the Red Ledge quartz phenocrysts indicate that the primary $\delta^{18}O$ composition of QFP and plagioclase feldspar was between 6.5 and 8.5 permil. This range is consistent with that reported for their unaltered equivalents (see Taylor, 1968), as shown in Figure 28. Protoliths of mafic and intermediate rocks in the Red Ledge area

presumably had $\delta^{18}O$ values typical of fresh basalts and andesites; that is, between 5.5 and 7.5 permil (Taylor, 1968). These inferences suggest that the rocks of the Seven Devils Group in the Red Ledge and the Hells Canyon areas have been variably enriched in ^{18}O by an average of 2 to 6 permil as a result of hydrothermal-metamorphic processes.

The 1.6 permil difference in average $\delta^{18}O$ values between felsic and mafic rocks of comparable alteration grade is similar to differences between their unaltered equivalents. However, because these rocks are almost totally altered, the apparent preservation of their primary isotopic differences is doubtful or fortuitous. Rather, the relatively high proportion of chlorite and clay, two ^{16}O-rich minerals, and relatively low abundance of hydrothermal quartz, an ^{18}O-rich mineral, in the mafic rocks may account for the isotopic disparity between the two rock clans.

Origin of Fluid and Rock Compositions

A variety of geologic and geochemical evidence from oceanic rocks, ophiolites, volcanogenic massive sulfide deposits, and submarine hot springs collectively suggest that massive sulfide mineralization forms near the discharge sites of large subseafloor hydrothermal convection cells (see discussion in Franklin et al., 1981). Heat released from crystallizing magma supplies the energy required for convection. That such a model applies to the Red Ledge deposit is consistent with the presence of both strata-bound and stockwork styles of mineralization, the localization of the deposit adjacent to

the Red Ledge intrusion, the Mg enrichment in the altered host rocks, and the petrogenesis and secondary mineralogy of the rocks of the Seven Devils Group.

Figure 29 schematically portrays the geologic setting of the Red Ledge deposit at the time of mineralization. This representation suggests that: 1) convected and evolved (via interaction with rocks) seawater was the primary constituent in the Red Ledge fluids over the duration of the hydrothermal cell, 2) the admixing of seawater was prevalent in the vicinity of the vent, and 3) a pulse of magmatic fluid may have been predominant during a particular stage in the development of the deposit. Thus, in order to characterize the role of these different fluids, the isotopic evolution of convecting seawater, oceanic crust, and a magmatic fluid was modeled and the results compared to the isotopic data for the Red Ledge fluids. The discussion that follows first establishes the parameters, methods of calculation, and assumptions of a theoretical convection model through a consideration of oxygen isotopic exchange, then outlines the results for hydrogen isotopic exchange as predicted by the model, and finally considers the case of a cooling magmatic fluid.

The convection model simulates isotopic exchange between seawater and rocks along a lengthy streamline and over an undefined interval of time. Several parameters that influence isotopic fractionation between water and rock were presumed to vary with distance along this hypothetical flow path and incorporated in the model calculations. These parameters and the specific values utilized at discrete points (A through J in Figure 29) are listed in Table 15. The temperature of seawater was increased from an ambient 0 °C to

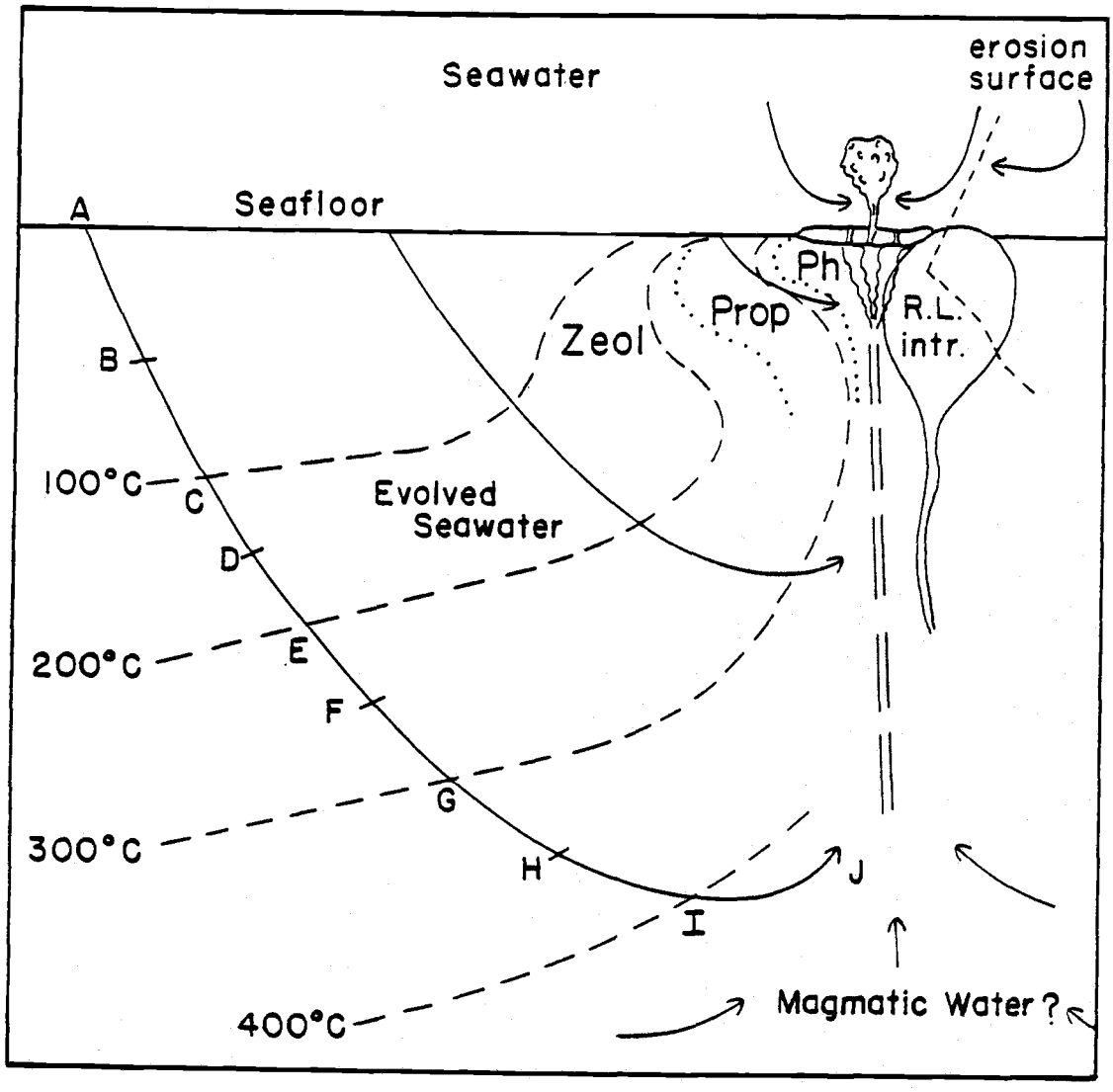

Figure 29. Schematic portrayal of the geologic setting of the Red Ledge deposit depicting isotherms (dashed line), streamlines (solid line), potential sources of hydrothermal fluids, and alteration assemblages (zeol-zeolite; prop-propylitic; phy-phyllic).

Table 15. Parameters Utilized in Calculating the Isotopic Evolution of Convecting Seawater

Step	T (°C)	ρH_2O (g/cm^3)	PH_2O (bars)	ϕ (%)	$\dot{w}/r_i$	$\delta^{18}O_{r-w}$ (°/oo)	δD_{r-w} (°/oo)
A	0	1.0	200	---	---	---	---
B	50	0.99	250	10	7	22.1	-70
C	100	0.97	300	9	5	15.7	-64
D	150	0.94	350	8	3	11.4	-60
E	200	0.89	400	7	1	8.4	-51
F	250	0.84	450	6	0.5	6.3	-49
G	300	0.78	500	5	0.5	4.6	-43
H	350	0.70	550	4	0.5	3.4	-41
I	400	0.61	600	3	0.5	2.4	-39
J	450	0.50	650	3	0.5	1.6	-37

****

ρH_2O calculated from Table 1 in Burnham et al., (1969);

ϕ represents porosity;

450 °C, or the upper limit of greenschist metamorphism, along the descending limb of the flow path. However, isotopic ratios were not calculated for the ascending limb of the streamline where the fluids cool from 450 to 350 °C because it was assumed that, in the zone of upwelling, fluid flow rates exceeded isotopic equilibration rates and retrograde reactions were essentially limited to minor changes in the compositions of plagioclase feldspar and amphiboles. Concomitant with heating, the density of the fluid was assumed to decrease from approximately 1 g/cc at 250 bars P_{H2O} (corresponding to a depth of about 2500 meters below sealevel) to 0.50 g/cc at 650 bars P_{H2O} (6500 meters below sealevel). Porosity was assumed to range from 10% at depths less than one kilometer below the seafloor to 3% at depths of 4 kilometers.

The calculations in this model were performed in a stepwise manner. Oxygen isotopic exchange between seawater and rock was computed at 50 °C intervals from 50 to 450 °C, and these "packets" of evolved seawater were then reequilibrated with rock at successively higher temperature intervals. At each step, the oxygen isotopic composition of the fluid was calculated from:

$$S\delta^{18}O_{(w)} = \frac{\delta^{18}O_{(r)} - \delta^{18}O_{(r-w)} + (w/r_{inst})\,\delta^{18}O_{(iw)}}{1 + (w/r_{inst})} \quad (6)$$

where iw and fw refer to the $\delta^{18}O$ ratio of the initial and final water, respectively, $S^{\delta 18}O_{(r-w)}$ is the oxygen isotopic fractionation factor between rock (r) and water (w), and w/r_{inst} denotes the

"instantaneous" water to rock ratio in grams of oxygen. The fractionation of oxygen isotopes between rock and water was computed from the relationship:

$$1000 \ln a_{r-w} = 2.68 \times 10^6 (T^{-2}) - 3.53 \quad (7)$$

where T is in degrees Kelvin. This equation describes the exchange of oxygen isotopes between water and plagioclase feldspar (An_{30}), and also closely approximates the exchange between water and rocks of intermediate composition (Taylor, 1979). Fractionation factors at the temperatures of interest are listed in Table 15.

In the model calculations, the "instantaneous" w/r determines the proportion of water oxygen to rock oxygen that is equilibrated at each step. Since the amount of oxygen in water was fixed by the porosity of the crust and density of water, the selection of w/r_{inst} determined the amount of rock oxygen involved in each equilibration. Under hydrothermal conditions, oxygen isotopic exchange between rock and fluids is governed by surface chemical reactions and the diffusion of oxygen-bearing species through crystal structures (Cole et al., 1983). Experimental exchange rates for the former mechanism are orders of magnitude higher than for the latter (ibid.). This implies that oxygen isotope exchange in a convection system may be governed essentially by the chemical alteration of fresh rock rather than by isotopic equilibration with previously formed secondary minerals. However, because the model utilized in this investigation does not provide for chemical reactions, flow rates, or kinetic isotopic exchange rates, a specific w/r_{inst} could not be determined for a

given set of conditions. In a chemical and physical analysis of a Kuroko hydrothermal system, Cathles (1983) calculated that the fraction of rock undergoing alteration at any time is approximately 1 percent. The w/r_{inst} (O mass) ratios selected for the model calculations in this investigation range from 7 at 50 °C to 0.5 at temperatures of 250 to 450 °C (Table 15). The variation in this parameter reflects a smaller amount of reaction at lower temperatures and corresponds to alteration of 1% of the rock per step at 50 °C, 7% per step at 250 °C, and about 3% per step at 400 and 450 °C.

In the model, the fluid was equilibrated only with unaltered rock with an average $\delta^{18}O$ composition of 7 °/oo and a density of 2.7 g/cc. Consequently, the fluid was not in isotopic equilibrium with the whole rock (altered + unaltered). The $\delta^{18}O$ ratio of the hypothetical alteration rind produced during each step was computed from the $\delta^{18}O$ value of water with which it equilibrated, and the $\delta^{18}O$ composition of the whole rock was calculated as a weighted average of the altered and unaltered fractions. The calculations at each step were normalized to a block of crust (rock + pore space) 100 cm^3 in volume.

The results of calculations from this model are portrayed in Figure 30. Under the specified conditions, the whole rock $\delta^{18}O$ values increase with extent of alteration (and time), expressed as an integrated water/rock ratio for the rock (w/r_r), at temperatures below approximately 150 °C. This effect is primarily a function of the large fractionation factors at low temperatures which result in ^{18}O-depleted fluids, but correspondingly ^{18}O-enriched alteration assemblages. At temperatures greater than 150 °C the whole rock

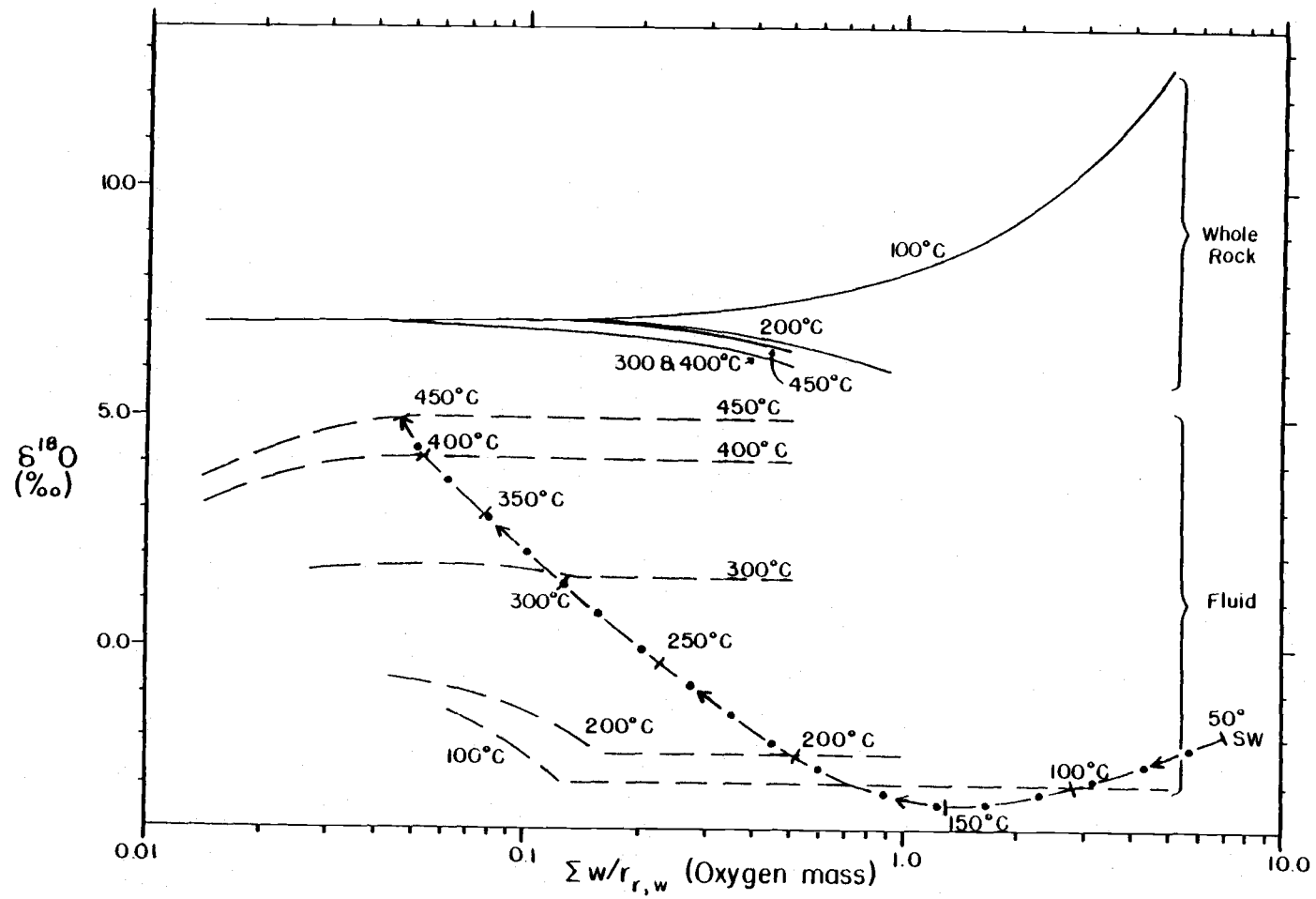

Figure 30. Variations in the $\delta^{18}O$ ratios for whole rocks (solid lines) and fluids (dashed lines) as a function of integrated water to rock ratio for the rock (w/r_r) and at selected temperatures. Also shown is the $\delta^{18}O$ evolution of a packet of seawater (dash-dot line) as a function of integrated water to rock for the water (w/r_w).

compositions decrease by one permil or less with progressive alteration. Such a limited depletion in ^{18}O is a function of fractionation factors less than 7 $^{o}/_{oo}$, and w/r_{inst} ratios less than one (i.e. rock dominated system). The decrease in whole rock values is apparently greater in rocks at 300 and 400 °C than those at 450 °C because the former are more strongly influenced by the ^{18}O-depleted fluids produced at low temperatures and shallow depths. The $\delta^{18}O$ values of evolved seawater are less than 0 $^{o}/_{oo}$ at temperatures below about 250 °C and decrease at integrated w/r_r ratios less than 0.3 but reach a steady state at higher ratios. Fluids at temperatures higher than 250 °C are greater than 0 $^{o}/_{oo}$ and either maintain a constant value (~300 °C) or increase to a steady state with higher integrated w/rk_r ratios. A packet of seawater traversing streamline A-J (Fig. 29) would decrease from 0 $^{o}/_{oo}$ to approximately -3 $^{o}/_{oo}$ at 150 °C and then increase to about +5 $^{o}/_{oo}$ at 450 °C (Fig. 30). The integrated w/r ratio with respect to this quantity of water would decrease with distance along the flow path as it exchanged with progressively greater quantities of rock oxygen.

These results are critically dependent on the fractionation curve used to represent oxygen isotopic exchange between water and rock and on the w/r_{inst} ratios. The smectite-water fractionation curve, which was utilized by Cathles (1983) to model the $\delta^{18}O$ evolution of seawater, yields fluid and rock compositions that are depleted in ^{18}O relative to those computed from the feldspar-water curve. For example, the smectite-water curve results in a maximum fluid composition of 1.9 $^{o}/_{oo}$ whereas the plagioclase feldspar-water curve produces a maximum value of 5.0 $^{o}/_{oo}$ under the same conditions.

Similarly, an increase or decrease in the w/r_{inst} ratios causes an inverse shift in fluid and rock $\delta^{18}O$ values. Thus, a w/r_{inst} ratio of 5 yields maximum fluid $\delta^{18}O$ compositions of 1.5 to 2.3 permil at 400 to 450 °C, or about 2.6 °/oo less than those resulting from a ratio of 0.5. In addition to increasing with temperature and chemical potential, it is probable that the w/r_{inst} also increases with time as unaltered rock is progressively shielded from the fluid by secondary minerals in alteration rinds, pores and fractures. This would cause the fluid $\delta^{18}O$ curves in Figure 30 to gradually converge toward 0 °/oo with an increase in the integrated w/r_r ratio from relatively moderate to high values.

To the extent this model applies to the Red Ledge hydrothermal convection system, the results imply that both the range and variations in the isotopic compositions of fluid and rock at the site of mineralization can be produced through the interaction of seawater and volcanic rocks. Specifically, the model calculations suggest four important inferences.

1. Stage 1 vein fluids ($\delta^{18}O$ = ~0 °/oo) are the result of isotopic exchange at approximately 250 °C and low to moderate integrated w/r_w ratios (~0.2-0.3). Such conditions are probable within 1 to 2 km of the intrusion. Also, the incorporation of weakly modified seawater into the stockwork system during this early period is isotopically permissible where flow rates exceed isotopic exchange rates near the vent.

2. The vein fluids of stages 2 and 3 ($\delta^{18}O$ = 4-5.5 °/oo) originated at temperatures of 400 to 450 °C and low integrated w/r_w ratios (~0.1). These fluids may have been produced by fluid-mineral

reactions characteristic of the upper greenschist facies and at depths of several kilometers within the volcanic pile. Extensional faulting possibly provided the mechanism to tap these fluids and the conduit for their ascent to the seafloor. Perhaps a minor proportion of the isotopically heavy fluids was generated in a narrow high temperature zone surrounding the Red Ledge intrusion.

3. Assuming that stringer quartz and syngenetic chert formed during the period corresponding to vein deposition of stages 2 and 3, then the fluids near the seafloor (~2.8-2.9 $^{o}/_{oo}$) probably represented mixtures of ascending hydrothermal fluids of stages 2 and 3 (5.0 $^{o}/_{oo}$) and pristine or weakly evolved seawater (~0 $^{o}/_{oo}$).

4. Stage 4 fluids ($\delta^{18}O$ = 0-1 $^{o}/_{oo}$) may have been produced under conditions similar to those of Stage 1 fluids; specifically at 250-290 °C and moderate integrated w/r_w ratios (0.1-0.3). The rocks in the vicinity of the Red Ledge deposit were intensely altered by the later stages of mineralization and, therefore, some of the Stage 4 fluids probably represent weakly modified seawater that had infiltrated the stockwork zone as suggested by the isotopic variability of vein sulfate and carbonate.

5. The curves presented in Figure 30 suggest that the ^{18}O-enriched rocks of the phyllic alteration zone were produced at temperatures of 150 °C or less by the interaction of evolved seawater and rocks of $\delta^{18}O$ = 7.0 permil. Yet this interpretation is inconsistent with the inferred temperature of ~300 °C for sericite crystallization and the simultaneous formation of ^{18}O-enriched rocks (~9.6 $^{o}/_{oo}$ for felsic varieties) and fluids (~4.9 permil) by equilibrium or partial equilibrium isotopic exchange. However,

calculations indicate that the whole rock ^{18}O values can be generated at 300 °C and at high integrated w/r_r ratios (~>or = 6) if the fluids were initially 5 °/oo. Thus, it is possible that the ^{18}O enriched vein fluids of stages 2 and 3 infiltrated the wallrocks and produced the isotopically heavy phyllic alteration assemblage. Similarly, the final $\delta^{18}O$ compositions of the calcite-bearing fluids (~3.1 °/oo) and dacitic rocks (~10.6 °/oo) in the zone of propylitic alteration may have resulted from isotopic exchange with fluids of 5 °/oo provided the integrated w/r_r was about 1. Higher integrated w/r_r ratios (e.g. 10) would require fluids with smaller initial $\delta^{18}O$ values (e.g. 4.5 °/oo) to produce the observed final rock and fluid compositions. Spilitized rocks of Triassic age (~9.9 °/oo) in Hells Canyon apparently equilibrated with evolved seawater at temperatures of 200 °C or less.

The hydrogen isotopic evolution of seawater was calculated similarly to that for the evolution of oxygen isotopes, although the w/r_{inst} (hydrogen mass) ratio had to be adjusted to maintain the same bulk water/rock mass ratios for each reaction step. It was assumed that the chlorite-H_2O fractionation curve approximated rock-H_2O hydrogen isotopic exchange. The fractionation factors used at each step are listed in Table 15. Results of these interpretations indicate that the δD composition of evolved seawater decreased at all temperatures. Thus, at 250 °C the estimated δD ratio is -16 °/oo and at 400 to 450 °C it is -30 to -32 °/oo. Moreover, the results are consistent with the calculated δD ratio of the Red Ledge fluids that deposited vein chlorite (-16 °/oo at 275 °C). However, the δD composition of the fluids associated with sericitic wallrock

alteration (-5 $^{o}/_{oo}$) is not compatible with that predicted for seawater that has evolved at high temperature.

Finally, an injection of magmatic fluid into the convection cell must be considered as a potential cause of the positive shift in the $\delta^{18}O$ ratios of the Red Ledge fluids. This potentially viable mechanism was investigated by modeling the isotopic evolution of a magmatic fluid ($\delta^{18}O$ = 7.5 $^{o}/_{oo}$, δD = -60 $^{o}/_{oo}$) through equilibration with rock ($\delta^{18}O$ = 7.0 $^{o}/_{oo}$, δD = -70 $^{o}/_{oo}$) while cooling from 750 to 350 °C. These calculations were performed at w/r_{inst} ratios of 0.5 and 0.3 for oxygen and hydrogen isotopic exchange, respectively. The results suggest that at 350 °C the magmatic fluids ($\delta^{18}O$ = 4.1 $^{o}/_{oo}$, δD = -30 $^{o}/_{oo}$) are isotopically indistinguishable from evolved seawater that was generated at 400 to 450 °C. Thus, magmatic fluids are an isotopically permissible component in the Red Ledge submarine hydrothermal system during the intermediate stages of mineral deposition. Because the Red Ledge igneous complex formed near the seafloor, a magmatic fluid expelled from this intrusion would have been cooled and diluted by circulating fluids within a distance of perhaps 1 kilometer of the seafloor. However, these inferences of steep thermal and chemical gradients are inconsistent with the uniform isotopic compositions of paragenetically equivalent quartz and sulfide throughout the stockwork zone and between veins that crosscut the intrusive QFP and the volcaniclastic rocks. Furthermore, other contemporaneous intrusions of sufficient size to provide the requisite components (e.g. see Cathles, 1983, Table 2) are not exposed within the vicinity of the Red Ledge deposit.

Genetic Model

The following discussion concerning the origin of the Red Ledge deposit integrates a wide variety of pertinent data into a "best fit" genetic model. The strength of the model relies not only on the constraints imposed by the different sets of data but, more importantly, on the extent to which independently derived conclusions provide supportive or complementary evidence for the various aspects of ore genesis. For example, the accumulated data are consistent with an origin that entails only evolved seawater and pristine seawater but is somewhat contradictory with regard to the possible role of magmatic fluid. Thus, magmatic fluid is apparently unessential to the formation of the Red Ledge deposit. Implicit in such conclusions is the assumption that hydrothermal ore deposits are a normal, but rare, consequence of common geologic processes which typically operate on rocks and magmas of "average" composition.

The available geologic and geochemical data for the rocks of the Seven Devils Group, Hunsaker Creek Formation, and Red Ledge deposit provide a general framework for the tectonic setting of the deposit and the processes that resulted in mineralization. The Red Ledge deposit originated in an island arc, probably back arc, tectonic setting during Early Permian time (258-286 Ma.). Modern analogs of such a setting are characterized by extensional tectonics (expressed by block faulting), caldera formation, bimodal volcanism, and high heat flow. Rocks of the Hunsaker Creek Formation record a considerable interval of subaerial and submarine explosive volcanism, reworking of volcanic detritus, and the local extrusion of magma as

flows and domes. This interval was punctuated by a few relatively short episodes of carbonate sedimentation. The Red Ledge domal complex represents one locale where felsic magma reached the seafloor and formed a volcanic dome. Growth of the dome was accomplished through the repeated intrusion of sills and plugs, extrusion of small pyroclastic deposits, and the accumulation of an apron of volcanic debris produced by phreatic and phreatomagmatic explosions, and by gravity slides.

Mineralization was intimately related to the development of the Red Ledge domal complex. This relationship is particularly evident in the consistent and exclusive association of stringer mineralization with beds of felsic volcaniclastic rocks in the stratigraphic section immediately overlying the dome. This relationship implies that mineralization was triggered by episodes of explosive volcanism. Repetition of these explosive events resulted in the cyclic deposition of mineralization as stacked couplets of stringer sulfides +/- massive sulfides. Textural features suggest that the precipitation of some stringer mineralization in the volcaniclastics may have coincided with explosive activity, whereas massive sulfide lenses largely formed on the seafloor during periods of volcanic quiescence and synchronously with the deposition of extraneous volcanic rocks of mafic composition and clastic sediments. If the volcanic explosions were caused by pulses of magma intruding the dome and if the cycles of mineralization were related to discreet episodes of fracturing in the stockwork zone, then the mineralization may have been a direct consequence of a repetitive sequence of events involving both tectonism and volcanism.

Evolved seawater undoubtedly played a major role in the origin of the Red Ledge deposit. The evolution of seawater into a potential ore fluid via interaction with rocks at elevated temperatures has been established by experimental studies and the presence of metal sulfides around hydrothermal springs on the seafloor. The convection of seawater during the mineralization event at the Red Ledge is consistent with a variety of circumstantial evidence, most notably the Mg enrichment in the hydrothermally altered rocks. Theoretical modeling of the exchange of oxygen isotopes between convecting seawater and volcanic rocks suggests a possible origin for the Red Ledge fluids and, by implication, the mineralization. Early fluids ($\delta^{18}O$ = 0 $^{o}/oo$) were generated through isotopic exchange with rocks at peak temperatures of approximately 250 °C, moderate w/r_w ratios, and along flow paths perhaps within 2 kilometers of the seafloor. Intermediate fluids ($\delta^{18}O$ = 4-5.5 $^{o}/oo$) originated at maximum temperatures of 400-450 °C, relatively low integrated w/r_w ratios, and in a zone that encompassed the deeper portions of the volcanic pile and a restricted area around the Red Ledge dome and its feeder conduit. These fluids were responsible for alteration of the wall-rocks to a phyllic assemblage and deposition of the majority of the sulfides. Many of the elements that are enriched in the rocks and ores of the Red Ledge deposit (e.g. Si, K, Fe, Ba, Cu, Zn, and Ag) were leached from the country rocks during the generation of the intermediate fluids, as suggested by seawater-rock experiments. Late stage fluids ($\delta^{18}O$ = 0-1 $^{o}/oo$) consisted of various mixtures of evolved seawater (250-290 °C, moderate w/r_w ratios, and short, shallow flow paths) and pristine seawater.

The isotopic systematics of the Red Ledge sulfides, sulfates, and carbonates indicate that fluid mixing played a major role in the formation of the deposit. For example, the mixing of ingressing moderately evolved seawater and egressing highly evolved seawater (intermediate fluids) in a zone surrounding the deposit may have resulted in the propylitic assemblage of hydrothermal alteration. By contrast, the phyllic assemblage corresponds to the zone where fluid mixing was inconsequential and intermediate fluids were predominant. Sulfide and sulfate species of seawater derivation and carbon leached from the country rocks were incorporated into the hydrothermal system through the addition of moderately evolved seawater to the ascending intermediate fluids in the conduit below the site of mineralization. The H_2S of seawater origin was produced through the inorganic reduction of seawater sulfate in a shallow zone surrounding the Red Ledge complex. Pristine seawater was entrained into the rising hydrothermal fluids below the seafloor, primarily in permeable volcaniclastic sediments, and into the vented fluids above the seafloor. The addition of seawater to the hydrothermal fluids caused a decrease in temperature and an increase in pH, fO_2, and several ionic species, such as Ca^{++}, Mg^{++}, SO_4^{--}, and HCO_3^-. The sulfides and quartz precipitated in response to the decrease in temperature, barite largely in response to the influx of SO_4^{--}, and dolomite in response to local heating and possibly the increase of Ca^{++}, Mg^{++}, and HCO_3^-. Equilibrium isotopic exchange between aqueous sulfide and sulfate species was limited to the initial stages of mixing when seawater comprised 10% or less of the solution and the temperature was approximately 240 °C and above. Accordingly, the $\delta^{34}S$ composition of

sulfides and barite decreased upward from vein mineralization (-2.8 & 15.2 $^{o}/_{oo}$, resp.) to stringer (-5.1 & 14.5 $^{o}/_{oo}$, resp.) mineralization. The incorporation of additional seawater into the solutions (greater than 10%) caused cooling below 240 °C, inhibited further sulfur isotopic exchange and resulted in a decrease in the $\delta^{34}S$ ratios of stringer and massive barite (12.7 $^{o}/_{oo}$) because of the addition of isotopically light seawater sulfate. Seawater comprised up to 40% of the solutions in the zone of stringer mineralization and 75% of the solutions in the area above or on the seafloor. During the last stage of mineralization, when the thermal anomaly and convection system were waning, seawater infiltrated fractures and voids up to depths of at least 1000 feet below the seafloor. Mixing in this environment yielded solutions with a maximum of 30% seawater during vein barite deposition and a maximum of 60% during vein dolomite deposition.

With cessation of the hydrothermal system and burial, the Red Ledge deposit was subjected to two periods of metamorphism and tectonism. These events caused the local recrystallization of the sulfides, sulfates, carbonates and quartz, disturbed the intermineral fractionation of sulfur isotopes, and partially reconstituted the arrays of the fluid inclusions and homogenization temperatures. Deuterium depleted fluids (-112 to -78 $^{o}/_{oo}$) may have been trapped in secondary inclusions during the periods of metamorphism or subsequently during uplift and erosion.

The involvement of magmatic fluids in the formation of the Red Ledge deposit is permitted by the isotopic data but is contradictory and poorly supported by geologic evidence. For example, the isotopic

composition of the intermediate fluids, total sulfur, and total carbon are consistent with a magmatic derivation for these components under specified conditions. However, the sulfur data suggest equilibration with an oxidized magma (above the QFM buffer) and the carbon data imply equilibration with a reduced magma (below the QFM buffer). Moreover, if the magmatic fluids and their contained components were expelled from the Red Ledge igneous complex, then steep thermal and chemical gradients should be evident within the delineated dimensions of the deposit. These hypothesized gradients are contradictory to the uniform isotopic compositions of paragenetically equivalent quartz and sulfide throughout the stockwork zone and between veins that crosscut the intrusive QFP and the volcaniclastic rocks. Other contemporaneous intrusions of the size required to supply the requisite components are not exposed within the region surrounding the Red Ledge. Finally, it is implausible to suggest that only a few select components were derived from a magma (e.g. metals) and that all other components of a magmatic fluid were either swamped by components from other sources (seawater) or were preferentially removed.

Conclusions

The major conclusions of this investigation regarding the origin of the Red Ledge deposit are summarized as follows:

1. Footwall alteration assemblages in QFP grade outward from silicified vein selvages through zones of sericite and sericite-chlorite to a propylitic halo. The major oxides SiO_2, $Fe_2O_3^*$ (total iron), K_2O, and H_2O+ have been enriched, and Na_2O depleted, in all these alteration zones. In contrast, MgO, CaO, and CO_2 are variably enriched in the outer alteration zones and strongly depleted in the inner zones.

2. Rocks surrounding the Red Ledge deposit have been enriched in ^{18}O by an average of 2 to 6 permil as a consequence of hydrothermal alteration. Average $\delta^{18}O$ compositions of felsic rocks in the footwall of the deposit vary with respect to the mineralogy of the alteration assemblage and proximity to mineralization: from 10.6 $^{o}/oo$ in the propylitic zone, through a minimum of 9.6 $^{o}/oo$ in the phyllic zone, to a maximum of 12.2 $^{o}/oo$ in the silicified vein selvages.

3. Concentrations of Zr, Ti, and Y suggest that the altered and metamorphosed rocks of the mafic and felsic clans were originally basaltic and dacitic-rhyodacitic in composition, respectively.

4. Mineral deposition in the stockwork system varied with relative time from amethyst quartz through gray quartz-sulfide, white quartz-(sulfide), barite-(sulfide), orange dolomite-(calcite-sulfide) to olive dolomite-(calcite). In strata-bound mineralization the sulfides precipitated first and were followed sequentially by quartz

and barite. Carbonate is not present in stringer or massive sulfide mineralization.

5. Fluid inclusions in vein quartz have characteristics of both hydrothermal and metamorphic environments. Primary-appearing inclusions have vapor homogenization temperatures that average 274 °C, whereas all inclusion fluids (secondary and primary) have δD values between -112 and -78 permil.

6. Differences in the $\delta^{34}S$ composition of syngenetic pyrite and barite from volcanogenic massive sulfide deposits of Phanerozoic age exhibit a remarkable correlation with the $\delta^{34}S$ variations of seawater sulfate through time. This correlation, for certain intervals of geologic time, can be used to distinguish deposits of various ages. This relationship also implies that seawater sulfate was the prime source of sulfur in these deposits and that most of the H_2S incorporated in the sulfides was produced through the inorganic reduction of seawater sulfate. Furthermore, the anomalously low $\delta^{34}S$ composition of Permian oceanic sulfate accounts for the anomalously low $\delta^{34}S$ composition of the Red Ledge mineralization (-9.5 to -0.6 $^{o}/oo$ for sulfides and 11.1 to 19.0 $^{o}/oo$ for sulfates) relative to that of analagous deposits of different age. Thus, the sulfur isotopic data indirectly corroborate the Early Permian age of the Red Ledge mineralization as determined by a recent paleontological date.

7. The upward decrease in the average $\delta^{34}S$ compositions of sulfides and barite from vein (-2.8 & 15.2 $^{o}/oo$, resp.) through stringer (-5.1 & 14.5 $^{o}/oo$, resp.) to massive (-5.1 & 12.7 $^{o}/oo$, resp.) mineralization resulted from an upward decrease in fluid temperature that was caused by the addition of progressively greater

quantities of cold seawater (~0 °C) to the rising hydrothermal fluids (250-275 °C). The sympathetic decrease in sulfide and barite compositions was produced by equilibrium isotopic exchange between aqueous sulfate and sulfide in solutions containing up to ~10% seawater and at temperatures as low as ~240 °C. Cooling below 240 °C through the admixing of greater quantities of seawater greatly inhibited further isotopic exchange, but resulted in the decrease of the barite compositions because the $\delta^{34}S$ ratio of Permian seawater sulfate was less than that of the hydrothermal sulfate.

8. Calculated $\delta^{18}O$ compositions of the feeder vein fluids varied from ~0 $^{o}/_{oo}$ during the early amethyst deposition, to 4-5.5 $^{o}/_{oo}$ during intermediate quartz-sulfide, quartz-(sulfide), and barite deposition, and finally to 0-1 $^{o}/_{oo}$ during late barite and carbonate deposition. This paragenetic trend is consistent with isotopic exchange between convecting seawater and volcanic host rocks at variable temperatures and integrated water to rock ratios with respect to the water (w/r_w): early fluids at 250 °C and moderate w/r_w, intermediate fluids at 400-450 °C and low w/r_w (hydrothermal -metamorphic fluids generated deep within the volcanic pile), and late fluids at 250-290 °C and moderate w/r_w. The hydrogen isotopic composition of the intermediate fluids was about -10 +/- 6 $^{o}/_{oo}$.

9. The ranges in isotopic compositions of vein barite ($\delta^{34}S$ = 13.6-19.0 $^{o}/_{oo}$ and $\delta^{18}O$ = 7.8-10.5 $^{o}/_{oo}$) and carbonate ($\delta^{13}C$ = -10.8 to -0.8 and 9.1 to $\delta^{18}O$ = 20.1 $^{o}/_{oo}$) are consistent with variable mixtures of pristine seawater and hydrothermal fluid. Thus, during the waning of the thermal anomaly and the collapse of the convection system seawater infiltrated the stockwork zone up to depths of at

least 1000 feet below the seafloor and mixed with the late hydrothermal fluids.

References Cited

Addy, S. K., and Ypma, P. J. M., 1977, Origin of massive sulfide deposits at Ducktown, Tennessee: an oxygen, carbon, and hydrogen isotope study: Econ. Geol., v. 72, p. 1245-1268.

Albee, A. L., 1962, Relationships between the mineral association, chemical composition and physical properties of the chlorite series: American Mineralogist, v. 47, p. 851-870.

Albers, J. P., 1981, A lithologic-tectonic framework for the metallogenic provinces of California: Econ. Geol., v. 76, p. 765-790.

Albers, J. P., and Robertson, J. F., 1961, Geology and ore deposits of east Shasta County, California: U. S. Geol. Survey Prof. Paper 338, 107 p.

Armstrong, R. L., Taubeneck, W. H., and Hales, P. O., 1977, Rb-Sr and K-Ar geochronometry of Mesozoic granitic rocks and their Sr isotopic composition, Oregon, Washington, and Idaho: Geol. Soc. America Bull., v. 88, p. 397-411.

Ault, W. V., and Jensen, M. L., 1963, Summary of sulfur isotope standards, in Biogeochemistry of Sulfur Isotopes, M. L. Jensen, ed., Natl. Sci. Found., Symposium Proc., Yale University.

Ave Lallement, H. G., 1976, Structure of the Canyon Mountain (Oregon) ophiolite complex and its implication for sea floor spreading: Geol. Soc. America Spec. Paper 173, 49p.

-----, 1983, The pre-Tertiary tectonics of the Blue Mountains region, NE Oregon: Geol. Soc. America Abs. w. Prog., v. 15, no. 5, p. 372.

Ayers, D. E., Burns, M. S., and Smith, J. W., 1979, Sulfur-isotope study of the massive sulfide orebody at Woodlawn, New South Wales: Geol Soc. Australia Jour., v. 26, p. 197-201.

Bailey, S. A., and Smith, J. W., 1972, Improved method for the preparation of sulfur dioxide from barium sulfate for isotope ratio studies: Anal. Chem., v. 44, p. 1542-1543.

Barton, P. B., Jr., and Skinner, B. J., 1967, Sulfide mineral stabilities in Barnes, H. L., ed., Geochemistry of Hydrothermal Ore Deposits (1st ed.): New York, Holt, Rinehart, and Winston, p. 236-333.

Barton, P. B., Jr., Bethke, P. M., and Roedder, E., 1977, Environment of ore deposition in the Creede Mining District, San Juan Mountains, Colorado: Part III. Progress toward interpretation of the chemistry of the ore-forming fluid for the OH Vein: Econ. Geol., v. 72, p. 1-24.

Beaty, D. W., and Taylor, H. P., Jr., 1980, The oxygen isotope geochemistry of the Kidd Creek mine: evidence for a high ^{18}O ore-forming solution and implications regarding the genesis of volcanogenic massive sulfide deposits: Geol. Soc. America Abs. w. Prog., v. 12, no. 7, p. 384.

-----, 1982, Some petrologic and oxygen isotopic relationships in the Amulet mine, Quebec, and their bearing on the origin of Archean massive sulfide deposits: Econ. Geol., v. 77, 95-108.

Brooks, H. C., 1979, Plate tectonics and the geologic history of the Blue Mountains: Oregon Geology, v. 41, no. 5, p. 71-80.

Brooks, H. C., McIntyre, J. R., and Walker, G. W., 1976, Geolgoy of the Oregon part of the Baker 1 by 2 Degree Quadrangle: Oregon Dept. of Geology and Mineral Industries, Map GMS-7.

Brooks, H. C., and Vallier, T. L., 1978, Mesozoic rocks and tectonic evolution of eastern Oregon and western Idaho, in Howell, D. G., and McDougall, K. A., eds., Mesozoic paleogeography of the western United States: Pacific Section, Society of Economic Paleontologists and Mineralogists Pacific Coast Paleogeography Symposium 2, p. 133-146.

Bryndzia, L. T., Scott, S. D., and Farr, E. J., 1983, Mineralogy, geochemistry, and mineral chemistry of siliceous ore and altered footwall rocks in the Uwamuki 2 and 4 deposits, Kosaka Mine, Hokuroku District, Japan: Econ. Geol. Mono. 5, p. 507-522.

Burnham, W. C., Holloway, J. R., and Davis, N. F., 1969, Thermodynamic properties of water to 1000 C and 10,000 bars: Geol. Soc. America Spec. Paper 132, 96 p.

Casey, W. H., and Taylor, B. E., 1982, Oxygen, hydrogen, and sulfur isotope geochemistry of a portion of the West Shasta Cu-Zn District, California: Econ. Geol., v. 77, p. 38-49.

Cathles, L. M., 1983, An analysis of the hydrothermal system responsible for massive sulfide deposition in the Hokuroko basin of Japan: Econ. Geol. Mono. 5, p. 439-487.

Chiba, H., Kusakabe, M., Hirano, S., Matsuo, S., and Somiya, S, 1981, Oxygen isotope fractionation factors between anhydrite and water from 100 to 550 °C: Earth and Planetary Sci. Letters, v. 53, p. 55-62.

Claypool, G. E., Holser, W. T., Kaplan, I. R., Sakai, H., and Zak, I., 1980, The age curves of sulfur and oxygen isotopes in marine sulfate and their mutual interpretation: Chem. Geol., v. 28, p. 199-260.

Clayton, R. N., and Mayeda, T. K., 1963, The use of bromine pentafluoride in the extraction of oxygen form oxides and silicates for isotopic analysis: Geochim. Cosmochim. Acta, v. 22, p. 43-52.

Cole, D. R., Ohmoto, H., and Lasaga, A. C., 1983, Isotopic exchange in mineral-fluid systems. I. Theoretical evaluation of oxygen isotopic exchange accompanying surface reactions and diffusion: Geochim. Cosmochim. Acta, v. 47, p. 1681-1693.

Craig, H., 1957, Isotopic standards for carbon and oxygen and correction factors for mass-spectrometric analysis of carbon dioxide: Geochim. Cosmochim. Acta, v. 12, p. 133-149.

-----, 1961, Standards for reporting concentrations of deuterium and oxygen-18 in natural waters: Science, v. 133, p. 1833-1834.

Cramer, R. S., and Taylor, B. E., 1983, Oxygen, hydrogen, and sulfur isotope geochemistry of the Gray Eagle Cu-Zn-Au deposit, Siskiyou Co., Ca.: Geol. Soc. America Abs. w. Prog., v. 15, no. 5, p. 297.

Cunningham, C. T., 1979, Geology and geochemistry of a massive sulfide deposit and associated volcanic rocks, Blue Creek District, southwestern Oregon: unpublished M. S. thesis, Oregon State Univ., 165 p.

Date, J., and Tanimura, S., 1974, Dacite and rhyolite associated with the Kuroko mineralization: Soc. Mining Geologists Japan, Spec. Issue 6, p. 261-265.

Date, J., Watanabe, Y., and Saeki, Y., 1983, Zonal alteration around the Fukazawa kuroko deposits, Akita Prefecture, northern Japan: Econ. Geol. Mono. 5, p. 365-386.

Derkey, R. E., 1982, Geology of the Silver Peak mine, Douglas County, Oregon: unpublished Ph. D. dissertation, Univ. of Idaho, 188 p.

Dickinson, W. R., 1979, Mesozoic forearc basin in central Oregon: Geology, v. 7, p. 166-170.

Dickinson, W. R., and Thayer, T. P., 1978, Paleogeographic and paleotectonic implications of Mesozoic stratigraphy and structure in the John Day inlier of central Oregon, in Howell, D. G., and McDougall, K. A., eds., Mesozoic paleogeography of the western United States: Pacific Section, Society of Economic Paleontologists and Mineralogists Pacific Coast Paleogeography Symposium 2, 147-161.

Eldridge, C. S., Barton, P. B., Jr., and Ohmoto, H., 1983, Mineral textures and their bearing on formation of the Kuroko orebodies: Econ. Geol. Mono. 5, p. 241-281.

Fifarek, R. H., 1982, Geology and mineralization of the Banfield and Rowley volcanogenic massive sulfide deposits, Douglas Co., Oregon: unpublished M. S. thesis, Oregon State Univ., 133 p.

Fifarek, R. H., Rye, R. O., and Field, C. W., 1983, Sulfur isotope geochemistry of the Red Ledge and other massive sulfide deposits of the Northwest: Geol. Soc. America Abs. w. Prog., v. 15, no. 5, p. 372.

Francheteau, J., Needham, H. D., Choukroune, P., Juteau, T., Seguret, M., Ballard, R. D., Fox, P. J., Normark, W., Carranza, A., Cordoba, D., Guerro, J., Rangin, C., Bougault, H., Cambon, P., and Hekinian, R., 1979, Massive deep-sea sulfide ore deposits discovered on the East Pacific Rise: Nature, v. 277, p. 523-528.

Franklin, J. M., Kasarda, J., and Poulsen, K. H., 1975, Petrology and chemistry of the alteration zone of the Mattabi massive sulfide deposit: Econ. Geol., v. 70, p. 63-79.

Franklin, J. M., Sangster, D. M., and Lydon, J. W., 1981, Volcanic-associated massive sulfide deposits: Econ. Geol. 75th Anniv. Vol., p. 485-627.

Friedman, I., 1953, Deuterium content of natural water and other substances: Geochim. Cosmochim. Acta, v. 4, p. 89-103.

Fritz, P., Drimmie, R. J., and Nowicki, V. K., 1974, Preparation of sulfur dioxide for mass spectrometric analyses by combustion of sulfides with copper oxide: Anal. Chem., v. 46, p. 164-166.

Gill, J. B., and Stork, A. L., 1979, Miocene low-K dacites and trondhjemites of Fiji in Barker, F., ed., Trondhjemites, dacites and related rocks: Amsterdam, Elsevier, 660 p.

Gilluly, J., 1933, Copper deposits near Keating, Oreg.: U. S. Geol. Survey Bull. 830, p. 1-32.

Godfrey, J. D., 1962, The deuterium content of hydrous minerals from the east-central Sierra Nevada and Yosemite National Park: Geochim. Cosmochim. Acta, v. 26, p. 1215-1245.

Goodfellow, W. D., 1975, Major and minor element halos in volcanic rocks at Brunswick no. 12 sulphide deposit, New Brunswick, Canada, in Elliot, I. L., and Fletcher, W. K., eds., Geochemical exploration 1974: Amsterdam, Elsevier, p. 279-295.

Green, G. R., Solomon, M., and Walshe, J. L., 1981, The formation of the volcanic-hosted massive sulfide ore deposit at Rosebery, Tasmania: Econ. Geol., v. 76, p. 304-338.

Green, G. R., Ohmoto, H., Date, J., and Takahashi, T., 1983, Whole-rock oxygen isotope distribution in the Fukazawa-Kosaka area, Hokuroku District, Japan, and its potential application to mineral exploration: Econ. Geol. Mono. 5, p. 395-411.

Hattori, K., and Muehlenbachs, K., 1980, Marine hydrothermal alteration at a Kuroko deposit, Kosaka, Japan: Contr. Mineral. Petro., v. 74, p. 285-292.

Heaton, T. H. E., and Sheppard, S. M. F., 1977, Hydrogen and oxygen isotope evidence for sea-water hydrothermal alteration and ore deposition, Troodos complex, Cyprus, in Volcanic processes in ore genesis: London, Geol. Soc. London, Spec. Pub. 7, p. 42-57.

Hillhouse, J. W., 1977, Paleomagnetism of the Triassic Nikolai Greenstone, McCarthy quardrangle, Alaska: Canadian Jour. Earth Science, v. 14, p. 2578-2592.

Hillhouse, J. W., and Gromme, C. S., 1981, Paleolatitude of Triassic basalt in the Clearwater Mountains, south-central Alaska, in Albert, N. R. D., and Hudson, T., eds., The United States Geological Survey in Alaska: U. S. Geol. Survey Circ., 823-B, p. B55-B56.

Hillhouse, J. W., Gromme, C. S., and Vallier, T. L., 1982, Paleomagnetism and Mesozoic tectonics of the Seven Devils volcanic arc in northeastern Oregon: Jour. Geophysical Research, v. 87, no. B5, p. 3777-3794.

Holland, H. D., 1978, The chemistry of the atmosphere and oceans: New York, John Wiley, 351 p.

Holland, H. D., and Malinin, S. D, 1979, The solubility and occurrence of non-ore minerals, in Barnes, H. L., ed., Geochemistry of Hydrothermal Ore Deposits (2nd ed.): New York, John Wiley, p. 461-508.

Holser, W. T., and Kaplan, I. R., 1966, Isotope geochemistry of sedimentary sulfates: Chem. Geol., v. 1, p. 93-135.

Hotz, P. E., 1971, Plutonic rocks of the Klamath Mountains, California and Oregon: U. S. Geol. Survey Prof. Paper 684-B, 19 p.

Hotz, P. E., Lanphere, M. A., and Swanson, D. A., 1977, Triassic blueschist from northern California and north-central Oregon: Geolgoy, v. 5, no. 11, p. 659-663.

Iijima, A, 1974, Clay and zeolitic alteration zones surrounding Kuroko deposits in the Hokuroku district, northern Akita, as submarine hydrothermal-diagenetic alteration products: Soc. Mining Geologists Japan, Spec. Issue 6, p. 267-289.

Irvine, T. N., and Baragar, W. R. A., 1971, A guide to the chemical classification of the common volcanic rocks: Canadian Jour. Earth Science, v. 8, p. 523-548.

Irwin, W. P., 1972, Terranes of the western Paleozoic and Triassic belt in the southern Klamath Mountains, California, in Geological Survey Research 1972: U. S. Geol. Survey Prof. Paper 800-C, p. C103-111.

Izawa, E., Yoshida, T., and Saito, R., 1978, Geochemical characteristics of hydrothermal alteration around the Fukazawa Kuroko deposit, Akita, Japan: Mining Geology, v. 28, p. 325-335.

Jakes, P., and White, A. J. R., 1971, Composition of island arcs and continental growth: Earth and Planetary Sci. Letters: v. 12, p. 224-230.

-----, 1972, Major and trace element abundances in volcanic rocks of orogenic areas: Geol. Soc. America Bull., v. 83, p. 29-40.

Jones, D. L., Silberling, N. J., and Hillhouse, J., 1977, Wrangellia-A displaced continental block in northwestern North America: Canadian Jour. Earth Science, v. 14, p. 2565-2577.

-----, 1978, Microplate tectonics of Alaska-Significance for the Mesozoic history of the Pacific coast of North America, in Howell, D. G., and McDougall, K. A., eds., Mesozoic paleogography of the western United States: Pacific Section, Society of Economic Paleontologists and Mineralogists Pacific Coast Paleogeography Symposium 2, p. 71-74.

Juhas, A. P., and Gallagher, T. P., 1981, Kuroko type mineralization at the Red Ledge deposit, Idaho, in Silberman, M. L., Field, C. W., and Berr, A. L., eds., Proceedings of the Symposium on Mineral Deposits of the Pacific Northwest-1980: U. S. Geol. Surv. Open-file Report 81-355, p. 223-235.

Kajiwara, Y., 1971, Sulfur isotope study of the Kuroko-ores of Shakanai No. 1 deposits, Akita Prefecture, Japan: Geochem. Jour., v. 4, p. 157-181.

Kerrich, R., 1976, Some effects of tectonic recrystallization on fluid inclusions in quartz veins: Contr. Mineral. Petrol., v. 59, p. 195-202.

Kinkel, A. R., Jr., Hall, W. E., and Albers, J. P., 1956, Geology and base-metal deposits of West Shasta copper-zinc district, Shasta County, California: U. S. Geol. Survey Prof. Paper 285, 156 p.

Koski, R. A., 1981, Volcanogenic massive sulfide deposits in ocean-crust and island-arc terranes, northwestern Klamath Mountains, Oregon and California, in Silberman, M. L., Field, C. W., and Berr, A. L., eds., Proceedings of the Symposium on Mineral Deposits of the Pacific Northwest-1980: U. S. Geol. Surv. Open-file Report 81-355, p. 197-212.

Kowalik, J., Rye, R. O., and Sawkins, F. J., 1981, Stable-isotope study of the Buchans, Newfoundland, polymetallic sulphide deposits: Geol. Assoc. Canada, Spec. Paper 22, p. 229-254.

Kusakabe, M., and Robinson, B. W., 1977, Oxygen and sulfur isotope equilibria in the $BaSO_4$-HSO_4^--H_2O system from 110 to 350 °C and applications: Geochim. Cosmochim. Acta, v. 41, p. 1033-1040.

Kusakabe, M., and Chiba, H., 1979, Oxygen isotope geothermometry applicable to sulphate minerals from the Kuroko deposits: Mining Geology, v. 29, p. 257-264.

-----, 1983, Oxygen and sulfur isotope composition of barite and anhydrite from the Fukazawa deposit, Japan: Econ. Geol. Mono. 5, p. 292-301.

Large, R. R., 1977, Chemical evolution and zonation of massive sulfide deposits in volcanic terrains: Econ. Geol., v. 72, p. 549-572.

Levinson, A. A., 1974, Introduction to exploration geochemistry, Broadview, Illinois, Applied Publishing, 614 p.

Liou, J. G., Kuniyoshi, S., and Ito, K., 1974, Experimental studies of the phase relations between greenschist and amphibolite in a basaltic system: American Jour. of Sci., v. 274, p. 613-632.

Livingston, D. C., and Laney, F., 1920, The copper deposits of the Seven Devils and adjacent districts: Idaho Bur. Mines and Geology Bull. 1, p. 41-59.

Lloyd, R. M., 1968, Oxygen isotope behavior in the sulfate-water system: Geophys. Research, v. 78, p. 6099-6110.

Long, R. C., 1975, Geology and mineral deposits of the Red Ledge Mine area, Adams County, Idaho: unpublished M.S. thesis, Oregon State Univ., 115 p.

Lusk, J., and Crocket, J. H., 1969, Sulfur isotope fractionation in coexisting sulfides from the Heath Steele B-1 orebody, New Brunswick, Canada: Econ. Geol., v. 64, p. 147-155.

Marutani, M., and Takenouchi, S., 1978, Fluid inclusion study of stockwork siliceous orebodies of Kuroko deposits at the Kosaka mine, Akita, Japan: Mining Geology, v. 28, p. 349-360.

Matsuhisa, Y., Goldsmith, J. R., and Clayton, R. N., 1979, Oxygen isotopic fractionation in the system quartz-albite-anorthite-water: Geochim. Cosmochim. Acta, v. 43, p. 1131-1140.

McCrea, J. M., 1950, The isotopic chemistry of carbonates and a paleo-temperature scale: Jour. Chem. Phys., v. 18, p.849.

Meyer, C., and Hemley, J. J., 1967, Wall rock alteration, in Barnes, H. L., ed., Geochemistry of Hydrothermal Ore Deposits (1st ed.); New York, Holt, Rinehart and Winston, p. 166-235.

Mizukami, M., and Ohmoto, H., 1983, Controlling mechanisms for the major element chemistry of aqueous solutions in tuff-rich environments: Econ. Geol. Mono. 5, p. 559-569.

Mizutani, Y., and Rafter, T. A., 1969, Oxygen isotopic fractionation in the bisulphate ion-water system: New Zealand Jour. Sci., v. 12, p. 54-59.

Mottl, M. J., 1983, Metabasalts, axial hot springs, and the structure of hydrothermal systems at mid-ocean ridges: Geol. Soc. America Bull., v. 94, p. 161-180.

Mottl, M. J., and Holland, H. D., 1978, Chemical exchange during hydrothermal alteration of basalt by seawater-I. Experimental results for major and minor components of seawater: Geochim. Cosmochim. Acta, v. 42, p. 1103-1115.

Mukaiyama, H., Mononobe, S., and Yoshida, T., 1974, Genesis of the Iwami mine, Shimande Prefecture, Japan: Soc. Mining Geologists Japan, Spec. Issue 6, p. 221-234.

Nehring, N. L., Bowen, P. A., and Truesdell, A. H., 1977, Techniques for the conversion to carbon dioxide of oxygen from dissolved sulfate in thermal waters: Geothermics, v. 5, p. 63-66.

Nockolds, S. R., Knox, R. W. O'B., and Chinner, G. A., 1978, Petrology, New York, Cambridge University Press, 435 p.

Northrop, D. A., and Clayton, R, N., 1966, Oxygen-isotope fractionations in systems containing dolomite: Jour. Geology, v. 74, p. 174-196.

Ohmoto H., 1972, Systematics of sulfur and carbon isotopes in hydrothermal ore deposits: Econ. Geol., v. 67, p. 551-579.

Ohmoto, H., and Rye, R. O., 1979, Isotopes of sulfur and carbon in Barnes, H. L., ed., Geochemistry of Hydrothermal Ore Deposits (2nd ed.): New York, John Wiley, p. 509-567.

Ohmoto, H., and Lasaga, A., 1982, Kinetics of reactions between aqueous sulfates and sulfides in hydrothermal systems: Geochim. Cosmochim. Acta, v. 46, p. 1727-1745.

Ohmoto, H., Mizukami, M., Drummond, S. E., Eldridge, C. S., Pisutha-Arnond, V., and Lenagh, T. C., 1983, Chemical processes of Kuroko formation: Econ. Geol. Mono. 5, p. 570-604.

O'Neil, J. R., and Taylor, H. P., Jr., 1969, Oxygen isotope fractionation between muscovite and water: Jour. Geophys. Res., v. 74, p. 6012-6022.

O'Neil, J. R., Clayton, R. N., and Mayeda, T., 1969, Oxygen isotope fractionation in divalent metal carbonates: Jour. Chem. Phys., v. 51, p. 5547-5558.

Pearce, J. A., and Cann, J. R., 1973, Tectonic setting of basic volcanic rocks determined using trace element analyses: Earth and Planetary Sci. Letters, v. 19, p. 290-300.

Petersen, M. D., and Lambert, I. B., 1979, Mineralogical and chemical zonation around the Woodlawn Cu-Pb-Zn ore deposit, southeastern New South Wales: Geol. Soc. Australia Jour., v. 26, p. 169-186.

Pisutha-Arnond, V., and Ohmoto, H., 1983, Thermal history, and chemical and isotopic compositions of the ore-forming fluids responsible for the Kuroko massive sulfide deposits in the Hokuroko District of Japan: Econ. Geol. Mono. 5, p. 523-558.

Potter, R. W. II., Clynne, M. A., and Brown, D. L., 1978, Freezing point depression of aqueous sodium chloride solutions: Econ. Geol., v. 73, p. 284-285.

Reed, M. H., 1983, Seawater-basalt reaction and the origin of greenstones and related ore deposits: Econ. Geol., v. 78, p. 466-485.

-----, 1984, Geology, wall-rock alteration, and massive sulfide mineralization in a portion of the West Shasta District: Econ. Geol., v. 79, p. 1299-1318.

Ripley, E. M., and Ohmoto, H., 1977, Mineralogic, sulfur isotope, and fluid inclusion studies of the stratabound copper deposits at the Raul Mine, Peru: Econ. Geol., v. 72, p. 1017-1041.

Riverin, G., and Hodgson, C. J., 1980, Wall-rock alteration at the Millenbach Cu-Zn mine, Noranda, Quebec: Econ. Geol., v. 75, 424-444.

Roberts, R. G., and Reardon, E. J., 1978, Alteration and ore-forming processes at Mattagami Lake mine, Quebec: Canadian Jour. Earth Science: v. 15, p. 1-21.

Roedder, E., 1963, Studies of fluid inclusions II: Freezing data and their interpretation: Econ. Geol., v. 58, p. 167-211.

-----, 1979, Fluid inclusions as samples of ore fluids in Barnes, H. L., ed., Geochemistry of Hydrothermal Ore Deposits (2nd ed.): New York, John Wiley, p. 684-737.

Rye, R. O., and Ohmoto, H., 1974, Sulfur and carbon isotopes and ore genesis: A review: Econ. Geol., v. 69, p. 826-842.

Rye, R. O., Roberts, R. J., Snyder, W. S., Lahusen, G. L., and Motica, J. E., 1984, Textural and stable isotope studies of the Big Mike cupriferous volcanogenic massive sulfide deposit, Pershing County, Nevada: Econ. Geol., v. 79, p. 124-140.

Sakai, H., 1968, Isotopic properties of sulfur compounds in hydrothermal processes: Geochem. Jour., v. 2, p. 29-49.

Sangster, D. F., 1968, Relative sulphur isotope abundances of ancient seas and stratabound sulphide deposits: Geol. Assoc. Canada, Proc., v. 17, p.79-91.

Sarewitz, D., 1983, Seven Devils terrane: Is it really a piece of Wrangellia?: Geology, v. 11, p. 634-637.

Sato, T., 1972, Behaviors of ore-forming solutions in seawater: Mining Geology, v. 22, p. 31-42.

Schwarz, E. J., Muller, J. E., and Clark, K. R., 1980, Paleomagnetism of the Karmutsen basalts from southeast Vancouver Island: Canadian Jour. Earth Science, v. 17, p. 389-399.

Shenon, P. J., 1933a, Copper deposits in the Squaw Creek and Silver Peak districts and at the Almeda mine, southwestern Oregon, with notes on the Pennell and Farmer and Banfield prospects: U. S. Geol. Survey Circ. 2, 35 p.

-----, 1933b, Geology and ore deposits of the Takilma-Waldo district, Oregon, including the Blue Creek district: U. S. Geol. Survey Bull. 846, p. 141-194.

Silberling, N. J., 1983, Stratigraphic comparison of the Wallowa and Huntington terranes: Geol. Soc. America Abs. w. Prog., v. 15, no. 5, p. 372.

Solomon, M., Rafter, T. A., and Jensen, M. L., 1969, Isotope studies on the Rosebery, Mount Farrell and Mount Lyell Ores, Tasmania: Mineral. Deposita (Berl.), v. 4, p. 172-199.

Solomon, M., and Walshe, J. L., 1979, The formation of massive sulfide deposits on the sea floor: Econ. Geol., v. 74, p. 797-813.

Sorensen, M. R., 1983, The Queen of Bronze copper deposit, southwestern Oregon: An example of sub-sea floor massive sulfide mineralization: unpublished M. S. thesis, Univ. of Oregon, 205 p.

Spry, A., 1976, Metamorphic textures (3rd ed.): New York, Pergamon Press, 350 p.

Suzuoki, T., and Epstein, S., 1976, Hydrogen isotope fractionation between OH-bearing minerals and water: Geochim. Cosmochim. Acta, v. 40, p. 1229-1240.

Swanson, D. A., 1969, Lawsonite blueschist from north-central Oregon: U. S. Geol. Survey Prof. Paper 650-B, p. 8-11.

Taylor, H. P., Jr., 1968, The oxygen isotope geochemistry of igneous rocks: Contr. Mineral. Petrol., v. 19, p. 1-71.

-----, 1974, The application of oxygen and hydrogen isotope studies to problems of hydrothermal alteration and ore deposition: Econ. Geol., v. 69, p. 843-883.

-----, 1979, Oxygen and hydrogen isotope relationships in hydrothermal mineral deposits in Barnes, H. L., ed., Geochemistry of Hydrothermal Ore Deposits (2nd ed.): New York, John Wiley, p. 236-277.

Taylor, H. P., Jr., and Epstein, S., 1962, Relationship between $^{18}O/^{16}O$ ratios in coexisting minerals of igneous and metamorphic rocks, Pt. 1, Principals and experimental results: Geol. Soc. America Bull., v. 73, p. 461-480.

Thayer, T. P., 1963, The Canyon Mountain Complex, Oregon, and alpine mafic magma stem, in Geological Survey research 1963: U. S. Geol. Survey Prof. Paper 475-C, p. C82-C85.

-----, 1977, The Canyon Mountain Complex, Oregon, and some problems of ophiolites, in Coleman, R. G., and Irwin, W. P., eds., North American ophiolites: Oregon Dept. Geology Mineral Industries Bull. 95, p. 93-106.

Thayer, T. P., and Brown, C. E., 1964, Pre-Tertiary orogenic and plutonic intrusive activity in central and northeastern Oregon: Geol. Soc. America Bull., v. 75, no. 12, p. 1255-1262.

Thode, H. G., and Monster, J., 1965, Sulfur isotope geochemistry of petroleum, evaporites, and ancient seas: Am. Assoc. Petroleum Geologists Mem. 4, p. 367-377.

Thurlow, J. G., Swanson, E. A., and Strong, D. F., 1975, Geology and lithogeochemistry of the Buchans polymetallic sulfide deposits, Newfoundland: Econ. Geol., v. 70, p. 130-144.

Tokunaga, M., and Honma, H., 1974, Fluid inclusions in the minerals from some Kuroko deposits: Soc. Mining Geologists Japan, Spec. Issue 6, p. 385-388.

Urabe, T., Scott, S. D., and Hattori, K., 1983, A comparison of footwall-rock alteration and geothermal systems beneath some Japanese and Canadian volcanogenic massive sulfide deposits: Econ. Geol. Mono. 5, p. 345-364.

Vallier, T. L., 1974, Preliminary report on the geology of part of the Snake River Canyon: Oregon Dept. Geology and Mineral Industries, Map GMS-6, 28 p.

-----, 1977, The Permian and Triassic Seven Devils Group, western Idaho and northeastern Oregon: U. S. Geol. Survey Bull. 1437, 58 p.

Vallier, T. L., Brooks, H. C., and Thayer, T. P., 1977, Paleozoic rocks of eastern Oregon and western Idaho, in Stewart, J. H., Stevens, C. H., and Gritsche, A. E., eds., Paleozoic paleogeography of the western United States: Pacific Section, Society of Economic Paleontologists and Mineralogists Pacific Coast Paleogeography Symposium 1, p. 455-466.

Vallier, T. L., and Batiza, R., 1978, Petrogenesis of spilite and keratophyre from a Permian and Triassic volcanic arc terrane, eastern Oregon and western Idaho, U.S.A.: Canadian Jour. Earth Science, v. 15, p. 1356-1369.

Vernon, R. H., 1975, Metamorphic processes, reactions and microstructure development: New York, John Wiley, 243 p.

Walker, N. W., 1983, Pre-Tertiary evolution of northeastern Oregon and west-central Idaho: Constraints based on U/Pb ages of zircons: Geol. Soc. America Abs. w. Prog., v. 15, no. 5, p. 371.

Watanabe, M., and Sakai, H., 1983, Stable isotope geochemistry of sulfates from the Neogene ore deposits in the Green Tuff region, Japan: Econ. Geol. Mono. 5, p. 282-291.

Wenner, D. B., and Taylor, H. P., Jr., 1971, Temperatures of serpentinization of ultramafic rocks based on O^{18}/O^{16} fractionation between coexisting serpentine and magnetite: Contr. Mineral. Petrol., v. 32, p. 165-185.

White, W. H., 1973, Flow structure and form of the Deep Creek stock, southern Seven Devils Mountains, Idaho: Geol. Soc. America Bull., v. 84, p. 199-210.

Wilkins, R. W. T., and Barkas, J. P., 1978, Fluid inclusions, deformation and recrystallization in granite tectonites: Contr. Mineral. Petrol., v. 65, p. 293-299.

Wilson, D., and Cox, A., 1980, Paleomagnetic evidence for tectonic rotation of Jurassic plutons in Blue Mountains, eastern Oregon: Jour. Geophysical Research, v. 85, no. B7, p. 3681- 3689.

Winchester, J. A., and Floyd, P. A., 1977, Geochemical discrimination of different magma series and their differentiation products using immobile elements: Chemical Geol., v. 20, p. 325-343.

Winkler, H. G. F., 1976, Petrogenesis of metamorphic rocks (4th ed.): New York, Springer-Verlag, 334 p.

Woods, T. L., Bethke, P. M., Bodnar, R. J., and Werre, R. W., Jr., 1981, Supplementary components and operation of the U.S.G.S. gas-flow heating/freezing stage: U. S. Geol. Survey Open File Report 81-954, 13 p.

Wracher, D. A., 1969, The geology and mineralization of the Peck Mountain area, Hornet Quadrangle, Idaho: unpublished M. S. thesis, Oregon State Univ., 78 p.

Yamamoto, M., 1974, Distribution of sulfur isotopes in the Iwami Kuroko deposits, Shimane Prefecture, Japan: Geochem. Jour., v. 8, p. 27-35.

Yole, R. W., Irving, E., 1980, Displacement of Vancouver Island: Paleomagnetic evidence from the Karmutsen Formation: Canadian Jour. Earth Science, v. 17, 1210-1288.